

https://dspace.org/

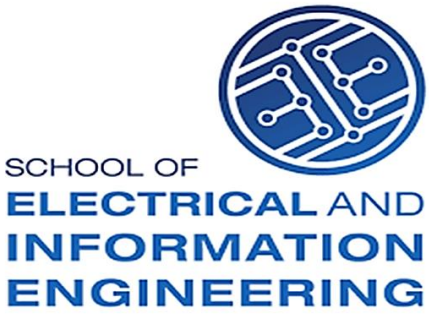
Developing an epoxy composite dielectric with hollow carbon nanospheres

Sitole, Sophy

2020

https://hdl.handle.net/10539/31110

Downloaded from a DSpace repository. https://dspace.org/



University of the Witwatersrand, Johannesburg, South Africa

MSc Engineering (Electrical) dissertation

Developing an epoxy composite dielectric with hollow carbon nanospheres

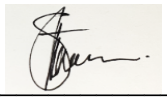
Sophy Sitole

This dissertation is submitted to the Faculty of Engineering and the Built Environment, University of the Witwatersrand, Johannesburg, in fulfilment of the requirements for the degree of Master of Science in Engineering

October 2020

DECLARATION

I declare that this dissertation is my own unaided work. It is being submitted for the degree of Master of Science in engineering at the University of the Witwatersrand, Johannesburg. It has not been submitted before for any degree or examination at any other University.

Signature: 

Date: 15 – 10 – 2020

Abstract:

This dissertation presents the feasibility of developing an epoxy nanocomposite with hollow carbon nanospheres. The work entailed synthesis of the hollow carbon nanoparticles and then fabrication and characterisation of the epoxy nanodielectric. A template method with polystyrene nanoparticles as a prototype was used to synthesize the hollow carbon nanospheres (HCNs). The characterisation techniques which are scanning electron microscopy, transmission electron microscopy, Branauer Emmett-Teller, Raman spectroscopy and thermogravimetric analysis were used to confirm the chemical and physical properties of the synthesized HCNs. It was found that the synthesized HCNs have a relatively high surface area of 341.5 m^2/g and an average diameter of 410±70 nm. A direct dispersion method incorporated with rheology analysis was used to fabricate the epoxy resin and nanodielectric material at different nanofiller loading levels. It was found that incorporating rheology analysis in the nanodielectric fabrication protocol can improve the efficiency of determining the optimal nanoparticle filler loading level for electrical tree endurance of the resultant nanodielectric. An electrical treeing test was used to characterise the fabricated nanodielectric material. A partial discharge measuring circuit according to the IEC 60270 was used to characterise the electrical trees grown in epoxy resin and nanocomposite material with either solid carbon nanospheres (SCNs) or HCNs. The performance of SCNs in epoxy of type araldite® FR476D and hardener® was used as a benchmark in comparing electrical tree endurance between SCNs/Epoxy and HCNs/Epoxy nanodielectric. It was found that HCNs improve the electrical insulation properties of epoxy but not to the same extent as the corresponding solid carbon nanospheres. This finding could be regarded as an indication that the electron scavenging properties of carbon nanoparticles (that has been reported in the literature) contributes to the superior properties of the carbon-based nanodielectrics. For the same particle size, solid carbon nanoparticles have more carbon content than mesoporous hollow carbon nanoparticles. Furthermore, there is a material type dependent compatibility relationship between nanoparticles and host material. Different types of epoxy showed different characteristics of the resultant nanodielectric for the same type of nanoparticle fillers.

Dedication

To my lovely grandmother, mom and uncle for their love, support and prayers.

To my siblings for cheering me up.

To my loving husband for the support and motivation throughout the years.

Acknowledgements

First and foremost, I would like to thank my supervisor Prof Nyamupangedengu for his excellent supervision, contribution, support, encouragement and guidance. It was a privilege to be supervised by him and I am greatly indebted to him.

I would like to acknowledge merSETA for funding my studies, and Eskom and National Research Foundation (NRF) for their support of the High Voltage Engineering Research Group at the University of Witwatersrand.

Sincere gratitude to Prof Coville, Dr Matuma and Ms Magubane from Wits school of Chemistry for sharing their knowledge with me on how to synthesize the hollow carbon nanoparticles. Special thanks to Prof. Ziegler, Dr. Maubane, Dr. Tetana and Mr. Gerber from Microscopy and Microanalysis unit (MMU) for the trainings and support on how to use microscopic techniques.

I would like to acknowledge my co-supervisor Prof Sigalas for granting me access and resources at the laboratories of Wits school of Chemical and Metallurgical engineering to fabricate the nanodielectric material. Special thanks to Dr. Rokeband and Dr. Ntholeng for the training provided.

I would like to acknowledge Mr Cornish for training me on how to manufacture the nanocomposite material and for those valuable discussions and debates we used to have about nanodielectric research. I would like to thank the technicians Mr Mabaso and Mtsweni for their assistance in the Germin and High voltage laboratories at the university of Witwatersrand.

Finally, I would like to thank God for the opportunity to pursue my MSc degree and meeting wonderful people during my studies.

List of research publications

1. S. Sitole, C. Nyamupangedengu and A.M Hank, "*Evaluation of AC and DC breakdown strength of carbon nanosphere/Epoxy nanodielectrics*", 26th Southern African Universities Power and Engineering Conference (SAUPEC), Johannesburg, 2018.

2. S. Sitole, C. Nyamupangedengu, "*Comparing Electrical Tree Inception in Epoxy and Polyethylene Using Fowler-Nordheim Based Model*", Proceedings of the 21st International Symposium on High Voltage Engineering (ISH) published by Springer Lecture Notes in Electrical Engineering, vol 599, 2019.

3. S. Sitole, A. Magubane, C. Nyamupangedengu and N. Coville, "*Synthesis of hollow carbon spheres for fabrication of C\Epoxy nanocomposite insulation*", IEEE AFRICON conference, Ghana, 2019.

Table of Contents

DECLARATION ..... **i**

Dedication ..... **iii**

Acknowledgements ..... **iv**

List of research publications ..... **v**

List of figures ..... **ix**

Chapter 1: Introduction **1**

1.1 Introduction 1

1.2 Problem statement 2

1.3 The research questions and objectives 2

1.4 The research methodology landscape 3

1.5 The dissertation structure 6

Chapter 2: Literature review of nanocomposites material technology **7**

2.1 Introduction 7

2.2 The models for the interfacial area 7

2.2.1 Multi-layered core model [17] 8

2.2.2 New potential barrier model [16] 9

2.2.3 The Interphase Volume Model [18] 9

2.2.4 Polymer chain alignment Model [19] 10

2.3 A literature review of nanofillers 11

2.3.1 Inorganic nanofillers 11

2.3.2 Organic nanofillers 14

2.4 Some challenges in the nanodielectrics technology 15

2.5 Chapter Conclusion 16

Chapter 3: The synthesis and characterization of the Mesoporous Hollow Carbon Nanospheres (HCNs) **18**

3.1 Introduction 18

3.2 The template method of Hollow Carbon Nanospheres (HCNs) synthesis 19

3.2.1 Template method of synthesising HCNs using silica nanoparticles as prototype 19

3.2.2 Template method of HCNs synthesis using polystyrene nanoparticles as template 23

3.3 Characterization techniques of the nanoparticles 26

3.4 Characterisation results of HCNs that were manufactured using polystyrene nanoparticles as templates 27

3.5 Chapter Conclusion 30

Chapter 4: The fabrication of the nanocomposite material: a conventional process modified to include rheology analyses 31

4.1 Introduction and background to nanodielectric fabrication techniques 31

4.2 The fabrication of the HCNs/Epoxy and SCNs/Epoxy nanodielectrics using the direct dispersion method incorporating rheological analysis 35

4.3 The rheological results of unfilled araldite (epoxy monomer), SCNs/Araldite and HCNs/Araldite mixture 37

4.4 Chapter Conclusion 41

Chapter 5: Electrical tree time-to-failure characterisation of the (HCN/Epoxy) nanodielectric in comparison with unfilled epoxy as well as SCN/Epoxy 43

5.1 Introduction 43

5.2 Some background literature on electrical treeing mechanisms 44

5.2.1 Electrical treeing in conventional polymer material 44

5.2.2 Electrical treeing mechanisms in nanocomposites 46

5.3 The electrical treeing experimentation with the hollow and solid carbon nanospheres in epoxy dielectric 47

5.4 The electrical treeing experimental test results 49

5.4.1 Electrical tree PD inception voltage results 49

5.4.2 Electrical tree time-to-failure test results 51

5.4.3 Partial discharge magnitude time-evolution results 52

5.4.4 Partial discharge phase-resolved-patterns (PDPRP) associated with electrical tree growth 56

5.4.5 Electrical tree microscopic imaging 59

5.5 Overall evaluation of the research results in the context of answers to the research questions .. 61

5.6 Chapter Conclusion 63

Chapter 6: Conclusion and possible future research **65**

6.1 The conclusions that can be drawn from the present work 65

6.2 Recommendations for future work 66

References **68**

Appendix A: Detailed electrical treeing result of unfilled epoxy resin, SCNs/Epoxy and HCNs/Epoxy nanodielectric **73**

Appendix B: Extra rheological results of SCNs/Araldite mixture 74

Appendix C: A paper presented at the 2018 Southern African Universities Power Engineering Conference (SAUPEC) held at University of Witwatersrand, Johannesburg. 75

Appendix D: The paper presented at the 2019 International Symposium on High Voltage Engineering (ISH) conference held at Budapest, Hungry. 81

Appendix E: The paper presented at the 2019 IEEE AFRICON conference held at Accra, Ghana. 88

List of figures

Figure 1.1:The flow chart diagram of research methodology 5
Figure 2.1 The multi- layered core model adapted from [17] 8
Figure 2.2 The polymer chain alignment model (a) the particle which is not surface modified and (b) a surface modified particle adapted from [19]. 10
Figure 2.3: Nanoparticles with different dimensions 11
Figure 2.4:Band diagram of the conductor, semiconductor and insulator. 13
Figure 3.1: A schematic overview of the template method using silica nanoparticles……..19
Figure 3.2: The modified Stober method used to make the silica nanoparticles 20
Figure 3.3: A horizontal chemical vapour deposition setup used for carbonization process adapted from [45]. 21
Figure 3.4: The SEM images of the synthesized HCNs using silica nanoparticles a template (a) SEM image of HCNs with few which are broken (b) A SEM image with many broken HCNs (c) A SEM image of HCNs with the region analysed using Energy-Dispersive X-ray spectroscopy (EDS) (d) Surface morphology of HCNs at high magnification. 22
Figure 3.5: The particle size distribution of HCNs. 22
Figure 3.6: The TEM images of HCNs synthesized using silica a template 23
Figure 3.7: EDS result of the region labelled spectrum 1 in Figure 3.4c 23
Figure 3.8: Images of (a) the experimental setup used to reflux (b) a centrifuge 24
Figure 3.9: A schematic diagram and image of the setup used for carbon reaction 25
Figure 3.10: The temperature profile as function of time 25
Figure 3.11: The SEM images showing the surface morphology of HCNs at different magnification 28
Figure 3.12: The TEM images of the HCNs manufactured using polystyrene nanoparticles as a template. 28
Figure 3.13: The particle size distribution of the synthesised hollow carbon nanospheres. 29
Figure 3.14:The TGA and D-TGA curves of (a) polystyrene nanoparticles (b) HCNs nanoparticles 29
Figure 3.15: Raman spectroscopy results of the synthesised HCNs 30
Figure 4.1: Ideal graphs of shear rate as a function of viscosity for Newtonian and non-Newtonian fluids adapted from [52]……...……..32
Figure 4.2: A flow diagram of in-situ polymerisation adapted from [60] 33
Figure 4.3: Sol-gel manufacturing method adapted from [65] 34
Figure 4.4: A melt blend method adapted from [2] [66]. 35
Figure 4.5: Direct mixing technique incorporated with rheology analyses used to fabricate the nanocomposite material adapted from Hank [10] 36
Figure 4.6: (a)A high shear mixer used to mix the mixture of araldite, hardener and nanoparticles (b) aluminium molds used to cast the nanocomposite material. 36
Figure 4.7: An image of the rheometer used to measure the rheological properties of a mixture of araldite with either SCNs or HCNs nanoparticles. 37
Figure 4.8: Viscosity profiles as a function of shear rate for SCNs/Araldite mixture with 0.21 wt% nanofiller concentration at different mixing times on the high shear mixer 38

Figure 4.9: The viscosity profiles of araldite at different temperature levels. 38
Figure 4.10: Comparison of unfilled araldite in comparison to SCNs/Araldite mixture with nanofiller loading levels of 0.35 wt% and 0.5 wt% (a) Viscosity profiles (b) Shear stress profiles. 39
Figure 4.11: Comparison of rheological properties of unfilled araldite and HCNs/araldite mixture at different nanofiller loading levels (a) Shear stress profiles (b) Viscosity profiles 40
Figure 4.12: Comparison of rheological properties of unfilled araldite and HCNs/araldite mixture at 0.04 wt% nanofiller loading levels(a) Shear stress profiles (b)Viscosity profiles. 40
Figure 5.1: The circuit diagram used in initiating and growing the electrical trees whilst simultaneously measuring the corresponding partial discharges according to IEC 60270……47

Figure 5.2: A drawing of electrical tree test specimen and images of a) Unfilled epoxy, b) Nanocomposite with carbon nanofillers. 47
Figure 5.3: The flow chart of the methodology used to measure electrical tree inception voltage and time-to-failure..... 48
Figure 5. 4: (a) Background noise level in the High Voltage Laboratory, (b) A snapshot of PDPRP of 1 pC signal used to calibrate the circuit. 48
Figure 5.5: (a) Min-Average-Max chart for inception voltage of SCNs/Epoxy nanodielectric as a function of nanofiller concentration (b) Min-Average-Max chart for inception voltage of HCNs/Epoxy nanodielectric as a function of nanofiller concentration. 50
Figure 5.6: Average electrical tree inception voltage of epoxy, SCNs\Epoxy and HCNs\Epoxy nanocomposites as a function of nanofiller loading level. 50
Figure 5.7: An example of PDPRP associated with the first PD pulses at electrical tree inception voltage (a) unfilled epoxy resin (b) SCNs/Epoxy nanodielectric with 0.31 wt% (c) HCNs/Epoxy nanodielectric with 0.04 wt%..... 50
Figure 5.8: Min-Average-Max chart for electrical tree time-to-failure as a function of nanofiller concentration of (a)SCNs/Epoxy nanodielectric (b) HCNs/Epoxy nanodielectric..... 51
Figure 5.9: Comparison of average electrical tree time-to-failure in SCNs\Epoxy and HCNs\Epoxy nanodielectric as a function of nanofiller loading level. 52
Figure 5.10: Typical results of electrical tree partial discharge magnitude as a function of time for the unfilled epoxy resin..... 52
Figure 5.11: Electrical tree PD magnitude as a function of time for SCNs/Epoxy nanodielectric at 0.044wt% nanofiller loading level. 53
Figure 5. 12: Electrical tree PD magnitude as a function of time for SCNs/Epoxy nanodielectric at 0.088wt% nanofiller loading level. 53
Figure 5.13: Electrical tree PD magnitude as a function of time for SCNs/Epoxy nanodielectric at 0.19wt% nanofiller loading level. 53
Figure 5.14: Electrical Tree PD magnitude as a function of time for SCNs/Epoxy at 0.31wt% nanofiller loading level 54
Figure 5.15: Electrical tree PD magnitude as a function of time for SCNs/Epoxy nanodielectric at 0.44wt% nanofiller loading level. 54

Figure 5.16: Electrical tree PD magnitude as a function of time for HCNs/Epoxy nanodielectric at 0.02wt% nanofiller loading level. 54
Figure 5. 17: Electrical tree PD magnitude as a function of time for HCNs/Epoxy nanodielectric at 0.04wt% nanofiller loading level. 55
Figure 5.18: Electrical tree PD magnitude as a function of time for HCNs/Epoxy at 0.088wt% nanofiller loading level. 55
Figure 5.19: Electrical tree PD magnitude as a function of time for HCNs/Epoxy at 0.19wt% nanofiller loading level. 55
Figure 5. 20: Electrical tree PD magnitude as a function of time for HCNs/Epoxy at 0.31wt% nanofiller loading level. 55
Figure 5.21: The typical PDPRP snapshots of unfilled epoxy every 8 minutes for the first 1 hour of 30 minutes 56
Figure 5.22: The PDPRP snapshots of sample 2 of SCNs/Epoxy nanocomposite at 0.31wt% nanofiller loading for every 2.5 minutes for the first hour. 57
Figure 5.23: The different types of PDPRP snapshots observed 27 minutes before the SCNs/Epoxy sample breaks down. 57
Figure 5.24: The partial discharge magnitude time evolution for a) unfilled epoxy b) SCNs/Epoxy nanodielectric c) HCNs/Epoxy nanodielectric 58
Figure 5.25: Different types of PDPRP snapshots observed on HCNs/Epoxy nanodielectric sample 58
Figure 5.26: The SEM images of (a) unfilled epoxy, (b) HCNs/Epoxy nanodielectric at 0.04 wt%. 59
Figure 5.27: The SEM image of a) A top view of the electrical tree in HCNs/Epoxy nanodielectric b) A top view of the electrical tree channel in HCNs/Epoxy nanodielectric. 59
Figure 5.28: The partial discharge cavity around the ogura needle tip for (a) HCNs/Epoxy nanodielectric (b) SCNs/Epoxy nanodielectric. 60
Figure 5. 29: The regions inside the cavity for HCNs/Epoxy nanodielectric. 61
Figure 5.30: The region inside the cavity for SCNs/Epoxy nanodielectric at different magnifications. 61
Figure B.1: The comparison of shear stress profiles of SCNs/Epoxy nanodielectric at different nanofiller loading levels and unfilled epoxy measured at 24.6℃ 74
Figure B.2: The comparison of viscosity profiles of SCNs/Epoxy nanodielectric at different nanofiller loading levels and unfilled epoxy measured at 24.6℃. 74

List of tables

Table 2.1:The characteristics of commonly investigated nanoparticles in the literature. 12
Table 2.2: Different types of carbon fillers with their applications [36] [40] [41] 15
Table 6.1: The research questions with corresponding answers as drawn from the research findings 65
Table A.1: The experimental data of electrical tree time-to-failure and inception voltage of unfilled epoxy, HCNs/Epoxy and SCNs/Epoxy nanodielectric data. 73

Acronyms and abbreviations

BET	Branauer Emmett-Teller
HCNs	Hollow Carbon Nanospheres
LDPE	low density polyethylene
MWCNTs	Multi-walled carbon nanotubes
PD	Partial discharges
PDPRP	Partial discharge phase resolved patterns
SCNs	Solid Carbon Nanospheres
SEM	Scanning electron microscopy
TEM	Transmission electron microscopy
TGA	Thermogravimetric analysis
Wt%	Weight percentage
XLPE	Cross-linked polyethylene
XRD	X-ray diffraction

Chapter 1: Introduction

1.1 Introduction

Reliability of electrical power equipment is largely dependent on that of the insulation. There are three forms of insulation which are solid, liquid and gas. The work of this dissertation focuses on solid insulation particularly epoxy resin. Epoxy resins have good chemical resistance, thermal conductivity, thermal shock, mechanical and dielectric properties [1]. The epoxy resins are used for encapsulating electrical and electronic components such as dry transformers, generators, switchgear and bushings. Necessarily, there is a need to explore development of the next generation of insulation material that will meet the evolving needs of modern and future electric power industry. The application of nanotechnology in electrical insulation seems to be a promising solution. The first polymer nanocomposite was manufactured by Toyota group in 1990, but Lewis was the first person to introduce the concept of nanodielectrics in 1994 [2] [3]. The research work done by Fothergill et al [4] and Nelson et al [5] to comprehend the fundamental concepts of nanodielectrics in the early 21st century re-invigorated interest in nanodielectrics research [2]. Fréchette et al [6] defined a nanodielectric as a dielectric which shows a dissimilar behaviour than the one expected in one of its properties due to an alteration on nanoscale. Nanodielectrics have good space charge performance, high breakdown strength, excellent resistance to electrical trees and partial discharges, thermal stability and good mechanical properties [2] [7].

The most investigated nanofillers in electrical insulation application are inorganic (such as silica, magnesium oxide, titanium oxide, alumina etc.) compared to organic nanofillers like carbon nanotubes, graphite platelets, carbon nanoballs, carbon black and fullerenes. The carbon-based organic nanofillers receive interest in mechanical applications, electromagnetic shielding applications and other applications where electrical conductivity is required. In 1997 Gustafsson et al [8] discovered that carbon black fillers reduce the space charge accumulation in crosslinked polyethylene (XLPE) but compromise the DC breakdown strength of the XLPE at 1 wt% nanofiller concentration. Later, carbon nanofillers such as fullerenes, solid carbon nanospheres and graphene were used and found to give nanocomposites with exceptionally improved electrical tree resistance [9] [10] [11]. It was hypothesised that the excellent properties of nanocomposites with carbon-based nanofillers is attributed to the electron scavenging properties of carbon. The present research work endeavours to prove whether this

hypothesis holds by investigating an epoxy nanocomposite that has hollow carbon nanospheres as fillers (HCNs/Epoxy) in comparison with that of solid carbon nanospheres.

The present dissertation presents the development of epoxy nanodielectric with hollow carbon nanospheres for application as a high voltage electrical insulation. The electrical treeing tests are used to characterise HCNs/Epoxy nanodielectric. Section 1.2 discusses the problem statement. The formulated research questions and objectives are presented in section 1.3. The research methodology that was used to answer the research questions is discussed in section 1.4. The structure of the rest of the dissertation document is outlined in section 1.5.

1.2 Problem statement

The problem is that conventional polymer-based insulation technology has limitations in meeting performance requirements of the modern and future electrical industry, which is characterized by stricter reliability requirements, increasing renewable energy sources, ultra-high voltage power transmission and the need for miniaturized equipment. Nanocomposites have proven to be the promising new generation of electrical insulation with better performance than conventional insulation. The existing literature shows that nanocomposite with carbon-based nanofillers have excellent resistance to electrical trees, but there is lack of knowledge on the mechanisms responsible for the improvement. Furthermore, it is still a challenge to ensure optimal nanofiller loading level for optimal dispersion and distribution when manufacturing nanodielectrics. Hence there is a need for real time techniques to monitor the nanofiller dispersion and determine the optimal nanofiller loading level during the manufacturing process. In literature rheology analysis has been used successfully to determine the optimal nanofiller concentration, and dispersion of nanoparticles within epoxy matrix but more research work is still required to fully understand the application of rheology in the nanodielectric development. The research questions and objectives which were derived from these problems are presented in the next section.

1.3 The research questions and objectives

From the work done by Jarvid et al [9] and that by Hank [10], the posit that the good properties of carbon-based nanocomposites is attributed to the electron scavenging properties of carbon still needs further validation. The objective of the present MSc research work is to show whether this hypothesis holds by developing a nanocomposite with hollow carbon nanospheres. If the hypothesis is true, the hollowness and mesoporosity of the nanoparticles will open other possibilities of further enhancing the electron scavenging properties of carbon by encapsulating

electron negative material in the carbon shell. The primary test is the electrical tree resistance since most insulation failure modes involve electrical trees in one way or another. The present research work therefore determines which nanofiller between solid carbon nanospheres (SCNs) and hollow carbon nanospheres (HCNs) cause better resistance to electrical trees in epoxy.

The main question is:

How do the properties of HCNs/Epoxy nanodielectric compare and contrast with those of SCNs/Epoxy nanodielectric?

The following sub-questions are on the specific dielectric properties investigated on the HCNS/Epoxy in comparison with SCNs/Epoxy and unfilled Epoxy. The sub-questions are as follows:

1. Which nanofiller loading level of hollow carbon nanospheres gives best electrical tree resistance in epoxy of type araldite® FR476D and hardener?
2. Which nanofiller loading level of solid carbon nanospheres gives best electrical tree resistance in epoxy; araldite® FR476D and hardener?
3. What are the rheological properties of unfilled araldite compared to HCNs/Araldite and SCNs/Araldite nanodielectrics in liquid state?
4. What are the electrical treeing characteristics of nanodielectric with hollow carbon nanospheres compared to those of unfilled epoxy and nanodielectric with solid carbon nanospheres?
5. Which nanofiller between SCNs and HCNs gives a nanodielectric with better resistance to electrical trees?

The key objective of the research work is to develop an epoxy nanocomposite with HCNs and then determine which nanofiller between SCNs and HCNs produce nanocomposite material with excellent resistance to electrical trees. This research work will further contribute knowledge of the mechanism responsible for improvement in electrical insulating properties related to carbon-based nanocomposites and the usage of rheology analysis to determine the optimal nanofiller concentration and monitor nanomaterial dispersion in real time during the nanocomposite manufacturing process.

1.4 The research methodology landscape

The research investigation incorporated knowledge areas from the following disciplines: Chemistry, Microscopy and microanalysis technology, Chemical Engineering and High

Voltage engineering. Consequently, therefore the work was executed in collaboration with the following departments at the University of the Witwatersrand, Johannesburg (Wits): School of Chemistry, Microscopy and Microanalysis Unit (MMU), School of Chemical and Metallurgical engineering and School of Electrical and Information engineering. The author had to develop the necessary competences in the requisite material science laboratory techniques as well as microscopic analyses techniques. The author therefore underwent various trainings to equip herself with necessary skills to operate the equipment used to synthesize nanoparticles and nanocomposites material and use microscopic techniques to analyse the nanoparticles. Figure 1.1 presents the key steps of the research methodology. The research was divided into three parts: synthesis and characterisation of the nanoparticles, fabrication of the nanocomposite and then characterisation of the nanocomposite.

The fabrication of the nanoparticles was conducted in the School of Chemistry laboratories. The tests to characterize the hollow carbon spheres were conducted in the laboratories of School Chemistry and Microscopy and Microanalysis unit (MMU) at the University and were as follows:

- Scanning Electron Microscopy (SEM)
- Transmission Microscopy (TEM)
- Branauer Emmett-Teller (BET)
- Thermogravimetric Analysis (TGA)
- Raman spectroscopy

The second part of the work was the fabrication of the epoxy nanocomposites and was conducted in the laboratories of the School of Chemical and Metallurgical Engineering. The nanofillers improve the polymer in specific nanofiller loading levels, therefore it was important to determine a nanofiller loading level of hollow carbon nanospheres that improved the epoxy resin. Since the type of epoxy resin that was used in the present research work was different from the one used on similar work by Hank [10], the study of electrical treeing behaviour of epoxy nanodielectric with solid carbon nanospheres was repeated in the present work. The repeat was to confirm whether experimental results obtained by Hank [10] were reproducible in different type of epoxy and therefore make sure that the comparison of epoxy nanodielectric with hollow and solid carbon nanospheres would be valid. The third part of the work was conducted in the high voltage laboratory of the School of Electrical and Information

Engineering and was on electrical properties characterisation of the fabricated epoxy nanodielectrics.

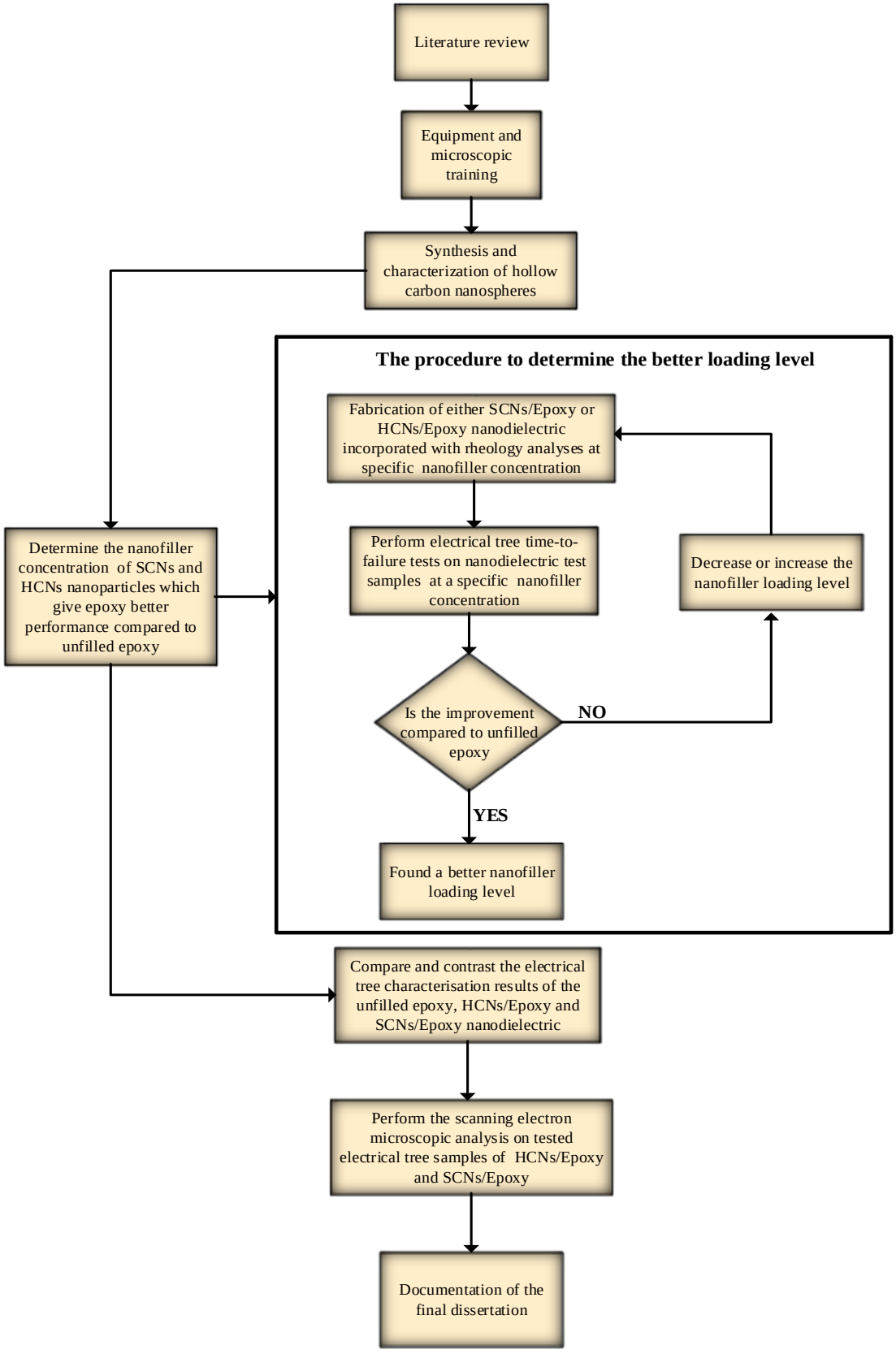


Figure 1.1:The flow chart diagram of the research approach

1.5 The dissertation structure

The structure of the dissertation document is as follows:

Chapter 2: presents the common models proposed to explain the structure and composition of interfacial regions in nanodielectrics. The models will be used to analyse the obtained results. It further outlines the literature review and challenges in nanodielectric research.

Chapter 3: presents the template methods used to synthesize hollow carbon nanospheres. Two types of templates were explored in the present work which are silica and polystyrene nanoparticles. The characterisation results of hollow carbon nanospheres using the following characterisation techniques are then presented. The characterisations are; scanning electron microscopy (SEM), transmission electron microscopy (TEM), Raman spectroscopy, Branauer Emmett-Teller (BET) and thermogravimetric analysis.

Chapter 4: presents a direct dispersion technique of the epoxy nanodielectrics fabrication that incorporated rheology analyses, The rheological results of unfilled araldite in comparison to HCNs/araldite and SCNs/araldite mixture in liquid state.

Chapter 5: It first introduces the literature review of electrical tree mechanisms in conventional insulation and then in nanocomposites material. The study of electrical treeing behaviour of unfilled epoxy, HCNs/Epoxy and SCNs/Epoxy nanocomposites is presented.

Chapter 6: Dissertation conclusion and possible future research.

Chapter 2: Literature review of nanocomposites material technology

2.1 Introduction

The first polymer nanocomposite with improved thermal and mechanical properties was developed by the Toyota group in 1990 and four years later Lewis introduced the concept of nanodielectric [2] [3]. Even though Lewis introduced the concept, it was still vague especially on how it would be applied in electrical insulation. In 1999, Heck et al [12] found that the silica nanoparticles improved the voltage endurance of epoxy resin. The concept of nanodielectric was reintroduced in 2001 by Fréchette et al [13]. The experimental works by Nelson and Fothergill et al [4] [5] in early 21^{th} century to comprehend the fundamental concepts of nanodielectrics re-invigorated interest in nanodielectrics research [2]. The first comprehensive review paper on nanodielectric was written in 2004 [2]. Research work conducted worldwide indicate that nanocomposites can have significantly enhanced electrical, thermal, chemical, optical, electrochemical and mechanical properties [6] [3]. It is widely agreed that the interfacial area between the nanoparticles and polymer matrix is what is responsible for the improvements in nanocomposite material.

The present chapter reviews the literature of nanodielectrics highlighting the basis for conceptualisation of the present research work. Section 2.2 presents the popular models used to explain the interfacial area. Section 2.3 gives further literature review of nanodielectrics. The nanodielectric research is still in the early stages and there still exist many unsolved questions. Some of the challenges in nanodielectric research are discussed in section 2.4.

2.2 The models for the interfacial area

Interfacial region is defined as an interaction area between the nanoparticle and host insulation and its size is in nanometer scale [14]. The nanoparticles have high surface area which results in corresponding large material of the interfacial regions within the nanocomposite material [15]. The interfacial region exhibits properties which are different from those of both the nanoparticles and host insulation [16]. This section briefly discusses four proposed models in the literature that are used to characterize the structure and composition of interfacial region.

2.2.1 Multi-layered core model [17]

Tanaka [17] proposed the multi-layered core model to explain why the silicate nanocomposite material is resistant to partial discharges. The model assumes that at least one dimension of the nanofillers should be less than 100 nm in size, the nanofillers are surface modified and spherical in shape. The model takes into account the diameter of the filler, inter-filler distance between the nanofillers, and nanofiller volume fraction and filler surface area per unit volume. The multi-core model comprises of three layers which are; the bonded (first), the bound (second) and the loose (third) layer as depicted in Figure 2.1. The first layer represents the tightly bonded strength between the nanofillers and host insulation. The addition of nanoparticles into the polymer changes the polymer chain structure and this results in the formation of second and third layers. The second and third layers represent the decreasing bonding strength in the interphase region. The spherulites and crystallites are formed in the second layer and this was confirmed by X-ray diffraction (XRD) spectra. XRD is an analytic technique used to identify the phase of crystalline material. The third layer is very thin and amorphous. The multi-core layered model states that if there is a charge injection or emission between the nanofiller and host insulation, the Gouy-Chapman diffuse layer will be created. The Gouy-Chapman diffuse layer overlaps the three layers and characterize the charge distribution, permittivity and conductivity. The multi-core model is a building block of many other proposed models for the interphase region, however it does not take the nanofiller loading and type of nanoparticle into account. Since the model does not factor in loading levels it does not take into the effect of possible existence of agglomerates/ agglomeration. The multi-core model is currently a working theory and not fully proved yet.

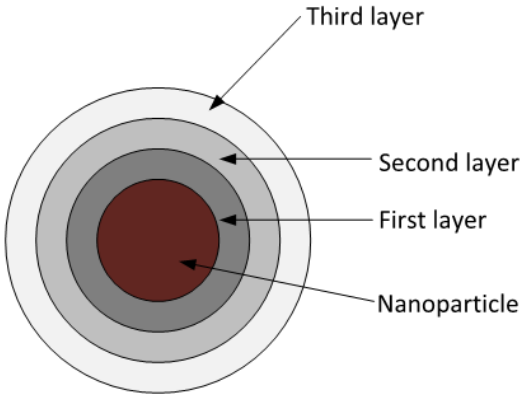


Figure 2.1 The multi- layered core model adapted from [17]

2.2.2 New potential barrier model [16]

The new potential barrier model is an extension of the multi-core model and was proposed by Li et al. [16]. The model takes the nanofiller level into consideration. The model combines the bound and loose layer of the multi-core model into a region called transition. The model states that at lower nanofiller loading the charge carriers are constrained within transition region. This causes the mobility and density of the carriers to decrease in nanodielectric, resulting into increased breakdown strength and decreased conductivity. The dielectric constant of nanodielectrics is less than that of host polymer due to dipole moments constrained within the interphase region. The opposite is true at higher nanofiller loading as the interface regions overlap to form conductive paths. Hence at higher nanofiller loading level the nanodielectrics have poor dielectric properties compared to conventional insulation.

2.2.3 The Interphase Volume Model [18]

The Interphase Volume Model is also based on the multi-core model and it was proposed in 2006 by Raetzke et al. [18]. The assumptions made in this model are that the thickness of the interface region is uniform, the nanoparticles have the same diameter and the nanoparticles are well distributed and dispersed within the host insulation. Mathematical equations were developed to approximate the interphase volume for three scenarios of nanofiller content. First scenario is when interphases of neighbouring particles do not overlap and nanofiller content is low and the interphase volume (P_i) is defined by equation 1. The second scenario is when the interphases of neighbouring particles slightly overlap, and interphase volume can be defined by equation 2. The third scenario is at higher nanofiller concentration where the interphases of neighbouring particles are extremely overlapping, and interphase volume can be defined by equation 3. In reality the volume of the interface is not constant as it is influenced by the nanofiller loading, particle size, and type of nanoparticle and host matrix. The maximum interface volume is found at the optimal nanofiller loading and once this point is reached then the nanoparticles cease to enhance the properties of nanocomposite. This model is consistent with many findings in the literature as the nanodielectrics give best performance at the optimal nanofiller loading level.

$$P_i = p.\left[\left(1 + {}^{2i}/_{d}\right)^3 - 1\right] \tag{1}$$

$$P_i = p.\left[\left(1 + {}^{2i}/_{d}\right)^3 - 1 - 8\left(\frac{1}{2} + \frac{i}{d} - \frac{\sqrt{3}a_0}{4d}\right)^2.\left(2 + \frac{4i}{d} + \frac{\sqrt{3}a_0}{2d}\right)\right] \tag{2}$$

$$P_i = 1 - p \tag{3}$$

Where:

p is nanofiller content.

i is a constant interface thickness.

d is the diameter of all nanoparticles.

a_0 is the distance between the centres of neighbouring particles.

2.2.4 Polymer chain alignment Model [19]

In 2011 Andritsch [19] proposed a polymer chain alignment model which integrates the multi-core layered, the intensity, the interphase volume and the double layer models. The model explains how the surface modification of the nanoparticle increases the interaction between the nanoparticle and host insulation. The polymer chains become aligned when the nanoparticle is surface modified as demonstrated in Figure 2.2. The model states that the interface is influenced by the physical properties of the nanoparticle (size and shape), type of nanoparticle and type of coupling agent used to modify the surface of nanoparticle.

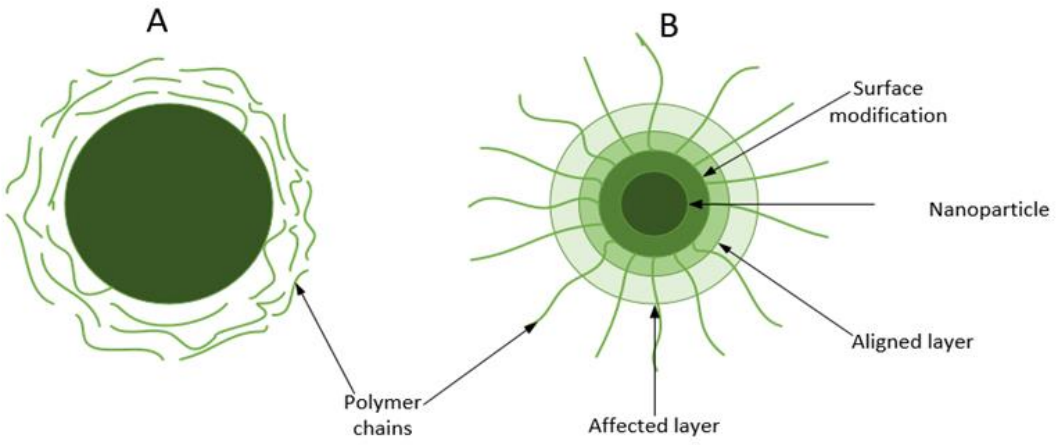


Figure 2.2 The polymer chain alignment model (a) the particle which is not surface modified and (b) a surface modified particle adapted from [19].

Even though these models explain what might cause enhancement in nanodielectric, there are still many experimentally established phenomena of the nanodielectrics which are still yet to be understood [14]. Some of these models will be used in the subsequent chapters to explain the obtained results in the present work. The models discuss the interaction between host insulation and nanofillers. The next section presents the different types nanofillers that are commonly investigated in the literature.

2.3 A literature review of nanofillers

The properties of nanocomposites are influenced by the type, geometry and size of the nanoparticle fillers. The smaller the nanoparticle size the more enhancement in the properties of nanocomposite [7].The nanofillers are classified according to their dimensions (one, two and three dimension) as illustrated in Figure 2.3 [20]. One-dimension nanofillers are defined as having a dimension of less than 100 nm and are of geometries of platelets, nanosheet and nanodisc. The two-dimension nanofillers have two dimensions which are less than 100 nm and have a geometry of tubes, fibers and filament [20]. Three-dimension nanofillers are spherical and cubical in geometry and are termed nanospheres, and this includes nanocrystals [20]. The shape of the nanoparticles should not allow local electric field reinforcement within the host insulation [7]. The selection of nanoparticles for the nanocomposite insulation depends on the desired electrical, thermal and mechanical properties [2] [7].The nanofillers can be classified into two categories which are organic and inorganic. This section presents literature review of inorganic and organic nanofillers in nanodielectrics.

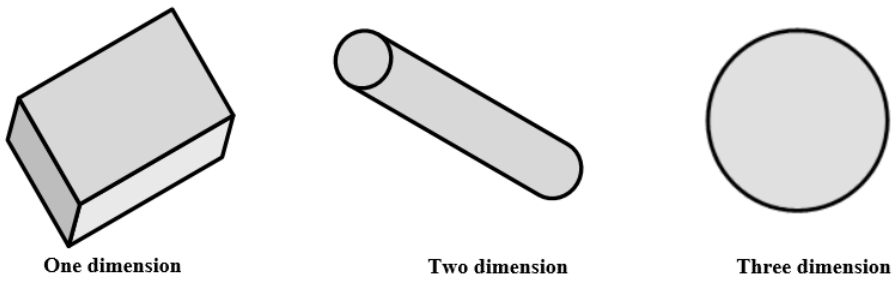


Figure 2.3: Nanoparticles with different dimensions

2.3.1 Inorganic nanofillers

The properties of commonly investigated inorganic nanoparticles are summarised in Table 2.1. When selecting a nanoparticle, it is desired that the nanoparticle enhances the host dielectric characteristics such as good space charge performance, high breakdown strength, resistance to electrical treeing induced degradation, good thermal and mechanical properties, among other important insulation properties at optimal nanofiller loading. Inorganic nanofillers have been reported in the literature to improve breakdown strength, space charge performance, partial discharge and electrical treeing resistance and thermal stability of the conventional polymer. The literature review of electrical trees in nanodielectric with inorganic nanofiller is discussed in detail in chapter 5.

Table 2.1:The characteristics of commonly investigated nanoparticles in the literature

Nanoparticles	**Properties**
Silicon Dioxide (SiO_2)	Has high breakdown strength, resistance to electrical treeing and poor thermal properties.
Titanium oxide (TiO_2)	Has high breakdown strength and good mechanical properties. The manufacturing process is long.
Alumina (AlO_3)	It has high breakdown strength and good thermal properties
Strotium titanate ($SrTiO_3$)	Has excellent thermal properties
Magnesium oxide (MgO_2)	Has good space charge performance, thermal properties, resistance to electrical treeing as well to Partial Discharge (PD) surface erosion
Boron nitride (BN)	Has excellent thermal properties
Zinc oxide (ZnO)	Has non-linear characteristics and good space charge performance
Silicon carbide	Has good thermal properties and high resistance to PD surface erosion but has high dielectric constant.

An insulation material with high breakdown strength is desired in the electric power industry. The AC, DC and impulse voltage breakdown strengths are enhanced at lower nanofiller loading of 0.5 wt% for silica and alumina nanoparticles in low density polyethylene (LDPE) [21] [22]. The DC breakdown strength of Alumina/LDPE nanodielectric is greater than that Silica/LDPE nanodielectric at 0.5 wt% nanofiller concentration by 18%. Hollow silica nanospheres can enhance DC breakdown strength of silicon rubber by 95% at 5 wt% nanofiller concentration [23]. The hollow silica nanospheres can enhance DC breakdown strength of nanocomposites better than solid silica nanospheres at 5 wt% nanofiller and it is speculated that the remarkable improvement caused by hollow silica nanoparticle is due to the hollowness structure of the nanoparticles which strengthen interface region between the nanoparticles and host material [23] . The better performance of hollow silica nanoparticles compared to the solid further inspired the present research work to investigate whether hollow carbon nanospheres would also give better performance than that of the solid nanospheres. The breakdown strength of nanodielectrics with solid nanospheres is poor at high nanofiller loading levels because interfacial areas overlap at high nano-filler loadings resulting in the formation of conductive paths [21] [22]. The dispersion of nanoparticles and space charge distribution play an important role in determining the breakdown strength of nanodielectrics [24]. There is still insufficient knowledge on the mechanisms that explain breakdown performance under DC, AC and impulse voltage in nanodielectrics.

Magnesia, titanium oxide and zinc oxide nanoparticles increase space charge suppression in conventional polymers [25] [26] [27]. The relationship between space charge suppression and nanofiller loading level is linear for magnesia and titanium oxide nanoparticles and non-linear

for zinc oxide nanoparticles. The mechanism of space charge suppression in nanodielectric can be explained using Tanaka's multi-core model. According to Zhou et al [26] the nanoparticles introduce many shallow traps which substitute the normal deep traps in the polymeric matrix. Traps are defined as defects or impurities, dangling bonds and surface states which function as trap sites for positive or negative charges. The difference between the deep and shallow traps is that the shallow traps are at the edges of conduction and valence band whereas the deep traps are close to the middle of the band gap. The band diagram of insulators is shown in Figure 2.4 in comparison to that of semiconductors and conductors. In nanocomposites the shallow traps are located at the third layer in the interaction zone, and the deep traps are in the first and second layers of the interaction zone. The third layer has a big volume compared to the second layer thus the shallow traps will become prevalent in the nanocomposites. This will result into high charge carrier mobility and therefore the space charge retention will be suppressed. As the concentration of nano-filler content increases, the number of deep traps decreases, and the number of shallow traps increases [26] . The trapped charges will produce their own electric field which will oppose the applied electric field and this leads to suppression of electric charge injection from the electrodes [28].

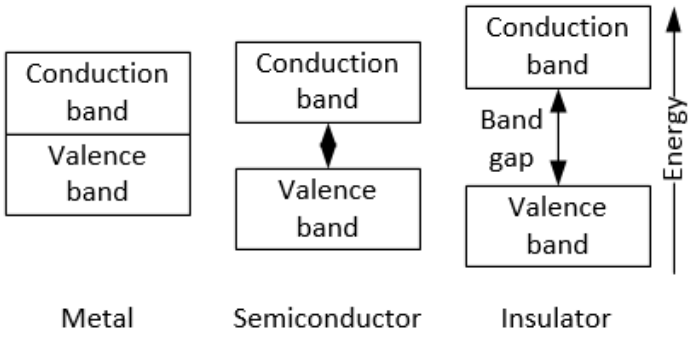


Figure 2.4:Band diagram of the conductor, semiconductor and insulator.

At low nanofiller loading, nanodielectrics incorporated with silica, alumina, aluminium nitride, magnesia and boron nitride nanofillers have low values of real permittivity and conductivity compared to the unfilled polymer matrix [29]. The values of permittivity and conductivity increase with the nanofiller content. Thermal ageing is the deterioration of the insulator over time caused by temperature. Temperature is very critical as it influences electrical, chemical, thermal and mechanical properties of the insulation. Zhang et al [30] found that Strontium titanate nanoparticles increase the thermal conductivity of epoxy by 200% at 40 wt% nanofiller concentration.

When the nanoparticles improve the breakdown strength, resistance to electrical treeing and permittivity of nanocomposites, it does not imply that they can reduce the partial discharge surface degradation of the insulation material [31]. Hence it is important to conduct the partial discharge surface erosion on nanocomposites material. Titania, silica, silica carbide and magnesia nanoparticles reduce surface erosion depth and roughness of epoxy, low density polyethylene and polyamide [7] [32] [33] [34] [35]. It can be deduced from the above discussion that breakdown strength, space charge performance and dielectric properties of nanocomposites with solid inorganic nanospheres are enhanced at lower nanofiller loading levels while thermal properties are enhanced at higher nanofiller loading. Nanocomposites with magnesia nanoparticles have been reported to possess good breakdown strength, space charge characteristics, partial discharge and electrical treeing resistance.

2.3.2 Organic nanofillers

The are several types of carbon-based nanoparticles such as fullerenes, carbon nanotubes, graphite, carbon nanospheres (solid and hollow), carbon nanohorns, carbon onions, carbon nanodiamonds. Various applications in the industry are summarised in Table 2.2. In nanodielectrics applications, carbon-based nanofillers are attractive because they have been found to have high electron affinity. The discovery of fullerene in 1985 caused some researchers to focus on carbon nanospheres [36]. The carbon nanospheres are made up of carbon layers (carbon chains) which are either parallel or perpendicular to the core. The physical and chemical properties of carbon nanospheres are dependent on the arrangement of carbon layer [36]. The organic nanofillers received much interest in mechanical properties applications, electromagnetic shielding application and other applications where electrical conductivity is required as shown in Table 2.2. Gustafsson et al [8] discovered that carbon black fillers reduce the space charge accumulation in crosslinked polyethylene (XLPE) but compromise the DC breakdown strength of XLPE at 1 wt% nanofiller concentration. Carbon nanofillers such as fullerenes, solid carbon nanospheres and graphene were used and found to give nanocomposites with exceptionally improved electrical tree resistance at a low nanofiller range of 0.1-0.2 wt% [9] [10] [11]. Zhang et al [37] investigated long and short multi-walled carbon nanotubes in epoxy resin and found that they improved thermal conductivity of epoxy by 16% and 26% respectively at a nanofiller concentration of 0.5 wt%. At 5 wt% nanofiller loading of the carbon nanospheres increased the tensile strength of thermoplastic polyurethane(TPU) by 43.9% but decreased the breakdown strength of TPU from 25 kV/mm to 6.3 kV/mm [38]. Gao et al [39] investigated the effect of chemical functionalization on multi-

walled carbon nanotubes (MWCNTs) in silicon resin at 0.1 wt% nanofiller content and found that MWCNTs and functionalized MWCNTs increase the tensile strength of silicon resin by 9% and 127% respectively. From the literature it can be deduced that most carbon-based nanofillers improve the electrical properties of conventional insulation at relatively low nanofiller loading levels. The carbon-based nanofillers at a specific nanofiller content can improve either space charge suppression or tensile strength of polymer while compromising its DC breakdown strength. The promising results of carbon nanospheres inspired conception of the present research work of further investigating the properties of carbon nanospheres in epoxy but the particles being hollow instead of solid.

Table 2.2: Different types of carbon fillers with their applications [36] [40] [41].

Nanoparticle type	**Fields of application**	**Elemental carbon content**
Carbon black	Manufacturing ink, makeup products, paints, coating and plastic, automotive accessories (e.g. tires, tubes), chemical industries	>97%
Fullerene	Photovoltaics, materials science, optics, water treatment and biological applications	99.9%
Carbon nanotubes	Car parts, tex-tiles to applications in electronics, polymer thermo-plastics, sporting goods, coatings, composites, and adhesives	60-97%
Graphene nanomaterials	Microchip components, conducting polymers, transport barriers, battery electrodes, supercapacitors, structural composites, printable inks, antibacterial, papers and biomedical technologies	>95%)
Carbon nanospheres (solid and hollow)	Water purification, energy storage, catalysis and biomedical application	Not found

2.4 Some challenges in the nanodielectrics technology

There is a problem of agglomeration of nanoparticles when fabricating nanocomposites materials. As a possible mitigation, coupling agents are used to achieve good dispersion of nanoparticles within polymer matrix. The coupling agents improve the compatibility between the nanoparticles and polymer matrix by increasing adhesion forces between the nanoparticle and host matrix and reduce the cohesion between the nanoparticles [7]. It is a challenge to ensure optimal nanofiller loading level for optimal dispersion and distribution when manufacturing nanodielectrics efficiently. The manufacturing techniques that can monitor and characterise dispersion quality in real time are required [42]. Currently a trial and error method is widely used to determine an optimal nanofiller loading where nanocomposites with different

nanofiller loadings are manufactured and characterized. The characterization results are then used to deduce which nanofiller loading is optimal. This is a time-consuming iterative process and is wasteful. Rheology was used in the work by Hank [10] to determine the optimal nanofiller concentration and dispersion. In this method, the rheology properties of nanodielectrics while in liquid state at different nanofiller concentration are measured. Then the rheological properties are then used to determine the best nanofiller loading level before complete manufacture and conducting electrical characterization tests. The rheological properties were correlated with the electrical tree test results and it was found that at optimal nanofiller loading for electrical tree resistance, the viscosity values were low compared to conventional polymer and other investigated nanofiller loading level. This technique is still at infancy stage because it is not yet applied on different types of nanoparticles and polymers to observe whether the findings will be consistent. Therefore, it cannot be used with confidence to determine the optimal nanofiller loading for electrical tree resistance. More research work is required to expand the concept of rheology analysis in nanodielectrics development. It is widely reported that the improvement of properties in nanodielectrics is attributed to an increased interface region between the nanoparticle and host insulation. There are models proposed to explain the interface region as presented earlier. But it is still vague on how the interfacial area controls the properties of nanocomposites. If this phenomena could be understood, it will become easy to tailor the nanodielectric to give specific desired properties. Comparing the literature on inorganic based nanodielectrics versus those of organic nanofillers, it is evident that the latter is less extensively investigated than the former. There is still need for more research on nanodielectrics with organic filler in order to comprehend how they improve conventional insulation, and this is the subject of the present research.

2.5 Chapter Conclusion

This chapter has presented the literature review of nanodielectrics. The electrical, thermal and mechanical properties, and mechanisms associated with properties in nanocomposites were discussed. The properties of nanocomposites are affected by the type of nanoparticle, physical properties of nanoparticles, nanofiller content and techniques used to manufacture nanocomposites material. In essence, for the particle type and host insulation at optimal loading level for electrical tree endurance is not necessarily the same for dielectric strength (DC and AC) and also not optimal for PD surface degradation. Even though there are many unsolved problems in nanodielectrics, with the direction that the research is heading the nanodielectrics are promising to be the next generation of insulation material.

In the present work, hollow carbon nanospheres are chosen as nanofillers and the next chapter presents a template method used to synthesise hollow carbon spheres followed by characterisation techniques and test results of the obtained nanoparticles.

Chapter 3: The synthesis and characterization of the Mesoporous Hollow Carbon Nanospheres (HCNs)

3.1 Introduction

The properties of nanodielectrics are significantly influenced by the type, size and shape of the nanoparticles [2] [7]. The nanoparticles are chosen based on the desired electrical, thermal and mechanical characteristics for the resultant nanocomposite material. In the literature it was found that organic nanofillers like fullerenes, carbon black, solid carbon nanospheres and graphene give nanocomposites with extraordinary properties compared to conventional insulation and some of the nanocomposites with inorganic nanofillers [8] [9] [10] [11]. The research of carbon-based nanofillers in nanodielectrics has gained momentum as a result of these findings. It is speculated that the good properties of nanodielectrics with carbon-based nanofillers is mainly attributed to the electron scavenging properties of carbon. The present research work investigates whether this hypothesis is true or not by studying an epoxy based nanodielectric with hollow carbon nanospheres. Hollow carbon nanospheres (HCNs) have profound properties which are high surface area, high mechanical strength, high capacitance, good thermal stability, low density and low electrical conductivity [36] [43] . Furthermore, the mesoporosity and hollowness of HCNs will open up the possibilities of further enhancing the electron scavenging properties of carbon by encapsulating an electronegative material inside the carbon shell. Some other application where HCNs have been used include water purification, energy storage, catalysis and biomedical application [43]. To the author's knowledge the use of HCNs as nanofillers in nanocomposites for high voltage applications has not yet been explored.

This chapter presents how the HCNs were synthesised and characterised. The HCNs were manufactured by the author assisted by Ms Magubane under the supervision of Prof Coville at Wits School of Chemistry. The structure of this chapter is as follows: Section 3.2 discusses the template method used to synthesize HCNs. In the present work two types of templates which are silica and polystyrene nanoparticles were explored. The synthesized HCNs were characterised using scanning electron microscopy (SEM), transmission electron microscopy (TEM), Branauer Emmett-Teller (BET), Raman spectroscopy and thermogravimetric analysis techniques. The characterization techniques and results are presented in section 3.3 and 3.4 respectively.

3.2 The template method of Hollow Carbon Nanospheres (HCNs) synthesis

The template method is commonly used to synthesize HCNs and it comprises of three main sequence of steps as follows:

1. Synthesis of the template nanoparticles (e.g. silica, polystyrene, micelle and metallic spheres). The template nanoparticles should be spherical in shape.
2. Coating the template nanoparticles with a carbon material to form a carbon shell (coating) around the template.
3. Removal of the template material to remain with the HCNs. Carbonization and etching process are commonly used to remove the template depending on the chemical nature of the template.

Another method to synthesize HCNs is by forming hollow carbon nanosphere bubbles in liquid state and then graphitising the carbon bubbles to get HCNs. This method is called template-free method and the method is rarely used as it is still under development [43]. This section presents the template method in detail using two types of templates which are silica and polystyrene nanoparticles. The challenge is that HCNs are synthesised in minute quantities which meant that relatively long time was required to manufacture the required quantities of the nanoparticles.

3.2.1 Template method of synthesising HCNs using silica nanoparticles as prototype

Figure 3.1 shows the overview of the template method using silica nanoparticles as a template. Each stage in the process is described in detail in the following subsections.

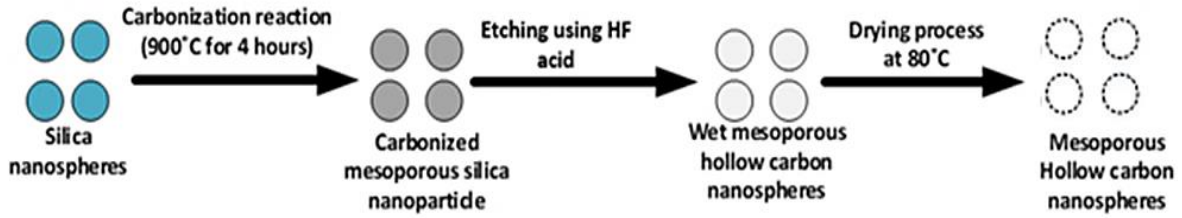


Figure 3.1: A schematic overview of the template method using silica nanoparticles.

3.2.1.1 Synthesis of mesoporous silica nanoparticles

The mesoporous silica nanospheres are made using a modified Stober method and the methodology is shown in Figure 3.2 [44] [45]. The purpose of washing the resultant solids and calcination is to remove unreacted precursors.

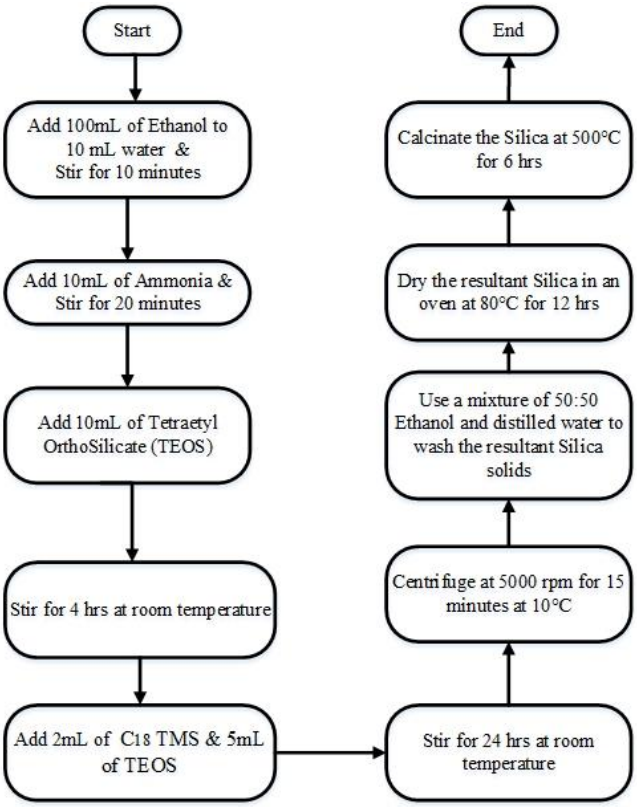


Figure 3.2: The modified Stober method used to make the silica nanoparticles

3.2.1.2 The carbonization process

Carbonization reaction is a process of converting the precursor into a carbon-based material [46]. There are different methods used to coat the template nanoparticles which are chemical vapour deposition (CVD), arc discharge, and laser ablation autoclave [36]. A horizontal chemical vapour deposition setup shown in Figure 3.3 was used in the present research work to coat the silica nanoparticles with carbon material as it is the most convenient technique. A pinch of 0.4 g of mesoporous silica nanoparticles is placed in a quartz boat which is then placed at the centre of a quartz tube. The quartz tube is then placed in a furnace. A volatile toluene solution is used as carbon source. Argon gas is used as the carrier to transport the toluene from the toluene bubbler into the furnace at a flow rate of 90ml/minute. The furnace is then ramped up to 900℃ at a rate of 10℃/minute and carbonation reaction is carried out at 900℃ for 4 hours. The carbonized silica nanospheres are then etched with 5% of hydrofluoric acid at room temperature for 12 hours to get wet HCNs. The wet HCNs are then dried in an oven for 12 hours at 80℃ to leave behind the HCNs nanoparticles. The chemical and physical properties of the synthesized HCNs are presented in the following subsection.

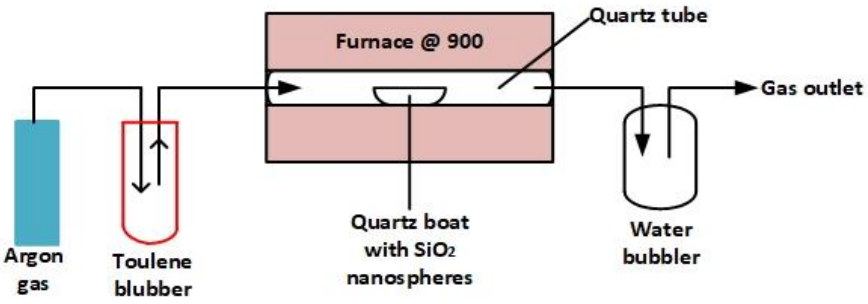


Figure 3.3: A horizontal chemical vapour deposition setup used for carbonization process adapted from [45].

3.2.1.3 The characterisation results of the HCNs that were synthesized using silica templates

A quantity of 10 g of carbonized silica nanoparticles were etched using hydrofluoric acid to yield 3.6 g of HCNs. The TEM and SEM images of HCNs are shown in Figure 3.4 and 3.6. The HCNs have an average diameter of 600±60 nm as shown in Figure 3.5 and a shell thickness of 40±10 nm. The SEM results revealed that most HCNs were broken as shown in Figure 3.4b. An Energy-Dispersive X-ray spectroscopy (EDS) analysis was done in an area labelled spectrum 1 on Figure 3.4c to confirm whether the silica was completely dissolved during the etching process. It was discovered that the HCNs still contained silica dioxide as shown on the EDS graph in Figure 3.7. The same was further confirmed by TEM images which showed that there were some HCNs with the silica template inside as shown in Figure 3.6c and Figure 3.6d.

The overall results therefore showed that the silica nanoparticles did not completely dissolve during the etching process. Hence the synthesized HCNs could not be used further to fabricate HCNs/Epoxy nanocomposite as they were deemed of poor quality. The silica template method did not work because the silica nanoparticles were not pounded before carbonization process to reduce the agglomeration of silica nanoparticles. This resulted into silica nanoparticles not being individual and therefore not coated properly. Furthermore, the mixture of carbonized silica nanoparticles and hydrofluoric acid was stirred for 12 hours during the etching process. Instead of debugging and perfecting the manufacturing technique the author decided to use polystyrene nanoparticles as a prototype instead. It was also an opportunity to avoid the usage of hydrofluoric acid during the etching process which is frequently a risky dangerous process. Furthermore, the process of synthesizing silica nanoparticles is lengthy compared the process of synthesizing polystyrene nanoparticles. The alternative method of synthesizing HCNs using polystyrene nanoparticles as a template which was subsequently adopted in the present research work is presented in the next subsection.

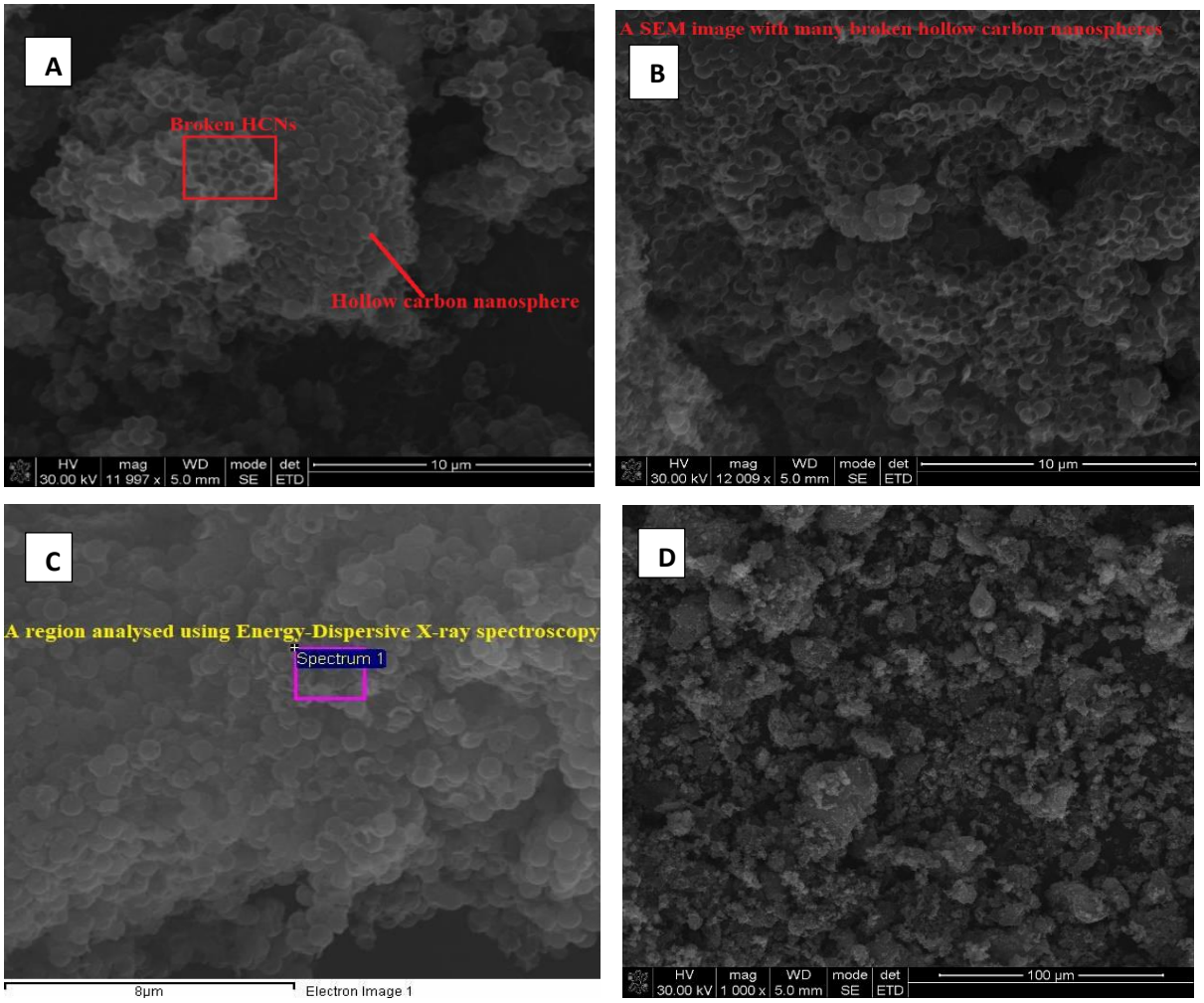


Figure 3.4: The SEM images of the synthesized HCNs using silica nanoparticles a template (a) SEM image of HCNs with few which are broken (b) A SEM image with many broken HCNs (c) A SEM image of HCNs with the region analysed using Energy-Dispersive X-ray spectroscopy (EDS) (d) Surface morphology of HCNs at high magnification.

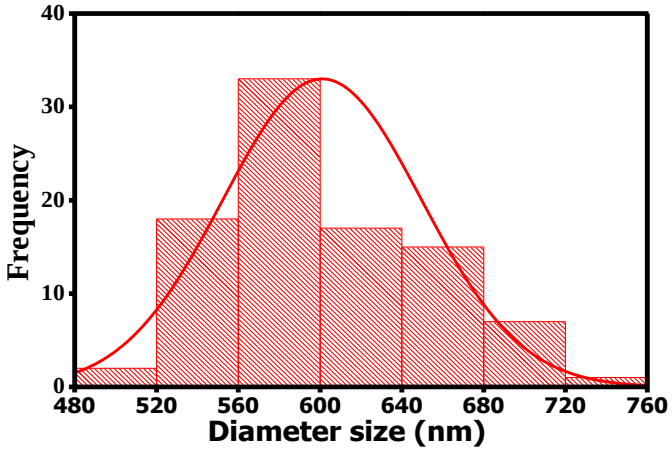


Figure 3.5: The particle size distribution of HCNs.

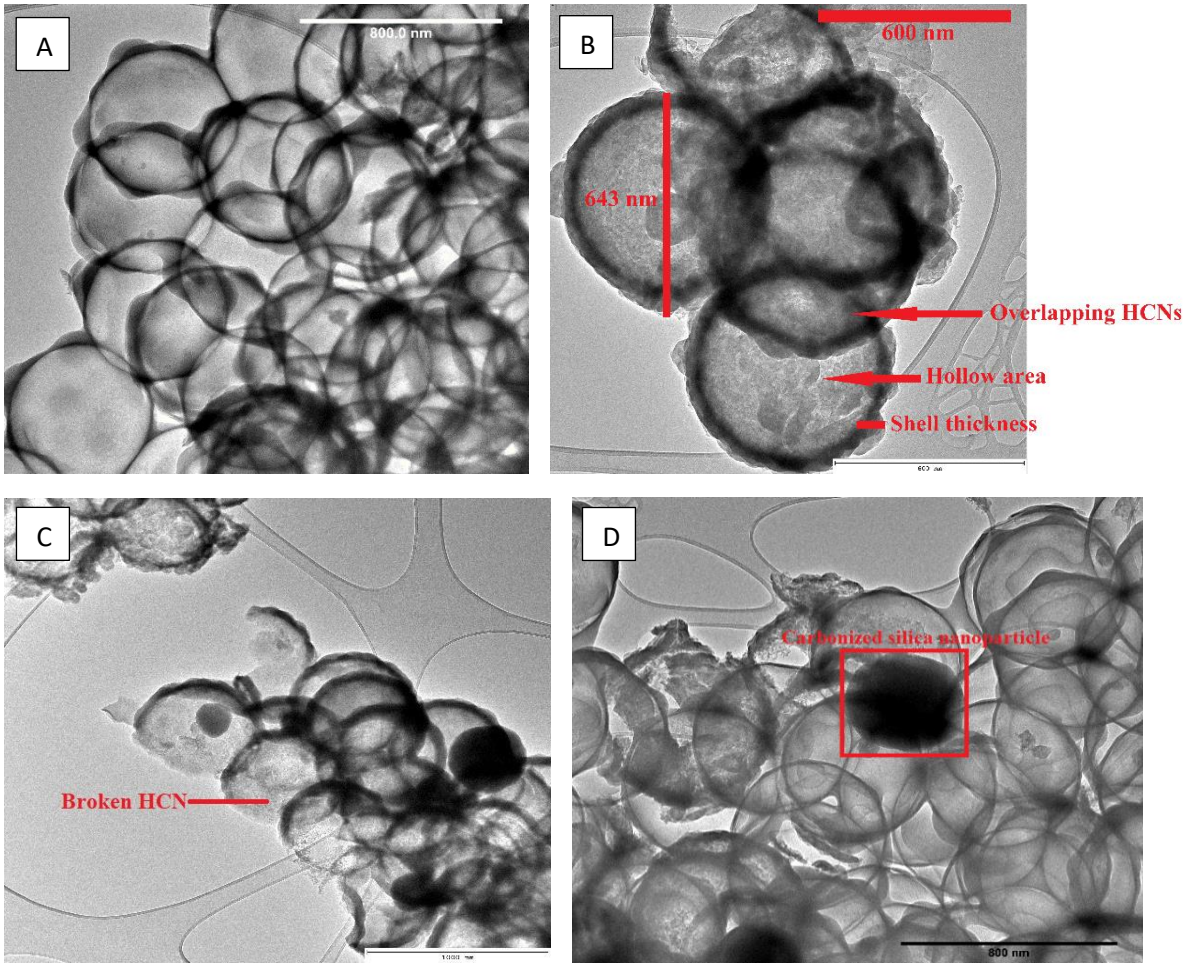


Figure 3.6: The TEM images of HCNs synthesized using silica a template

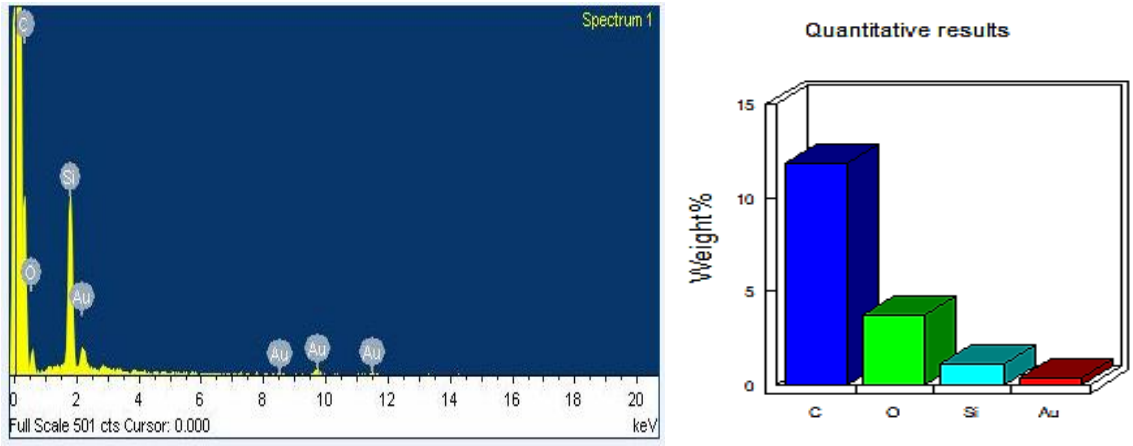


Figure 3.7: EDS result of the region labelled spectrum 1 in Figure 3.4c

3.2.2 Template method of HCNs synthesis using polystyrene nanoparticles as template

This subsection presents the polystyrene nanoparticle template method of synthesising HCNs. In summary the method involves synthesizing polystyrene nanoparticles first and then coating the particles using resorcinol-formaldehyde (RF) polymer to form a carbon shell around the

polystyrene nanoparticles. The polystyrene nanoparticles are then decomposed at 350℃ to leave behind the required HCNs.

3.2.2.1 Synthesizing the polystyrene template nanoparticles

A mixture of 16 mL of styrene and 0.2 g of polyvinyl pyrrolidone is added into a solution of 200 mL ethanol and 50 mL of distilled water and the resultant mixture is stirred for 10 minutes. As the first mixture is getting ready, another solution is made of 0.3 g of potassium persulfate is dissolved in 20 mL of distilled water. The two solutions are mixed, and the resultant mixture is refluxed at 80℃ for 24 hours as shown on Figure 3.8a. The mixture is then centrifuged at 15000 rpm for 15 minutes and the resultant solids are washed three times with ethanol to give wet polystyrene nanoparticles. The wet polystyrene nanoparticles are then dried at 60℃ for 3 hours in an oven.



Figure 3.8: Images of (a) the experimental setup used to reflux (b) a centrifuge

3.2.2.2 Coating of the polystyrene nanoparticles with resorcinol-formaldehyde (RF) polymer

The nanoparticles tend to agglomerate due to Van der Waals forces which cause the nanoparticles to attract each other. Hence polystyrene nanoparticles are dispersed in a solution of 1.5 ml ammonia and ethanol using a sonicator [47] [48]. While the resultant mixture undergoes sonication in a separate glass beaker, a 1.5 mL formaldehyde solution, 0.75 g of resorcinol, 1 g of hexadecyltrimethylammonium bromide and 50 mL of ethanol are mixed to form the resorcinol-formaldehyde (RF) polymer. The two mixtures are combined, and the resultant mixture is stirred at room temperature for 24 hours to initiate a reaction. The resultant mixture is refluxed at 100℃ for 24 hours. The solution is then filtered to give the solids which are then washed with distilled water to remove unreacted precursors. The solids would then be dried in an oven at 60℃ for 12 hours to give a polystyrene coated with resorcinol-formaldehyde polymer.

3.2.2.3 The carbonization reaction

The carbonization reaction is used to remove the polystyrene nanoparticles templates to give HCNs. A quantity of 0.5 g polystyrene coated with resorcinol-formaldehyde polymer is placed inside the quartz boat which is then placed at the centre of a quartz tube in the furnace as shown in Figure 3.9. Nitrogen gas is used as the carrier to transport the by-product gasses out of the quartz tube at a flow rate of 50 mL/minute. Figure 3.10 shows how the furnace temperature is ramped up to levels at which the polystyrene decomposes and temperatures where annealing of the carbon occurs. The annealing process is how carbon-carbon bond are formed to make a HCNs and any residual polystyrene is removed. It is notable that only 80 mg of HCNs are obtained at each run of the carbonization reaction which takes a total time of 7 hours. Therefore, in order to make adequate quantities required for the entire study in the present work, it required a total of 800 hours of laboratory time and that only for making the nanoparticles.

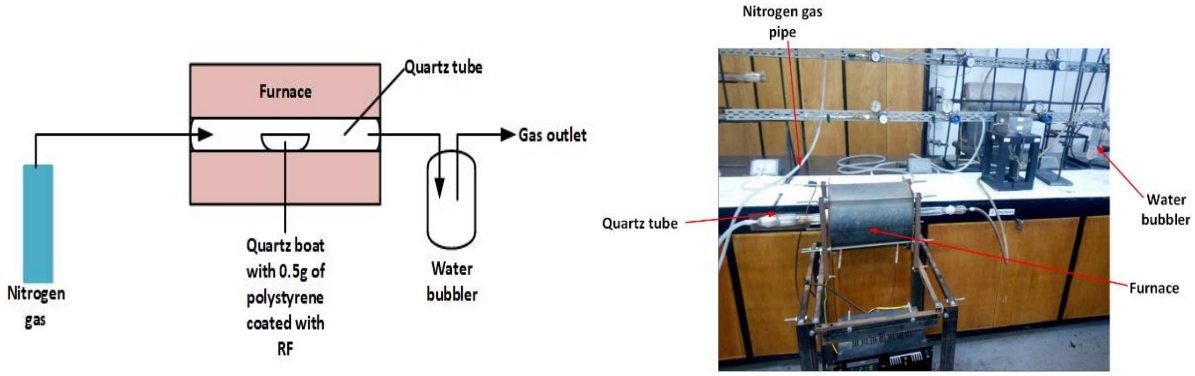


Figure 3.9: A schematic diagram and image of the setup used for carbon reaction

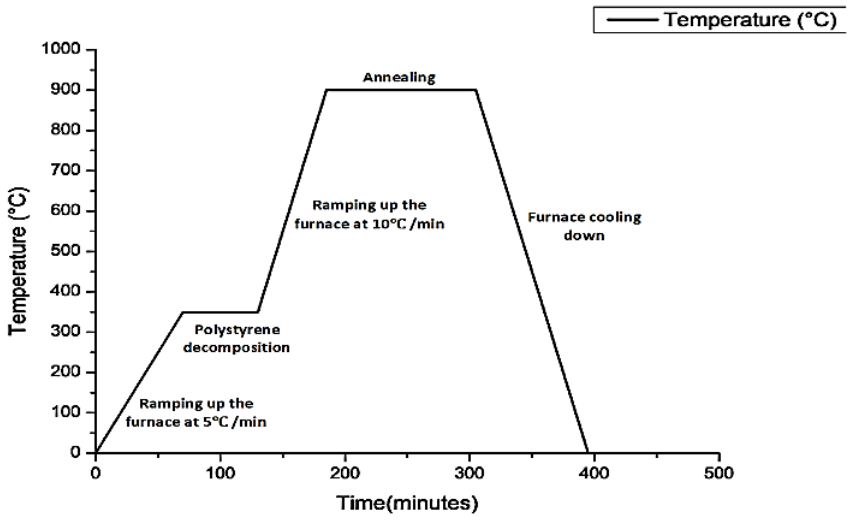


Figure 3.10: The temperature profile as function of time

After the nanoparticles have been synthesised the next stage is to verify the chemical composition and physical characteristics of the nanoparticles and this is the subject of the next section.

3.3 Characterization techniques of the nanoparticles

This section discusses the methods used to characterize the synthesized HCNs. The characterisation methods used are: Scanning Electron Microscopy (SEM), Transmission Electron Microscopy (TEM), Raman spectra, Branauer Emmett-Teller (BET), and thermogravimetric analysis techniques.

Scanning electron microscopy (SEM)

The FEI Nova nanolab 600 scanning electron microscopy determines the surface morphology and the diameter of the nanoparticles. For sample preparation the nanoparticles are uniformly dispersed on a carbon tape which is attached to an aluminium stab. The aluminium stab is then placed inside the vacuumed chamber of the SEM. The nanoparticles are then subjected to a beam of electrons and based on their interaction the detector will generate in image showing the details of the nanoparticles' surface [49].

Transmission electron microscopy (TEM)

Transmission electron microscopy is used to view the interior of the nanoparticles and confirm whether the manufactured nanoparticles are hollow or solid. TEM makes use of a beam of electrons to generate images of the tested sample. For sample preparation, a small quantity of nanoparticles is mixed with 3 ml of methanol in a small vase. The mixture is sonicated at room temperature for 15 minutes to disperse and distribute the nanoparticles within methanol solution. One drop of the mixture is placed on a copper grid and dried for few minutes. A dry copper grid is placed on the TEM holder which is inserted into the TEM chamber. A beam of electron is transmitted on the copper grid which contain the nanoparticles to generate a TEM image.

Branauer Emmett-Teller (BET)

BET is a characterisation technique used to measure the surface area and the pore size distribution of nanoparticles. An amount of 200 mg of the HCNs are placed in BET sample holder and degassed at 250 ºC in nitrogen gas for 4 hours. The BET method uses the nitrogen adsorption data to calculate the surface area and pore size distribution of the nanoparticles.

Thermogravimetric Analysis (TGA)

Thermogravimetric analysis (TGA) is a destructive characterization technique which measures mass loss of the nanoparticles as a function of temperature. The temperature of TGA analyser is increased from 36℃ to 900℃ at a rate of 10℃/minute [4]. A 10 mg of the test nanoparticles are placed on the sample pan inside the furnace of thermogravimetric analyser. The thermogravimetric analyser provides two curves which are thermogravimetric analyses and derivative thermogravimetric analyses (D-TGA) curves. The TGA curve gives information about the thermal stability of the sample and its sample composition. The D-TGA curves provide information about the rate of change of weight percentage loss with respect to temperature.

Raman spectroscopy

The Raman spectral analysis technique is used to characterise different structures of carbon materials and gives information about the molecular vibrations and crystal structure of the nanoparticles [23]. It quantifies the size, strength and arrangements of chemical bonds on the nanoparticles [36].

The obtained chemical and physical properties of synthesized HCNs using these characterisation techniques are provided in the next section.

3.4 Characterisation results of HCNs that were manufactured using polystyrene nanoparticles as templates

The SEM and TEM images of synthesized HCNs are shown in Figure 3.11 and 3.12. The HCNs have an average diameter of 410±70 nm as shown on Figure 3.13 and a shell thickness of 36±12 nm. Less than 5% of the nanoparticles were found broken in the analysed HCNs. From the TEM images in Figure 3.12 it can be observed that the surface of HCNs is uneven or not smooth because the nanoparticles are mesoporous. The synthesized HCNS have a BET surface area of 341.5 m^2/g (equivalent to about a third of a rugby field!) and a pore size of 2.5 nm. The results confirm that the HCNs have high surface area. It is evident from the microscopic pictures that there is agglomeration of HCNs nanoparticles, because of the Van der Waals forces of attraction between the nanoparticles.

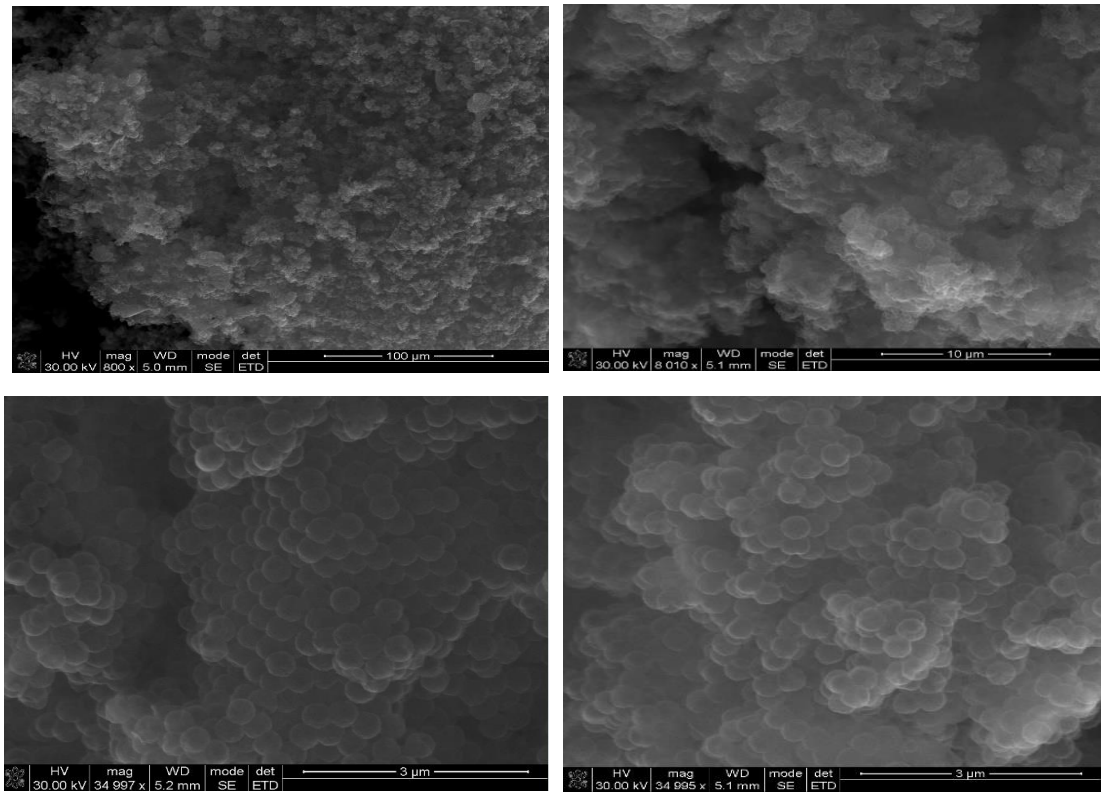


Figure 3.11: The SEM images showing the surface morphology of HCNs at different magnification

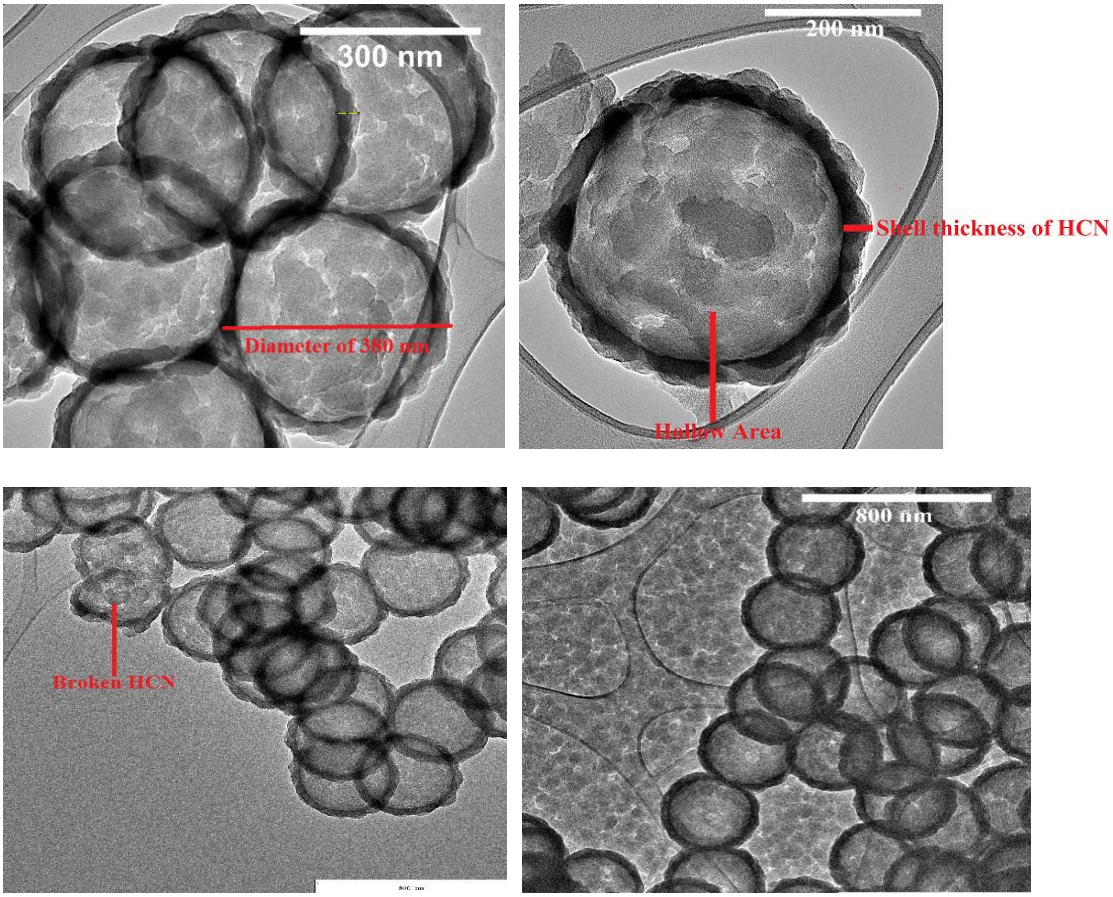


Figure 3.12: The TEM images of the HCNs manufactured using polystyrene nanoparticles as a template.

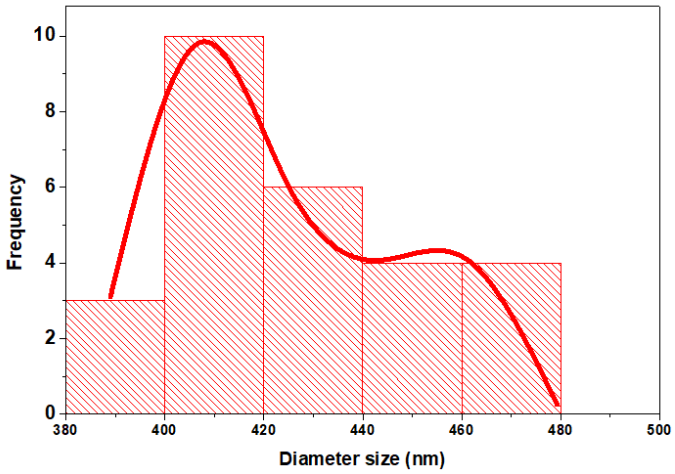


Figure 3.13: The particle size distribution of the synthesised hollow carbon nanospheres.

Figure 3.14 presents the TGA results of polystyrene nanoparticles and HCNs. Figure 3.14a shows that there is a 2% weight loss at 100-150℃ and this is attributed to moisture. The polystyrene nanoparticles start to decompose at 300℃ and the residual mass is zero at 430℃. The HCNs start to decompose at 500℃ as shown in Figure 3.14b and this confirms that all the polystyrene nanoparticles are decomposed during the carbonization process to give HCNs. The decomposition temperature of HCNs is above 450 °C which means that they have a graphitic type of carbon.

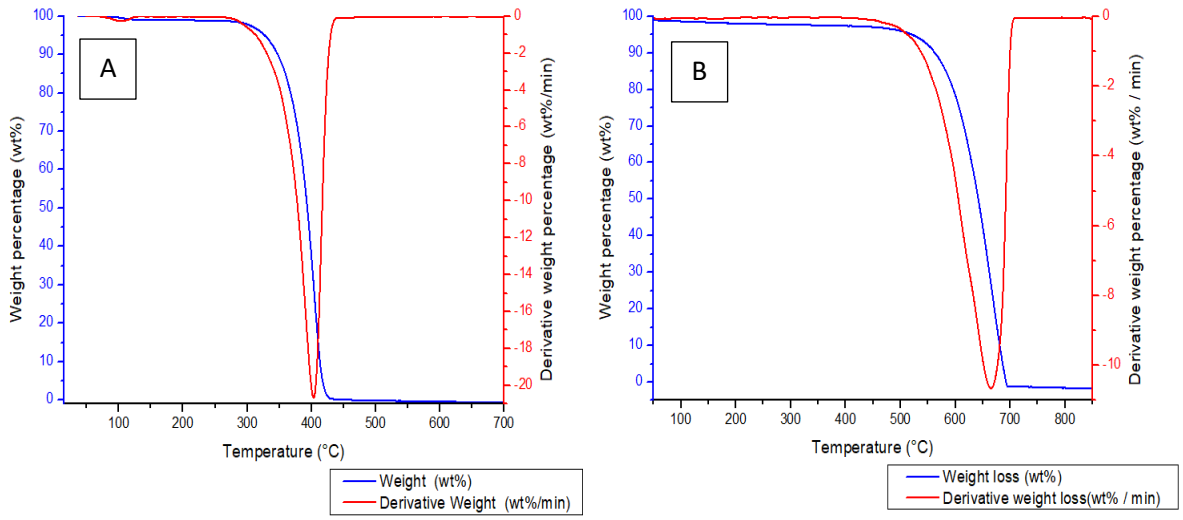


Figure 3.14:The TGA and D-TGA curves of (a) polystyrene nanoparticles (b) HCNs nanoparticles

There are two Raman bands detected which are D and G band at peak positions of 1350 cm^{-1} and 1597 cm^{-1} respectively as shown in Figure 3.15. The G band is attributed to the graphitic carbon material and D band is attributed to disordered carbon material [50]. The I_D/I_G (intensity of D peak to G peak) ratio is 0.98 as indicated on Raman spectroscopy results in Figure 3.15 and this means that the HCNs have a disordered carbon structure. The disordered

carbons comprise of sp^2 and sp^3 [50]. The HCNs have more sp^3 hybridized carbon than sp^2 carbon. Based on the obtained characterisation results these HCNs were deemed to be appropriate to be used in manufacturing nanocomposites with HCNs.

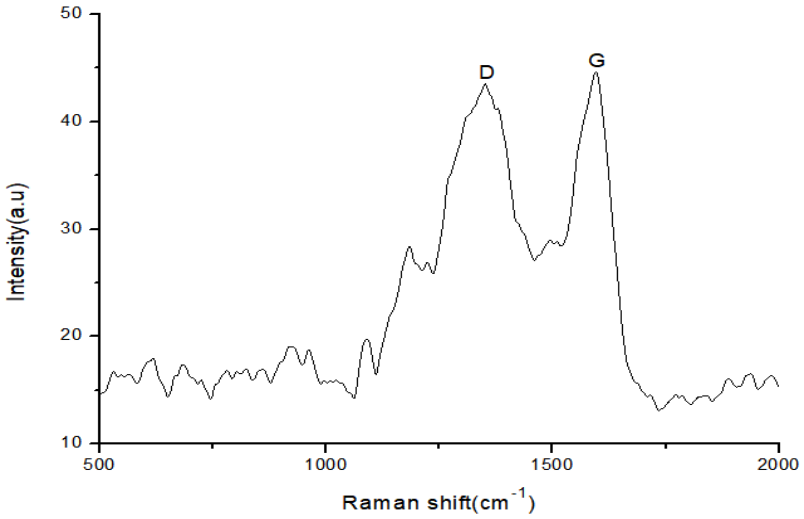


Figure 3.15: Raman spectroscopy results of the synthesised HCNs

3.5 Chapter Conclusion

This chapter has presented template methods of synthesising hollow carbon nanospheres using silica and polystyrene nanoparticles. The polystyrene template method was found to be simpler and more convenient method to synthesize HCNs. The polystyrene nanoparticles are easy to remove/decompose unlike silica nanoparticles which require hydrofluoric acid to decompose. The HCNs were characterised using five techniques namely SEM, TEM, BET, TGA and Raman spectroscopy. The synthesized HCNs have a diameter of 410±70 nm and a shell thickness of 36±12 nm. The BET technique confirms that the nanoparticles have a high surface area. From the microscopic images obtained it is evident that the HCNs nanoparticles are agglomerated. Silica template produce HCNs with bigger diameter size compared to polystyrene. The silica particle size can be reduced by modifying the reaction parameters in the Stober method in order to produce HCNs with smaller diameter [45]. The work of synthesizing HCNs is very critical in this study because properties of nanocomposites are greatly influenced by type and characteristics of the chosen nanofillers.

The synthesized HCNs were used to fabricate an epoxy nanocomposite with HCNs as presented in the next chapter.

Chapter 4: The fabrication of the nanocomposite material: a conventional process modified to include rheology analyses

4.1 Introduction and background to nanodielectric fabrication techniques

The manner at which the nanocomposite material is manufactured plays a critical role in determining the properties of the resultant nanodielectric. Ideally when fabricating nanocomposites, it is desired that the nanoparticles should be uniformly distributed and dispersed within the host insulation, and yet the nanoparticles have a tendency to agglomerate and become micro-sized cluster fillers [2]. The agglomeration of nanoparticles is caused by Van der Waals forces between the nanoparticles [36]. There is no improvement in nanodielectrics when the nanoparticles are agglomerated. The properties of nanocomposites are influenced by the method used to fabricate the nanocomposite and the nanofiller loading level. Especially with the conductive carbon nanofillers, the properties of the resultant nanocomposites can easily be poorer than those of the original unfilled polymer beyond the optimal nanofiller loading range and this was also reported by Hank [10]. Currently there are two methods to determine the optimal nanofiller loading level which are: the trial and error method and the use of rheology. For trial and error iterative method the nanocomposites with different nanofiller loadings are manufactured and characterized. The characterization results will then be used to deduce which nanofiller loading level is optimal. This method is time consuming and material wasteful.

Rheology is the study of flow and deformation of matter under the influence of exerted force [51] [52]. Rheology is commonly used in polymer processing, food processing, design of pumps and pipelines, mixing and agitation of dispersions and solutions, and manufacturing of cosmetic and pharmaceutical formulations [53]. For example the yoghurt manufacturing processes use rheology to make sure that the micro pieces of fruits are well dispersed and distributed within the yoghurt and the loading level of fruits is optimal, to avoid the fruits from sinking to the bottom or floating at the top [54]. Currently the polymer industries measure the rheological properties of suspensions and slurries which contain micro particles at high loading level. Viscosity describes the ability of the fluid to resist flow under the applied force (shear stress) and it is mathematically modelled using equation 1 [55]. The viscosity is directly

proportional to pressure and inversely proportional to temperature [55] [51]. The effect of temperature on viscosity is more dominant compared to pressure. There are two types of fluid behaviour which are Newtonian and non-Newtonian as shown in Figure 4.1. The shear stress of Newtonian fluids increases linearly with the shear rate and examples of Newtonian fluids are water, oil, honey and simple hydrocarbons [56] [55]. The non-Newtonian fluids behave contradictory to Newtonian fluids. There are two common types of non-Newtonian fluids which are shear thinning (pseudoplastic) and shear thickening (dilatant). Polymers are pseudoplastic in nature.

$$\eta = \frac{\sigma}{\gamma} \tag{1}$$

where: σ represents the applied force

γ represents the speed at which the fluid flows and it is called the shear rate

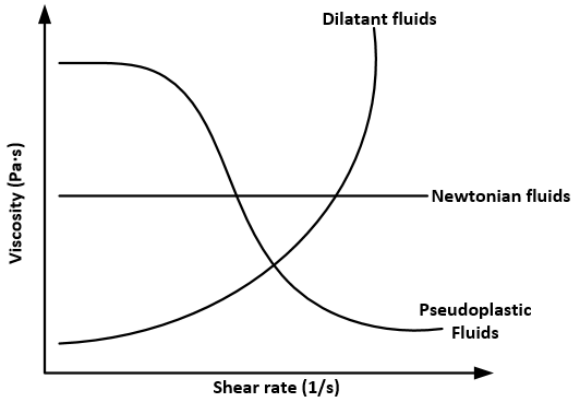


Figure 4.1: Ideal graphs of shear rate as a function of viscosity for Newtonian and non-Newtonian fluids adapted from [52].

Hank [10] investigated the rheological properties of the mixture of liquid araldite resin and nanoparticles in order to observe the correlation between rheological properties of mixture, nanofiller loading level and electrical tree resistance of epoxy nanocomposites with solid carbon nanospheres (SCNs) and boron nitrate (BN). It was found that at optimal nanofiller loading level of SCNs and BN nanoparticles for electrical tree resistance in epoxy, the araldite epoxy nanodielectrics have lower values of viscosity compared to unfilled araldite and other loading levels which were investigated. On the contrary Green et al [57] found that Silica/Epoxy nanodielectrics with 5 wt% nanofiller concentration have increased values of viscosity compared to an unfilled epoxy. The same nanofiller loading level of silica nanospheres prolonged the electrical tree inception voltage and time-to-failure of silicon rubber compared to unfilled silicone rubber and silicon rubber nanocomposites with 1 wt% and 3 wt% nanofiller concentrations [58]. Furthermore, an epoxy nanodielectric with functionalized

boehmite nanoparticles have high viscosity compared to unfilled epoxy and epoxy nanodielectric with unfunctionalized boehmite nanoparticles [57]. The compatibility between the nanoparticles and polymer matrix is very critical as it affects the performance of the resulted nanodielectric. Compatibility in nanodielectric can be enhanced by the functionalization of the nanofillers. Reading et al [59] used rheology to analyse the dispersion of silica microparticles within polyethylene and found out that the viscosity of microcomposite with silica microparticles increases with the nanofiller loading level.

Even though there is some work done in rheology of nanodielectrics it is still unknown on how the rheological properties of the nanodielectrics are related to the dispersion of nanofiller within the polymer matrix and the performance of the nanodielectric. The phenomenon of nanodielectrics rheological behaviour is not yet fully understood to such an extent that it can be used to find the optimal nanofiller loading level with confidence. Hence in the present work the rheological characteristics of araldite resin with solid carbon nanospheres (SCNs/Araldite mixture) and hollow carbon nanospheres (HCNs/Araldite mixture) at different nanofiller loading levels are studied. The epoxy used is of type Araldite® FR476D and hardener® and it is different from that one used by Hank [10] which was Araldite® CY231-1 CH and aradur® HY925 hardener.

There are five common techniques used in the literature to fabricate nanocomposites material which are: in-situ polymerization, intercalation, sol-gel, solution compound and direct mixing method. From these techniques one was chosen for use in the present research work. A flow chart of in-situ polymerization method is shown in Figure 4.2. The nanoparticles are dispersed within the monomer using a high shear force and the mixture is then polymerized using either radiation, heat or initiator diffusion [60] [61]. The in-situ polymerization technique can be used in a variety of host materials but it is not suitable for large scale production [62] . The nanoparticles do not bond properly with the host material and the polymer decomposes at high temperature [61] .

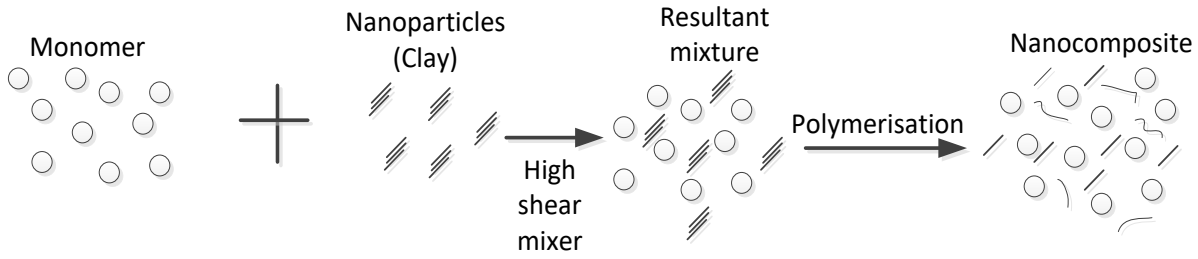


Figure 4.2: A flow diagram of in-situ polymerisation adapted from [60]

Intercalation is defined as a process of implanting or removing an atom or molecule into a layered material [63]. This method is used to fabricate nanocomposites that have layered nanofillers like layered silicates and clay nanoplates. The intercalation method is further divided into three types which are direct intercalation, melt intercalation and intercalation of monomer incorporated with in-situ polymerization [64]. Direct intercalation involves the usage of solvent to disperse and distribute the layered nanofillers in a polymer matrix. The resultant mixture of polymer, nanofiller and solvent is then mechanically mixed. The solvent will then be evaporated after dispersing and distributing the layer nanofillers within the polymer to form an intercalated nanocomposite. The melt intercalation method is commonly used in industrial scale productions [61]. The melt intercalation is like melt blend method, it involves high shear mixing of the polymer and nanofillers in a molten state at high temperature. After mixing, the resulted molten mixture undergoes either compression molding, injection molding or fiber production techniques to form the nanocomposite [61].

The other alternative fabrication method of nanocomposites is the Sol-gel method. This is a cost-effective technique used to synthesize ceramic and glass material at low temperatures [65]. The nanoparticles and the monomer solutions are the reactants which are converted into a colloidal solution which is also termed sol as shown in Figure 4.3. The colloidal solution is then gelled to form an interconnected network of polymers. A disadvantage of sol-gel method is that it is a lengthy process. The technique can disperse the nanoparticles much better compared to in-situ polymerization [62] .

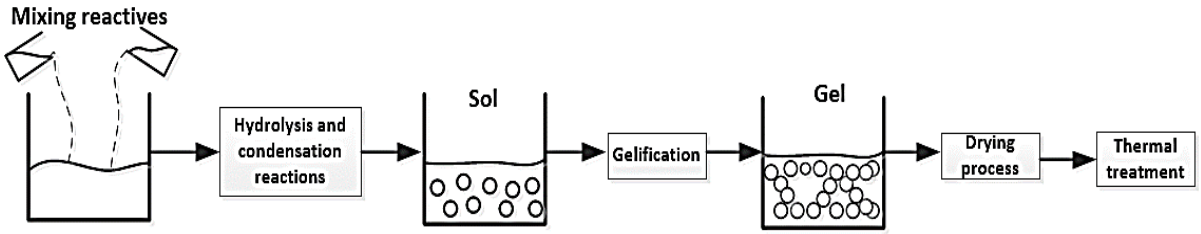


Figure 4.3: Sol-gel manufacturing method adapted from [65].

The melt blending technique of nanocomposite fabrication is similar to the melt intercalation method which is a direct mixing of nanoparticles and polymer matrix in a molten state during extrusion, molding and injection as shown in Figure 4.4 [7]. This technique is effective and cost efficient, but it cannot be used on thermosetting host matrix [62]. For solution compounding technique the nanoparticles are dispersed in a solvent and dissolved in polymer using sonication.

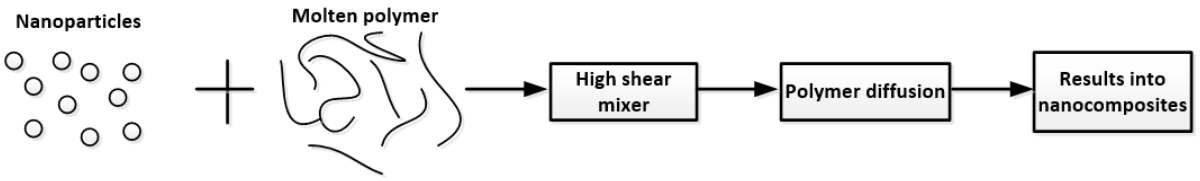


Figure 4.4: A melt blend method adapted from [2] [66].

In the direct mixing technique, the nanofillers and polymer matrix are mixed with or without the solvents at a temperature above that of glass transition temperature.

In the present research work, the choice was to use the direct dispersion method to fabricate the SCNs/Epoxy and HCNs/Epoxy nanocomposites. The direct dispersion method incorporated with rheology analyses are discussed in more detail in the next section. The rheological results are then presented and discussed in section 4.3. The conclusion is drawn out in section 4.4.

4.2 The fabrication of the HCNs/Epoxy and SCNs/Epoxy nanodielectrics using the direct dispersion method incorporating rheological analysis

The present research work uses direct dispersion technique incorporated with rheology analyses to fabricate SCNs/Epoxy and HCNs/Epoxy nanocomposite material as illustrated in Figure 4.5. The epoxy resin is of type Araldite® FR476D and hardener® obtained from Elite chemical industries (PTY) LTD ™. This epoxy is different from the one which was used by Hank [10] which is type Araldite® CY 231-1 CH and Aradur® HY 925 obtained from Huntsman™ . In the present work the hollow carbon nanospheres with an average diameter of 410±70 nm were synthesised as presented in the previous chapter. The solid carbon nanospheres with an average diameter of 165±31 nm were those leftover from Hank [10]'s work.

It is important to determine the best mixing time on the high shear mixer for the nanoparticles to be well dispersed and distributed within the epoxy. The high shear mixer shown in Figure 4.6a is used to disperse and distribute the nanoparticles within the epoxy monomer matrix. In the present work it is assumed that the high shear mixer reduces the agglomeration of nanoparticles. The aluminium moulds used to cast the epoxy nanodielectric are shown in Figure 4.6b. The rheological properties are measured before adding the hardener because the hardener causes the mixture to begin polymerising and harden (curing). A rheometer shown in Figure 4.7 is used to measure the rheological properties of unfilled araldite resin in comparison to SCNs/Araldite and HCNs/Araldite mixture in a liquid state. A measuring template (protocol)

from the previous work by Hank [10] was used and the measuring template on the rheometer consists of three phases which are as follows:

1. The mixture is sheared at a constant rate of $500s^{-1}$ for 30 seconds to remove the shearing history from the high shear mixer.
2. The mixture is left in the rest state for 30 seconds.
3. The viscosity and shear stress profiles are then measured at a linear shear rate from $0s^{-1}$ to $1500s^{-1}$.

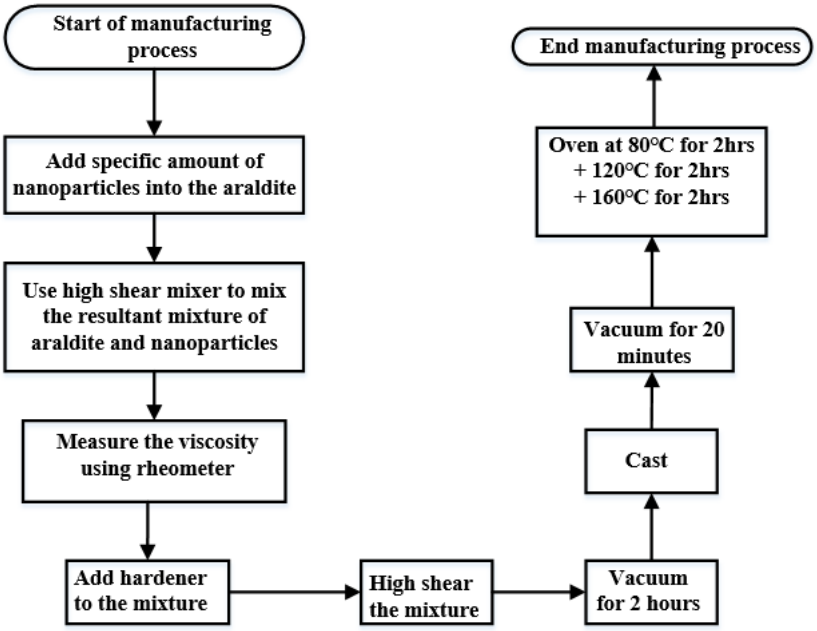


Figure 4.5: Direct mixing technique incorporated with rheology analyses used to fabricate the nanocomposite material adapted from Hank [10] .

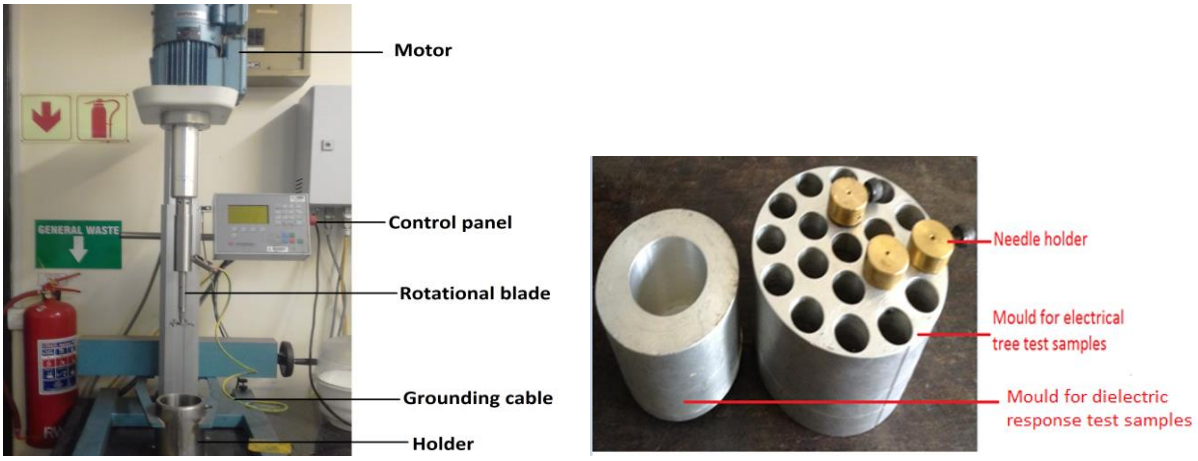


Figure 4.6: (a)A high shear mixer used to mix the mixture of araldite, hardener and nanoparticles (b) aluminium moulds used to cast the nanocomposite material.

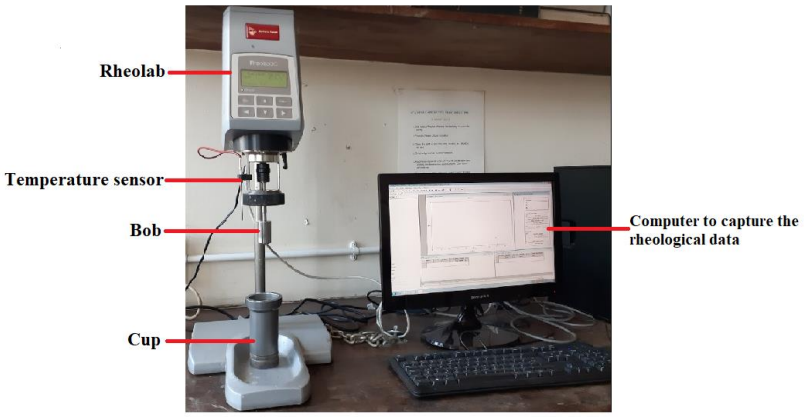


Figure 4.7: An image of the rheometer used to measure the rheological properties of a mixture of araldite with either SCNs or HCNs nanoparticles.

Firstly, the critical mixing time on the high shear mixer was determined using rheology analyses. A SCNs/Araldite mixture with the nanofiller loading level of 0.21 wt% was used to determine the critical mixing time on the high shear mixer. An araldite resin with 0.21 wt% nanofiller concentration of SCNs nanoparticles was mixed at different times of 10, 15 and 20 minutes on the shear mixer. The rheological properties were measured immediately after the high shear mixing process. The obtained rheological results would then be used to determine the best mixing time on the high shear mixer. The determined critical mixing time would then be the duration of the shear mixing process.

In the present work the rheological characteristics of SCNs/araldite mixture with different nanofiller loading levels of 0.05 wt%, 0.1 wt%, 0.15 wt%, 0.21 wt%, 0.35 wt% and 0.5 wt% were measured. Followed by the measurement of the rheological properties of HCNs/Araldite mixture at different nanofillers concentrations of 0.05 wt%, 0.1 wt%, 0.15 wt%, 0.21 wt% and 0.35 wt%. The obtained results of rheological properties are presented in the next section.

4.3 The rheological results of unfilled araldite (epoxy monomer), SCNs/Araldite and HCNs/Araldite mixture

The mixing time on the high shear mixer was varied for 10, 15 and 20 minutes using SCNs/Araldite mixture and the obtained results are shown in Figure 4.8. The critical mixing time was achieved at 15 minutes where the viscosity is low compared to 10 minutes mixing time. The viscosity values of 15 and 20 minutes mixing times are approximately the same. The obtained critical mixing time is greater than the one obtained by Hank [10] because the epoxy used in the present work has higher viscosity. The critical mixing time on the high shear mixer was validated using the electrical tree test to characterise the epoxy test samples which were

mixed for a period of 10 minutes and 15 minutes during the high shear mixing process in the nanocomposite fabrication. It was found that epoxy test samples with mixing time of 15 minutes had higher resistance to electrical treeing compared to epoxy test samples with a mixing time of 10 minutes. The electrical treeing results are presented in Table A1 in appendix A.

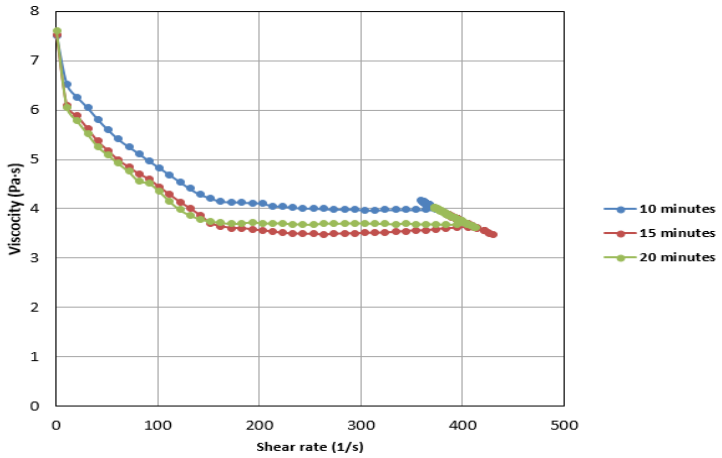


Figure 4.8: Viscosity profiles as a function of shear rate for SCNs/Araldite mixture with 0.21 wt% nanofiller concentration at different mixing times on the high shear mixer.

The temperature of the laboratory could not be controlled hence the viscosity profiles of araldite were measured on different days to observe how the temperature affected the viscosity profile of the unfilled araldite and the results are presented on Figure 4.9. The results show that the temperature significantly affects the viscosity magnitudes and profile of unfilled araldite. It was then decided to only compare the results which were measured on the same day where the room temperature change was insignificant instead of designing a temperature-controlled vessel on the rheometer. The results show that the araldite has a non-Newtonian behaviour and the viscosity decreases with an increasing shear rate.

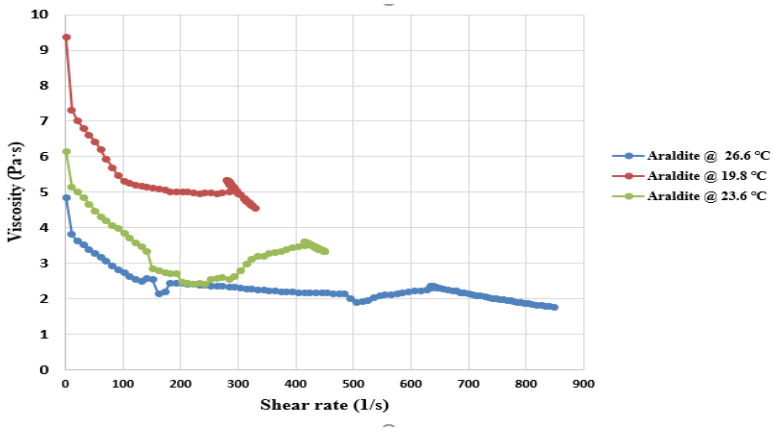


Figure 4.9: The viscosity profiles of araldite at different temperature levels.

Figure 4.10 presents the measured rheological properties of unfilled araldite in comparison to SCNs/Araldite mixture with 0.35 wt% and 0.5 wt% nanofiller concentration measured at a temperature of 27℃. The other nanofiller loading levels of SCNs/Araldite mixture with 0.05 wt%, 0.1 wt%, 0.15 wt% and 0.21 wt% nanofiller loading levels measured at 24.6℃ are presented in Figure B.1 in appendix B. The SCNs nanoparticles change the viscosity and shear stress profiles of unfilled araldite except at 0.35wt% nanofiller concentration. The viscosity profile of unfilled araldite at 27℃ decrease linearly until the shear rate of 152 s^{-1} where it drops significantly (kink) and then goes back to 2.45 Pa·s as shown in Figure 4.10a. After that the viscosity curve decreases gradually until at a shear rate of 496s^{-1} where another kink is observed. After the significant drop the viscosity gradually increases to 2.35 Pa·s at shear rate 646 s^{-1} which is the turning point where the viscosity begins to linearly decrease again. The shear stress curve increases with an increasing shear rate until at 646 s^{-1} where it becomes constant and the two kinks were observed on the shear stress curve as shown in Figure 4.10b.

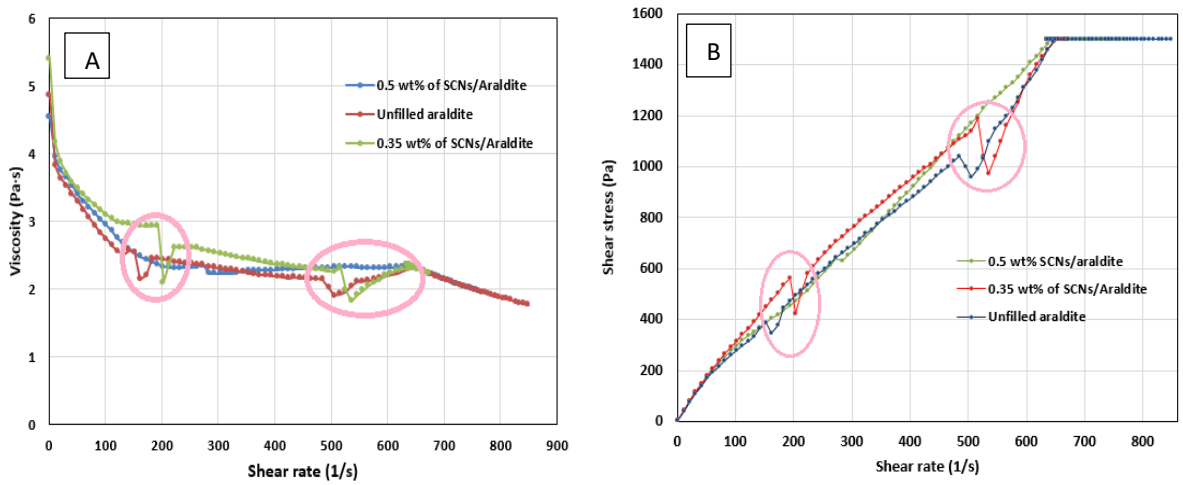


Figure 4.10: Comparison of unfilled araldite in comparison to SCNs/Araldite mixture with nanofiller loading levels of 0.35 wt% and 0.5 wt% (a) Viscosity profiles (b) Shear stress profiles.

The viscosity and shear stress profiles of SCNs/Araldite mixture at 0.35wt% nanofiller concentration are like that of unfilled araldite, but the viscosity magnitudes are greater than that of unfilled araldite and SCNs/Araldite mixture at 0.5 wt%. At the shear rate of 646 s^{-1} the viscosity magnitude of unfilled araldite and SCNs/araldite mixture at 0.35 wt% and 0.5 wt% nanofiller loading level are the same. The two kinks in the viscosity profiles of unfilled araldite and SCNs/Araldite mixture at 0.35wt% nanofiller loading level seem to be consistent with each other. These kinks signify a point of transition from one trend to another trend of flow mechanism. At 0.35 wt% nanofiller loading level the SCNs nanoparticles slightly increase the viscosity magnitude of araldite this corresponds with Green et al [57] findings that

nanoparticles increase the viscosity of the host polymer. The relationship between nanofiller concentration and viscosity magnitudes is non-linear. Using electrical treeing tests the best nanofiller loading level of SCNs nanoparticles for electrical tree resistance was found to be 0.35 wt% nanofiller loading level.

The viscosity and shear stress profiles of HCNs/Araldite mixture at different nanofiller levels as shown in Figure 4.11 were measured at a temperature of 26.4°C. Using electrical tree tests, the best nanofiller loading level for HCNs nanoparticles was found to be 0.05 wt%. HCNs/Araldite nanodielectric at 0.05 wt% nanofiller concentration has viscosity and shear stress profiles identical in shape to those of unfilled araldite as shown in Figure 4.12. The viscosity magnitude of HCNs/Araldite nanodielectric at 0.05wt% and unfilled araldite are approximately the same except at $700s^{-1}$ where the viscosity magnitude of HCNs/Araldite mixture is less than that of unfilled epoxy.

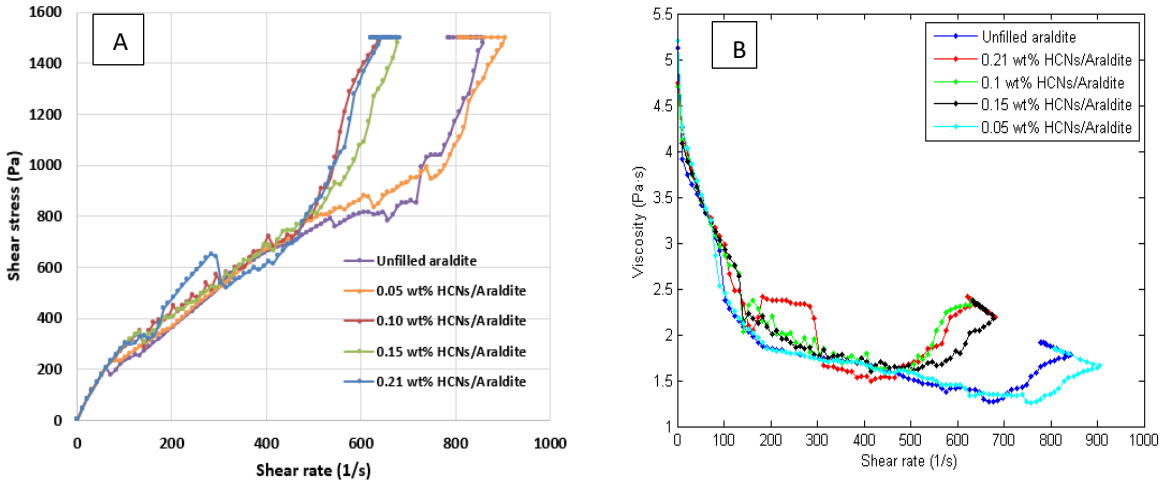


Figure 4.11: Comparison of rheological properties of unfilled araldite and HCNs/araldite mixture at different nanofiller loading levels (a) Shear stress profiles (b) Viscosity profiles

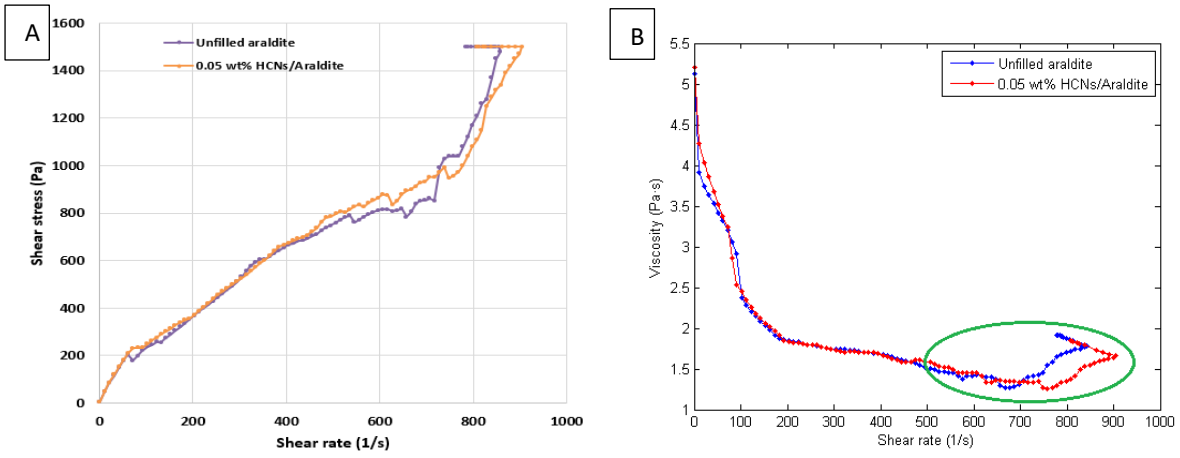


Figure 4.12: Comparison of rheological properties of unfilled araldite and HCNs/araldite mixture at 0.04 wt% nanofiller loading levels(a) Shear stress profiles (b)Viscosity profiles.

From the obtained results it can be concluded that the best nanofiller loading level of SCNs and HCNs nanoparticles for electrical treeing resistance are found where the viscosity and shear stress profiles are similar to those of unfilled araldite/host matrix. At the best nanofiller loading level of HCNs, both the viscosity profile and values are approximately the same with those of unfilled araldite. This behaviour corresponds with the results obtain by Mohammed [67] and Khumalo et al [68] where the viscosity profile and magnitude of polyethylene was not changed by the addition of boehmite nanoparticles at different nanofiller loading levels. Mohammed [67] claims that this is attributed to the good compatibility between boehmite nanoparticles and polyethylene matrix. As the addition of nanoparticles is not supposed to change the flow characteristics and polymer chain mobility of the host material. On the contrary Khumalo et al [68] claims that the similarity of viscosity magnitude is attributed to weak interactions between the nanofiller and the host polymer.

At the loading level of the nanofiller that gave the best electrical tree resistance, the SCNs nanoparticles slightly increased the viscosity magnitude of araldite and this does not correspond to the findings by Hank [10] who reported that at best nanofiller loading level for electrical tree resistance, the SCNs nanoparticles decrease the viscosity magnitude of unfilled araldite. Mohammed [67] speculate that when nanoparticles increase the viscosity magnitude of polymer it is due to the agglomeration of nanoparticles at high nanofiller loading which decreases the polymer chain mobility. The obtained best nanofiller loading level for electrical tree resistance in the present work is three times higher than that found by Hank [10]. The difference might explain why the SCNs nanoparticles increased the viscosity magnitude of the araldite in the present work. Blaszczak et al [69] reported that functionalized boehmite nanoparticles decrease the viscosity magnitude of polyethylene. The nanoparticles are functionalized to increase the compatibility between the nanoparticle and host matrix. It was speculated that the nanoparticles fill the spaces between the polyethylene chain branches and reduce the number of entanglements of the polymer thereby improving the flowability of the polymer [67] [69]. Using this speculation it can be concluded that SCNs are more compatible with the epoxy resin used [10] as they decreased the viscosity of unfilled araldite. This was further proven by the electrical treeing results presented in the next chapter.

4.4 Chapter Conclusion

This chapter has presented a direct dispersion method incorporated with the rheology analyses which is used to fabricate the experimental test specimens of unfilled epoxy resin, HCNs/Epoxy and SCNs/Epoxy nanocomposites. The rheological results of unfilled araldite in

comparison with HCNs/Araldite and SCNs/Araldite mixture are presented. It was found that the carbon-based nanofillers change the viscosity and shear stress profiles at different nanofiller loading levels except for that at the nanofiller loading level that gave the best performance for electrical tree resistance. At optimal nanofiller loading level of HCNs and SCNs nanoparticles for electrical tree resistance, the viscosity and shear stress profiles are similar to those of the unfilled host matrix. It was observed that an addition of 0.05 wt% nanofiller loading level of HCNs does not alter the viscosity magnitude of araldite. Whereas a 0.31 wt% nanofiller loading level of SCNs increased the viscosity magnitude of araldite. From the obtained results it can be concluded that incorporating rheology analysis in the nanodielectric fabrication method can improve the efficiency of determining the optimal nanofiller concentration. Since the temperature dominantly affects the viscosity profile a special controlled vessel will be required in the future to control the temperature on the rheometer and therefore the room temperature will not control temperature of the experimental setup.

The next chapter presents a study of the electrical tree characteristics of the fabricated epoxy nanocomposites with solid and hollow carbon nanospheres.

Chapter 5: Electrical tree time-to-failure characterisation of the (HCN/Epoxy) nanodielectric in comparison with unfilled epoxy as well as SCN/Epoxy

5.1 Introduction

Most electrical modes of failure in solid insulation involve electrical treeing phenomena either in the initial stages of the failure or during the course of failure or at the final phase of the failure process. Endurance to electrical treeing-induced failure becomes an important characteristic of electrical insulation. Electrical treeing is a pre-breakdown mechanism in solid insulation that initiate from a region of enhanced localised electric stress and causing gas-filled micro-tunnels that progressively grow through partial discharge activity [70]. The present work is a continuation of the work by Hank [10] that showed that the electrical tree endurance properties of epoxy can be significantly improved by adding an appropriate dosage of solid spherical carbon nanospheres. For the epoxy of type Araldite® CY 231-1 CH and Aradur® HY 925 used in Hank [10], the nanofiller loading of 0.11 wt% gave best electrical tree endurance. It is unknown why the carbon nanofillers cause excellent resistance to electrical trees but there are speculations that the good properties of carbon nanofillers are attributed to the electron scavenging properties of carbon. The present work therefore sought to extend the developments by investigating what happens to the nanodielectric if the carbon nanoparticles were to be made hollow. The hollowness of the nanoparticles will open other possibilities of further enhancing the electron scavenging properties of carbon by encapsulating electron negative material in the carbon shell. In the present work, a different type of epoxy was used. Since the solid nanospheres performance were the benchmark, the entire cycle of loading level optimisation of the nanospheres in another type of epoxy for best electrical tree endurance for the solid nanospheres had to be repeated for comparison with the hollow nanospheres. Furthermore, the work entailed choosing among available options the convenient synthesis technique for hollow carbon nanospheres and this was the polystyrene template method as explained in the previous chapter. The hollow carbon nanospheres were synthesised successfully and characterised using scanning electron microscopy, transmission electron microscopy, Raman spectroscopy, Branauer Emmett-Teller and thermogravimetric analysis techniques. Then the direct dispersion method incorporated with rheology analysis was used to fabricate the epoxy dielectric with HCNs and SCNs as presented in the previous chapter.

This chapter presents the electrical treeing studies of the HCNs/Epoxy nanodielectric in comparison with unfilled epoxy and SCNs/Epoxy nanodielectric. The different electrical treeing growth mechanisms in conventional polymer and in nanodielectric are discussed in section 5.2. Section 5.3 presents the experimental procedure used to characterise the electrical trees in unfilled epoxy and nanocomposite material. The results are presented and discussed in section 5.4. The chapter conclusion is drawn out in section 5.5.

5.2 Some background literature on electrical treeing mechanisms

Electrical treeing process is an amalgamation of four degradations which are electrical, chemical, thermal and mechanical [70]. This section discusses the mechanisms associated with electrical treeing growth in both conventional polymer and nanocomposites material.

5.2.1 Electrical treeing in conventional polymer material

Electrical treeing is a long-term degradation phenomenon which consist of three stages: inception, propagation and breakdown. The electrical trees initiate from a region of enhanced localised electric stress generated by anomalies such as metallic inclusion, cracks and small cavities [70] [71] [72]. In alternating electric field the electrical tree initiation process is driven by cyclic charge injection and extraction at the interphase region between the insulation and electrode/conductor [71] [72]. The evidence of charge injection in electrical treeing initiation in polyethylene was reported by Tanaka et al. [71] and in epoxy by Champion et al. [73]. The charges are injected by either Fowler-Nordheim tunnelling or Richardson-Schottky emission. During the negative half cycle of the applied voltage the electrons are emitted/injected into the insulation and drawn back during the positive half cycle of the applied voltage. In each cycle the injected/emitted electrons will extract energy from the applied electric field to initiate the physio-chemical reaction within the insulation. The physio-chemical reactions will cause the polymer molecular chains to breakdown. The electrical treeing process will then start when the polymer disintegration produces hollow channels (approximately 10 μm) that are sufficient enough to accommodate gaseous discharges [70] [71]. Alternatively, the micro-cracks may generate due to Maxwell compressive forces due to localised enhanced electric field. Hence the electrical tree process initiates from the generated micro-cracks. Even though there is some knowledge in the literature on electrical tree initiation mechanisms, the phenomenon is not yet fully understood due to the complexity and numerous factors influencing the process [74].

Of the three phases of electrical tree mechanisms, the most extensively researched is the electrical tree propagation phase. The electrical tree channels initiate and propagate as result of

partial discharges (PD) in either cavities or tree tubules, accompanied by thermal, chemical and mechanical degradations. There are several models proposed to explain the electrical treeing propagation in conventional polymers and these models are classified into two categories; stochastic and deterministic models [75] [76]. The stochastic models assume that electrical trees are conductive in nature and tree growth is a random process. The first field emission electron from either the electrode, surface of electrical tree channels or cosmic rays must be present to initiate avalanche discharges within the electrical tree [75]. The stochastic models can predict fractal dimension of the tree and structural distribution sub channels within the same tree [76]. The shortfall of stochastic models is that it does not explain the physical mechanism of how the main electrical tree channels are formed [76]. Deterministic models of electrical trees are based on the fact that the partial discharge activity in the trees produces space charges which will distort the local electric field within the tree. The distortion of electric field will result in intensified transient electric field which will further break the polymer chains and with time this effect will accumulate to cause electrical tree channels to extend [75]. The deterministic models assume that the electrical tree micro-tubules which can sustain partial discharge activity are formed during electrical tree initiation stage [76]. According to deterministic models the electrical tree growth rate is directly proportional to the electric field strength within electrical tree which exceeds a specific threshold value [77]. The threshold electric field is dependent on the insulation material and the applied voltage. The insulation will fail when electrical tree channels bridge the two electrodes.

There are three main types of electrical trees which are branch, bush and branch-bush. The shape of the electrical trees is determined by applied electric field strength, frequency of the voltage and morphological factors of the material [78] [76]. In epoxy resin the branch trees grow in relatively low electric field strength approximately 0.6 GVm^{-1} and bush trees grow in relatively high electric field approximately 1.2 GVm^{-1} [77]. The branch-bush trees grow between 0.6 GVm^{-1} and 1.2 GVm^{-1}electric field strengths. In silicone rubber there is high probability of branch trees developing at low frequency (50-500 Hz) and high probability of bush trees developing at high frequency (above 1kHz) [78] [79]. So far the studies of the effect of frequency in electrical trees in epoxy resin focused on frequency range of 50-500 Hz and it was found there is high probability of branch trees developing at this frequency range [80] [81]. The voltage frequency is directly proportional to the electrical tree growth rate and inversely proportional to the electrical tree inception voltage [78] [79]. The mechanisms associated with

electrical treeing growth in nanodielectric are different from those of conventional insulation and are discussed in the next subsection.

5.2.2 Electrical treeing mechanisms in nanocomposites

Properly engineered nanodielectrics generally have high resistance to electrical trees compared to conventional insulation. The nanoparticles increase the electrical tree inception voltage and PD resistance, therefore reducing electrical tree growth rate [82] [83] [84]. The electrical tree growth mechanism in nanocomposites is different from the one in conventional insulation. According to the physical model proposed by Alapati et al [85] to explain the electrical tree growth mechanism in epoxy nanocomposites, the tree grows through the epoxy resin and interfacial region between the nanofiller and the polymer. The electrical tree does not grow through the nanofillers because the nanofillers have higher resistance to partial discharges compared to host insulation. The electrical tree will form a zigzag pattern around the nanofillers thus expanding the electrical tree channels within the nanocomposite. Hildinger et al [86] stated that the electrical treeing in Silica/Epoxy nanocomposite is delayed due to the sintering of nanoparticles. The initial partial discharge pulses will erode the surface of the host polymer only and the free nanoparticles will agglomerate to form a barrier layer/ protective layer [86]. Hence the PD pulse energy will be absorbed by the new protective layer of nanoparticles and this will cause the electrical tree to lose its energy/momentum. The nanofillers act as obstacles hindering the propagation, therefore prolonging the electrical treeing process in nanocomposites.

The commonly investigated inorganic nanoparticles for electrical treeing experiments in nanodielectric are silica (SO_2), magnesia (MgO), alumina (Al_2O_3), titanium dioxide (TiO_2), boron nitride (BN) and zinc oxide (ZnO). For improvement to occur in the respective nanodielectric an appropriate nanofiller concentration must be determined which in turn is a function of the nanofiller type. According to Fréchette et al [7], generally the nanofiller concentration should be less than 5 wt% because beyond this loading level the nanoparticles will easily agglomerate.

There is lot of research work done on inorganic nanofillers compared to organic nanofillers in the field of electrical insulation. In the literature, organic nanofillers such as fullerenes, graphene and solid carbon nanospheres have been used and found to produce nanocomposites with significantly improved electrical tree resistance [9] [10] [11]. Enhancement in nanocomposites with fullerenes, solid carbon nanospheres and graphene nanoparticles was

found at relatively low nanofiller concentration of 0.1 wt%, 0.11 wt% and 0.2 wt% respectively. It is speculated that the excellent electrical tree resistance property of nanocomposites with carbon-based nanofillers is attributed to the electron scavenging properties of carbon. Hence the present research work investigates whether this hypothesis holds true when the carbon nanoparticles are of the hollow type. To the authors' knowledge the use of hollow carbon nanospheres as nanofillers in nanocomposite for electrical insulation application has not been explored yet. The next section presents the experimental procedure used to characterise the electrical trees in an epoxy nanodielectric material with carbon-based nanofillers.

5.3 The electrical treeing experimentation with the hollow and solid carbon nanospheres in epoxy dielectric

The circuit diagram shown in Figure 5.1 is used to measure electrical tree partial discharges grown in unfilled epoxy and nanocomposite material. The test sample is submerged in insulation oil to prevent surface discharges and flashovers. The needle-plane electrode configuration with a gap distance of 3 mm encapsulated in the nanodielectric under test is used to simulate accelerated growth of electrical trees. Ogura™ needles with a tip radius of 5 μm were used. The epoxy resin was of the type araldite® FR476D and hardener® obtained from Elite chemical industries (PTY) LTD ™. Since this type of epoxy is different from the one used by Hank [10], the study of electrical tree characteristics of nanocomposite with solid carbon nanospheres is repeated in the present work to confirm that the experimental results obtained by Hank [10] are reproducible in a different type of epoxy. Images of the fabricated test samples of epoxy and nanocomposite with either HNCs or SCNs nanoparticles are shown Figure 5.2.

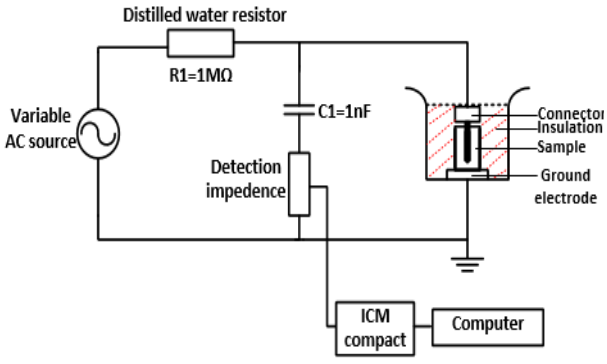


Figure 5.1: The circuit diagram used in initiating and growing the electrical trees whilst simultaneously measuring the corresponding partial discharges according to IEC 60270.

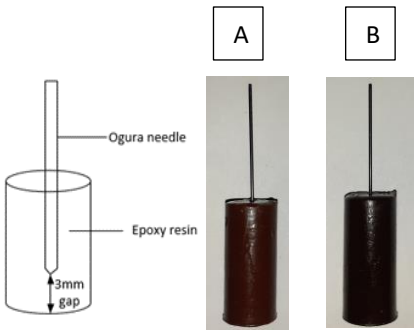


Figure 5.2: A drawing of electrical tree test specimen and images of a) Unfilled epoxy, b) Nanocomposite with carbon nanofillers.

Figure 5.3 shows the flow chart of the method used to measure electrical tree inception voltage and time-to-failure. The electrical treeing experiments were conducted in an electromagnetically shielded high voltage laboratory where the noise level averaged at 0.5 pC as shown in Figure 5.4. Assuming that at inception the electrical trees immediately give detectable PD, a voltage at which initial PD pulses appear is regarded as electrical tree inception voltage. The Power Diagnostix ICMcompact™ PD measurement system was used to measure the charge magnitude and partial discharge phase-resolved patterns (PDPRP) associated with the electrical trees. A computer is used to record the charge magnitude data and the flashback software is used to take the video of PDPRP associated with the electrical trees.

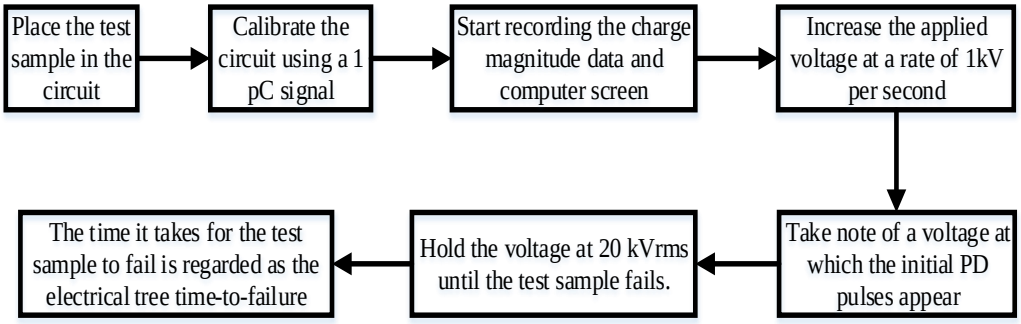


Figure 5.3: The flow chart of the methodology used to measure electrical tree inception voltage and time-to-failure.

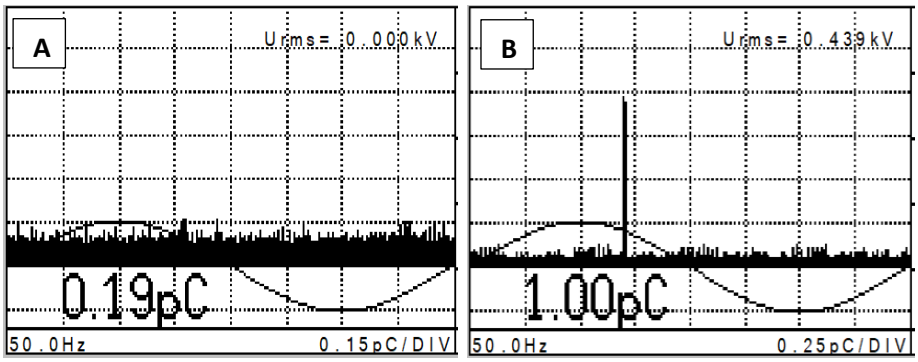


Figure 5. 4: (a) Background noise level in the High Voltage Laboratory, (b) A snapshot of PDPRP of 1 pC signal used to calibrate the circuit.

In the present work the nanofiller concentrations of 0.04 wt%, 0.09 wt%, 0.19 wt%, 0.31 wt% and 0.4wt% for nanodielectric with SCNs are investigated. For HCNs/Epoxy nanodielectric the nanofiller levels of 0.02 wt%, 0.04 wt%, 0.09 wt%, 0.19 wt% and 0.31wt% are investigated. The following characteristics of electrical tree partial discharges were measured for the unfilled

epoxy (as control tests), SCNs/Epoxy (as the benchmark) and HCNs/Epoxy (the new dielectric under investigation):

- The electrical tree partial discharge inception voltage
- Time-to-failure under electrical tree-induced degradation
- Partial discharge magnitude time-evolution trends
- Partial discharge phase-resolved-patterns (PDPRP) associated with electrical treeing growth.

The obtained electrical tree results are presented and analysed in the next section.

5.4 The electrical treeing experimental test results

This section presents the obtained results of electrical tree PD behaviour in unfilled epoxy in comparison to those in SCNs/Epoxy and HCNs/Epoxy nanocomposites.

5.4.1 Electrical tree PD inception voltage results

The plots of electrical tree inception voltages of SCNs/Epoxy and HCNs/Epoxy nanocomposites as a function of nanofiller concentration are shown in Figure 5.5. In both cases of SCNs/Epoxy and HCNs/Epoxy, electrical tree PD inception decrease with an increase in nanoparticles loading levels. Overall, the electrical tree inception voltage of SCNs/Epoxy nanocomposite is higher than that of HCNs/Epoxy nanocomposite as shown in Figure 5.6.

An example of PDPRP observed at inception voltage for unfilled epoxy resin, SCNs/Epoxy and HCNs/Epoxy nanodielectric at nanofiller filler concentration of 0.31 wt% and 0.04 wt% respectively are shown in Figure 5.7. The charge magnitudes of SCNs/Epoxy and HCNs/Epoxy nanodielectric are higher than that of unfilled epoxy. The PDPRP are observed in first and third quadrant at inception. It can be deduced from the obtained results that SCNs and HCNs nanoparticles compromise the electrical tree inception voltage of epoxy resin. There are different mechanisms for electrical tree inception and propagation processes. When the nanoparticles compromise electrical tree inception voltage it does not necessarily imply that they will compromise the electrical tree time-to-failure as well. Hence the electrical tree time-to-failure results are presented in the next subsection.

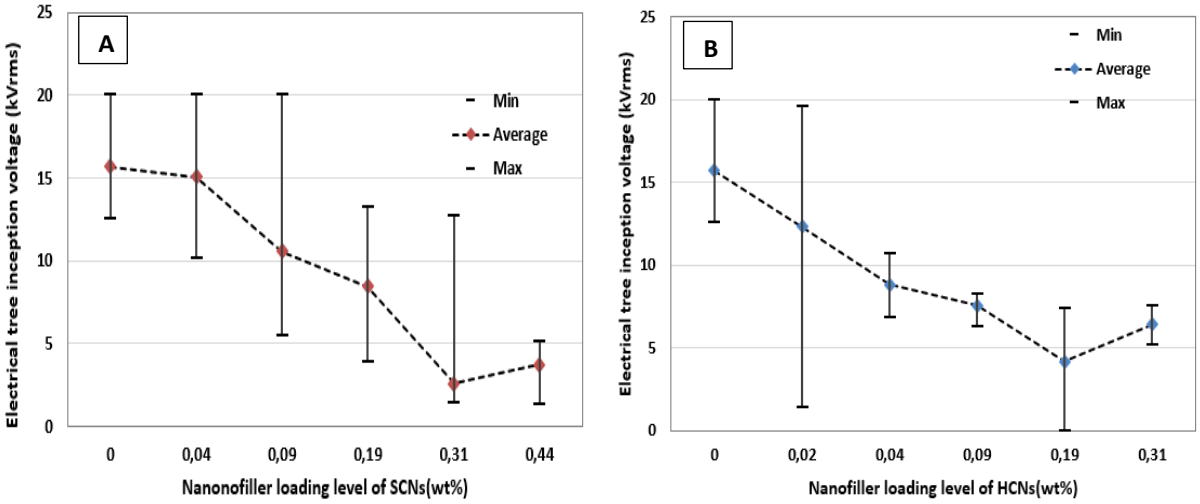


Figure 5.5: (a) Min-Average-Max chart for inception voltage of SCNs/Epoxy nanodielectric as a function of nanofiller concentration (b) Min-Average-Max chart for inception voltage of HCNs/Epoxy nanodielectric as a function of nanofiller concentration.

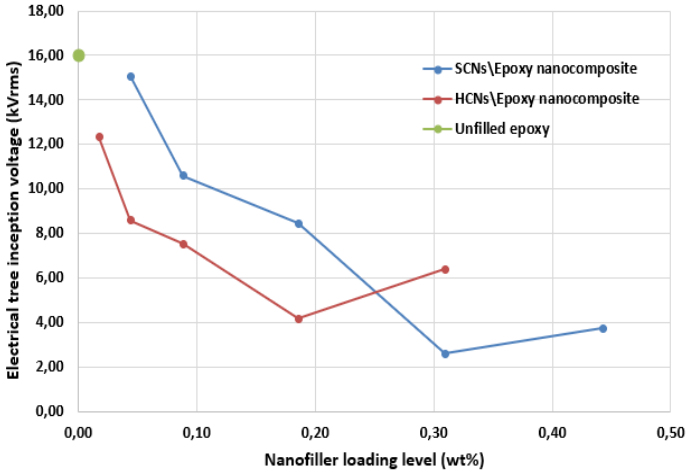


Figure 5.6: Average electrical tree inception voltage of epoxy, SCNs\Epoxy and HCNs\Epoxy nanocomposites as a function of nanofiller loading level.

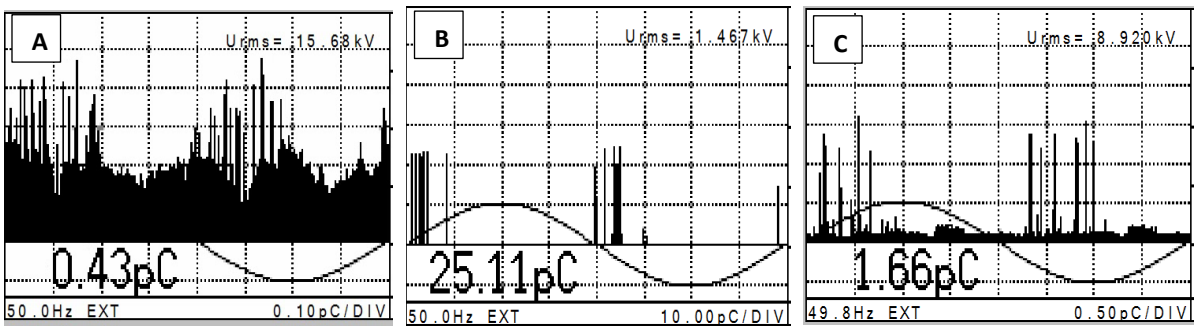


Figure 5.7: An example of PDPRP associated with the first PD pulses at electrical tree inception voltage (a) unfilled epoxy resin (b) SCNs/Epoxy nanodielectric with 0.31 wt% (c) HCNs/Epoxy nanodielectric with 0.04 wt%.

5.4.2 Electrical tree time-to-failure test results

Detailed experimental data of electrical tree time-to-failure of epoxy, SCNs/Epoxy and HCNs/Epoxy nanocomposites are presented in table A.1 in appendix A. The max-average-min charts of electrical tree time-to failure as a function nanofiller loading level for SCNs/Epoxy and HCNs/Epoxy nanodielectric in comparison to unfilled epoxy are shown in Figure 5.8. The SCNs nanoparticles give the best enhancement of the electrical tree time-to-failure at nanofiller loading of 0.31wt%. The HCNs nanoparticles on the other hand give the best electrical treeing endurance performance at a nanofiller loading level of 0.04 wt%. At this filler level however, only one test sample had superior performance as shown in appendix A and this performance was not reproducible and this raises concerns. In contrast, SCNs/Epoxy nanocomposites at 0.31wt% nanofiller concentration two samples performed better than unfilled epoxy. SCNs/Epoxy nanocomposite therefore has the highest average time-to-failure compared to both unfilled epoxy and HCNs/Epoxy nanocomposite. For SCNs/Epoxy nanocomposite, the electrical tree time-to-failure gradually increases with nanofiller concentration until it reaches the peak at 0.31wt% and after that the electrical tree time-to-failure decreases with continued increase in nanofiller concentration. A similar relationship is observed in HCNs/Epoxy nanocomposite. It can be concluded from the obtained results that SCNs/Epoxy nanodielectric with 0.31wt% nanofiller concentration has higher electrical tree time-to-failure compared to HCNs/Epoxy nanodielectric with 0.04 wt% nanofiller concentration and unfilled epoxy resin as shown in Figure 5.9. The electrical treeing process is driven by partial discharges activity. It is important to see how the SCNs and HCNs affect the partial discharge magnitude of the epoxy resin and this is the subject of the next subsection.

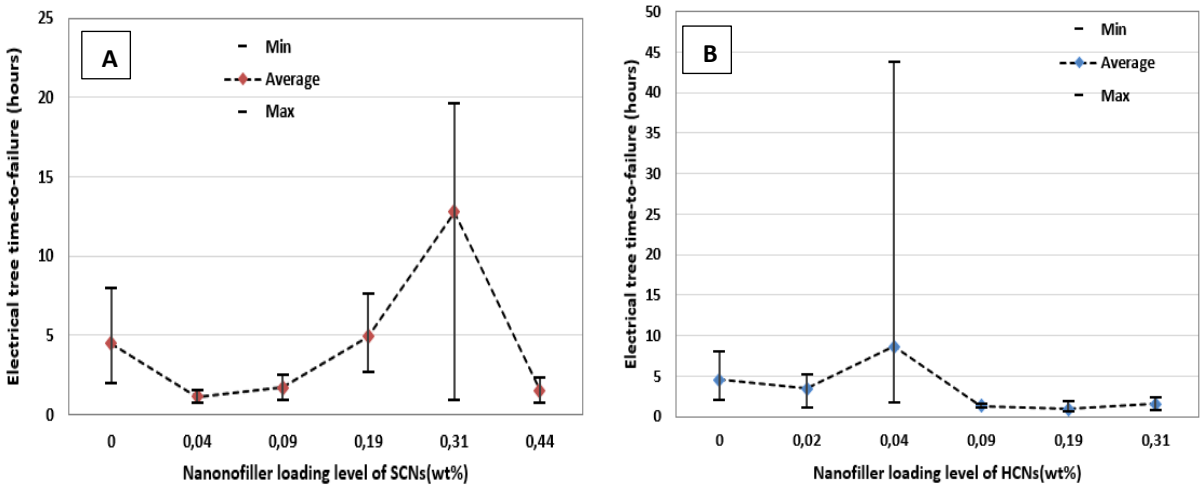


Figure 5.8: Min-Average-Max chart for electrical tree time-to-failure as a function of nanofiller concentration of (a)SCNs/Epoxy nanodielectric (b) HCNs/Epoxy nanodielectric.

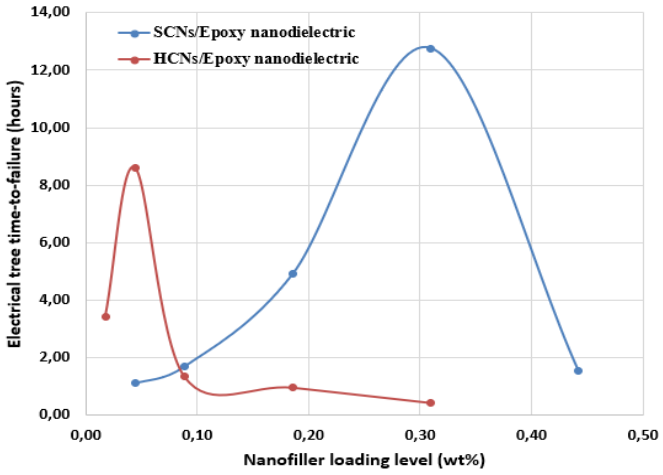


Figure 5.9: Comparison of average electrical tree time-to-failure in SCNs\Epoxy and HCNs\Epoxy nanodielectric as a function of nanofiller loading level.

5.4.3 Partial discharge magnitude time-evolution results

In unfilled epoxy test samples, the electrical tree partial discharge magnitude is small at the beginning of the electrical tree growth and then builds up as the electrical tree grows as shown in Figure 5.10. After some time, the partial discharge magnitude decreases before the test specimen completely fails.

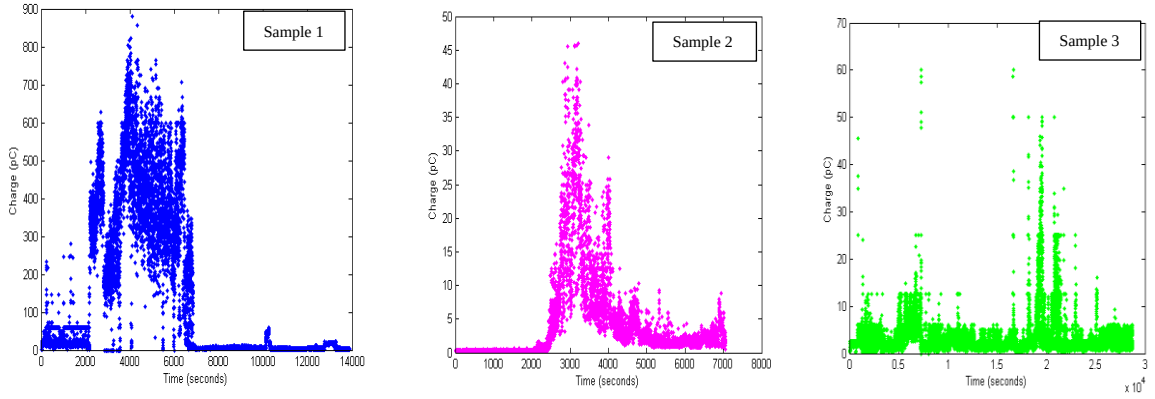


Figure 5.10: Typical results of electrical tree partial discharge magnitude as a function of time for the unfilled epoxy resin.

The electrical tree partial discharge magnitude time evolution of SCNs/Epoxy test samples at different nanofiller loading levels are shown from Figure 5.11 to Figure 5.15. Similar characteristics of partial discharge magnitude time evolution of unfilled epoxy are observed in SCNs/Epoxy test samples with nanofiller concentration of 0.04 wt% as shown in Figure 511. Most of SCNs/Epoxy test samples within nanofiller concentration range of 0.088-0.44 wt% had very high partial discharge magnitudes at the beginning of the electrical tree growth for a short period that then decreased to nearly zero as the trees grew. For some of the SCNs/Epoxy

samples the partial discharge magnitude remained low until the sample failed, whereas for some SCNs/Epoxy samples the partial discharge magnitude became high few minutes before the sample failed. SCNs/Epoxy sample 1 and 2 with nanofiller concentration 0.19 wt% and 0.44 wt% respectively had partial discharge magnitude behaviour similar to that of unfilled epoxy samples.

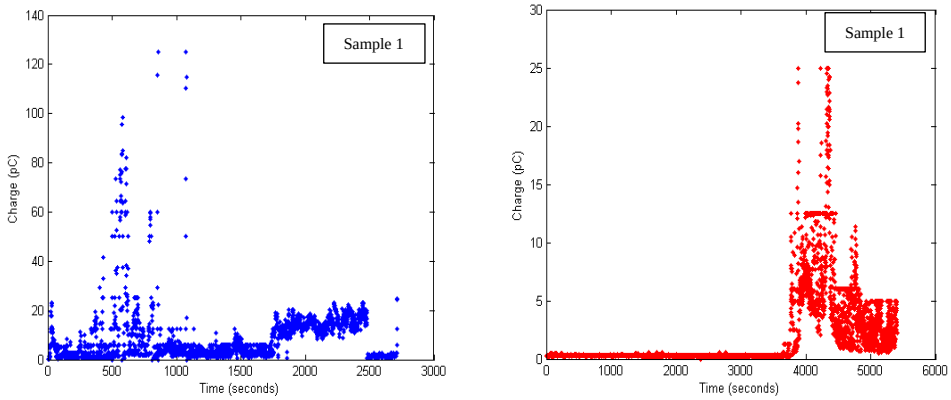


Figure 5.11: Electrical tree PD magnitude as a function of time for SCNs/Epoxy nanodielectric at 0.044wt% nanofiller loading level.

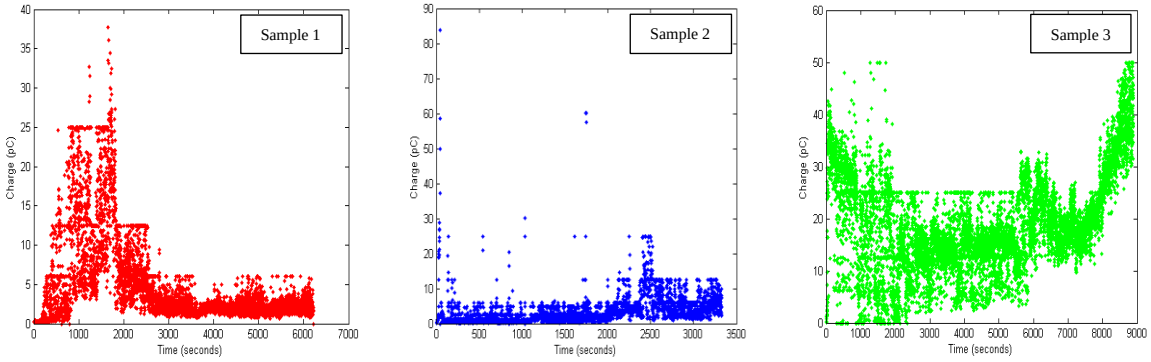


Figure 5. 12: Electrical tree PD magnitude as a function of time for SCNs/Epoxy nanodielectric at 0.088wt% nanofiller loading level.

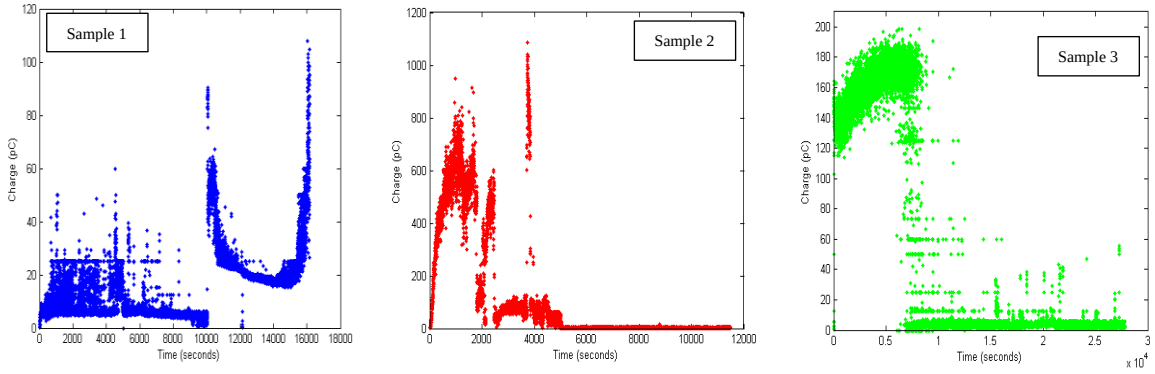


Figure 5.13: Electrical tree PD magnitude as a function of time for SCNs/Epoxy nanodielectric at 0.19wt% nanofiller loading level.

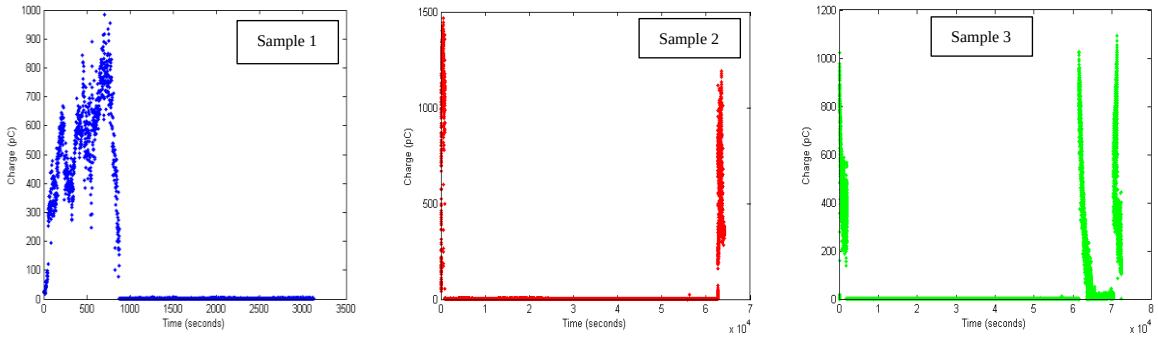


Figure 5.14: Electrical Tree PD magnitude as a function of time for SCNs/Epoxy at 0.31wt% nanofiller loading level .

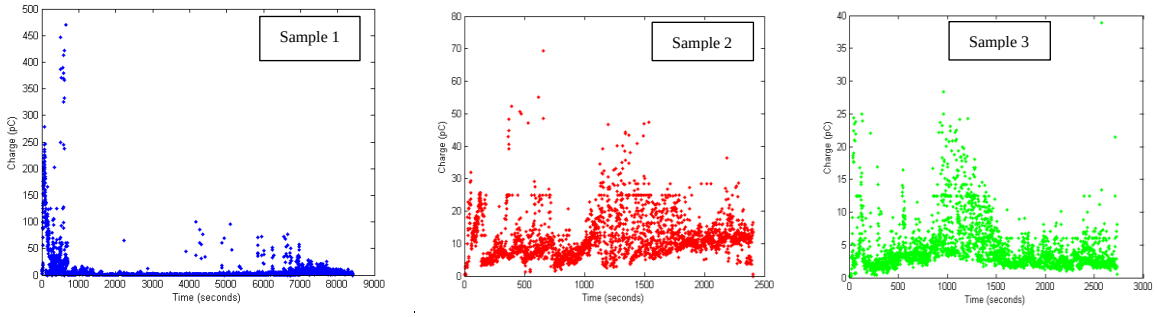


Figure 5.15: Electrical tree PD magnitude as a function of time for SCNs/Epoxy nanodielectric at 0.44wt% nanofiller loading level.

The partial discharge magnitude time evolution of HCNs/Epoxy test samples at different nanofiller loading levels are shown from Figure 5.16 to Figure 5.20. HCNs/Epoxy samples with 0.088wt% nanofiller concentration had partial discharge magnitude time evolution characteristics similar to those of most of SCNs/Epoxy samples as shown in Figure 5.12. Most of HCNs/Epoxy samples' partial discharge magnitudes fluctuated randomly over time and therefore giving no distinct patterns.

The next subsection presents the partial discharge phase-resolved-patterns which provides information regarding the type of PD in epoxy resin, SCNs/Epoxy and HCNs/Epoxy nanodielectric.

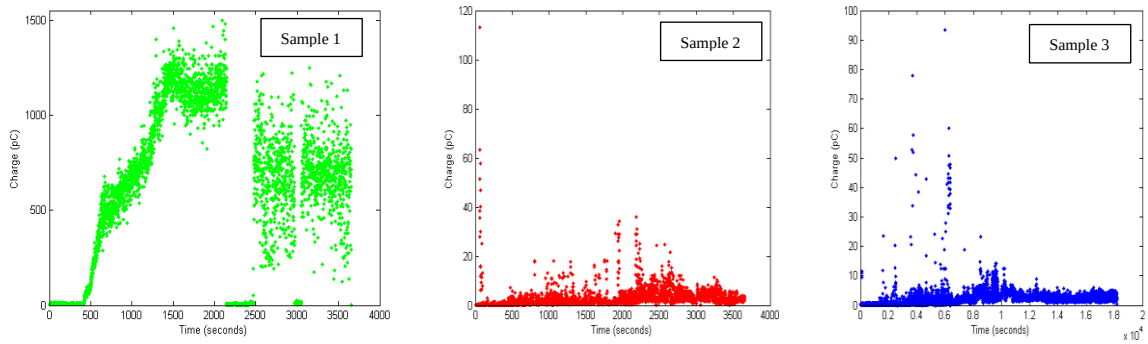


Figure 5.16: Electrical tree PD magnitude as a function of time for HCNs/Epoxy nanodielectric at 0.02wt% nanofiller loading level.

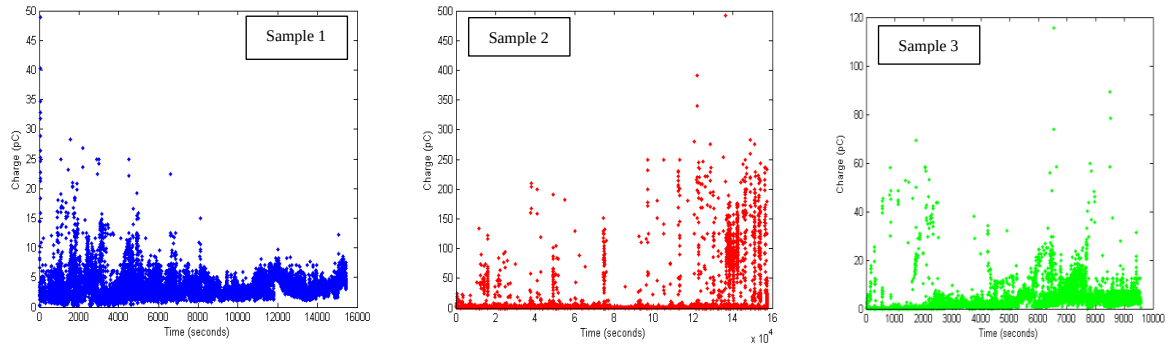


Figure 5. 17: Electrical tree PD magnitude as a function of time for HCNs/Epoxy nanodielectric at 0.04wt% nanofiller loading level.

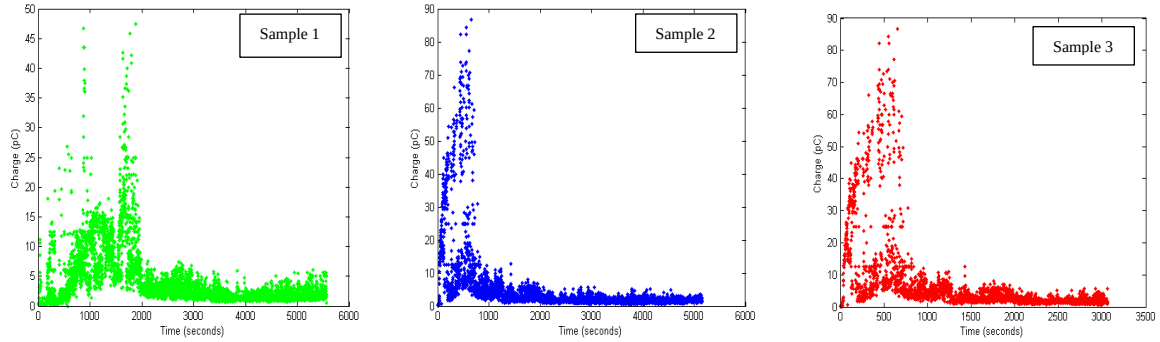


Figure 5.18: Electrical tree PD magnitude as a function of time for HCNs/Epoxy at 0.088wt% nanofiller loading level.

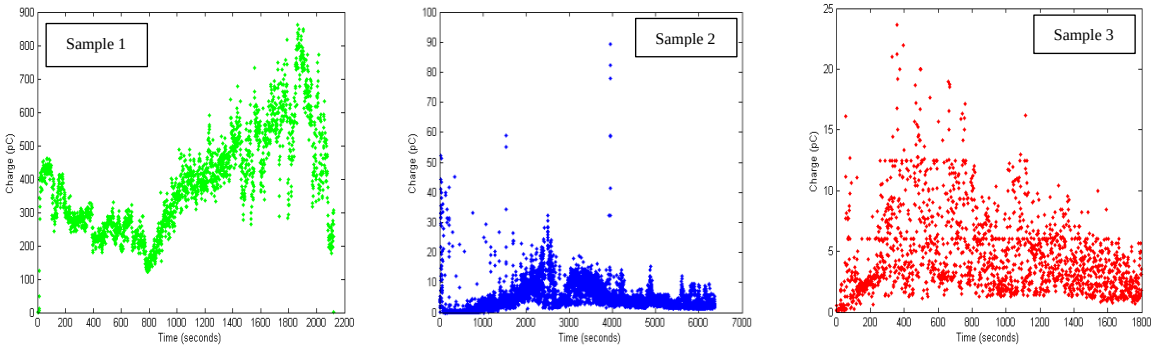


Figure 5.19: Electrical tree PD magnitude as a function of time for HCNs/Epoxy at 0.19wt% nanofiller loading level.

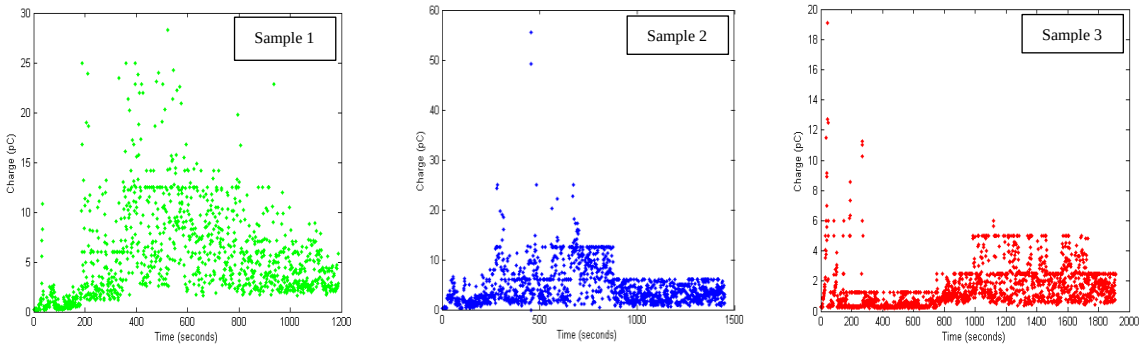


Figure 5. 20: Electrical tree PD magnitude as a function of time for HCNs/Epoxy at 0.31wt% nanofiller loading level.

5.4.4 Partial discharge phase-resolved-patterns (PDPRP) associated with electrical tree growth

This section presents electrical tree partial discharge phase-resolved-patterns (PDPRP) of unfilled epoxy in comparison to those of SCNs/Epoxy and HCNs/Epoxy nanodielectric that gave best electrical tree endurance. The respective loading levels of the SCNs/Epoxy and HCNs/Epoxy were 0.31wt% and 0.04 wt%. For unfilled epoxy sample there are barely any noticeable PD observed at the beginning of the electrical tree growth. Only after 32 minutes, PD appears continuously until the sample fails as shown in Figure 5.21. PDPRP with varying PD pulse magnitudes are observed on epoxy sample and PD patterns appear on both positive and negative half cycles. The observed PDPRP on epoxy sample and the applied electric field strength of approximately 1 MVm^{-1} corresponds to branch trees [75] [11].

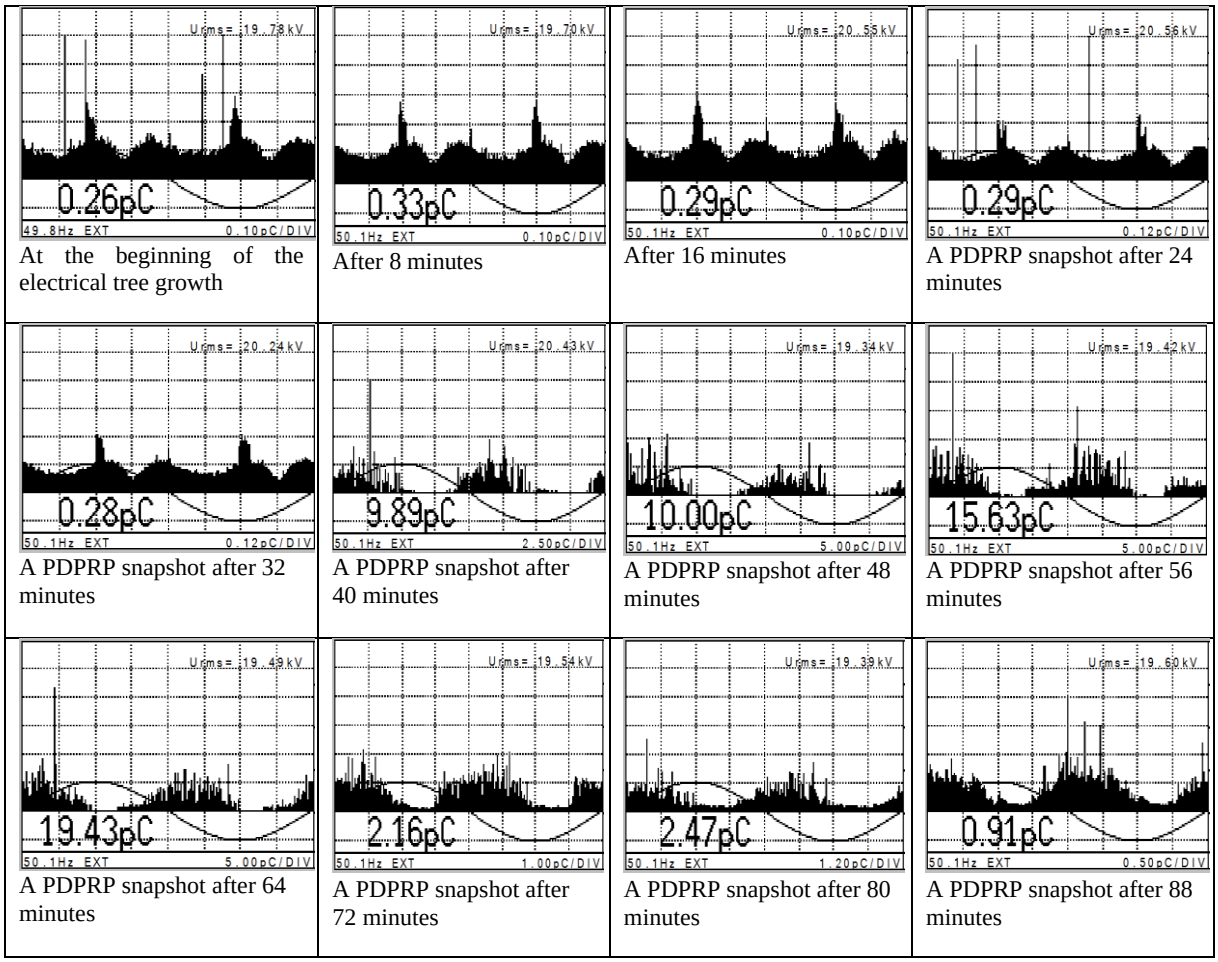
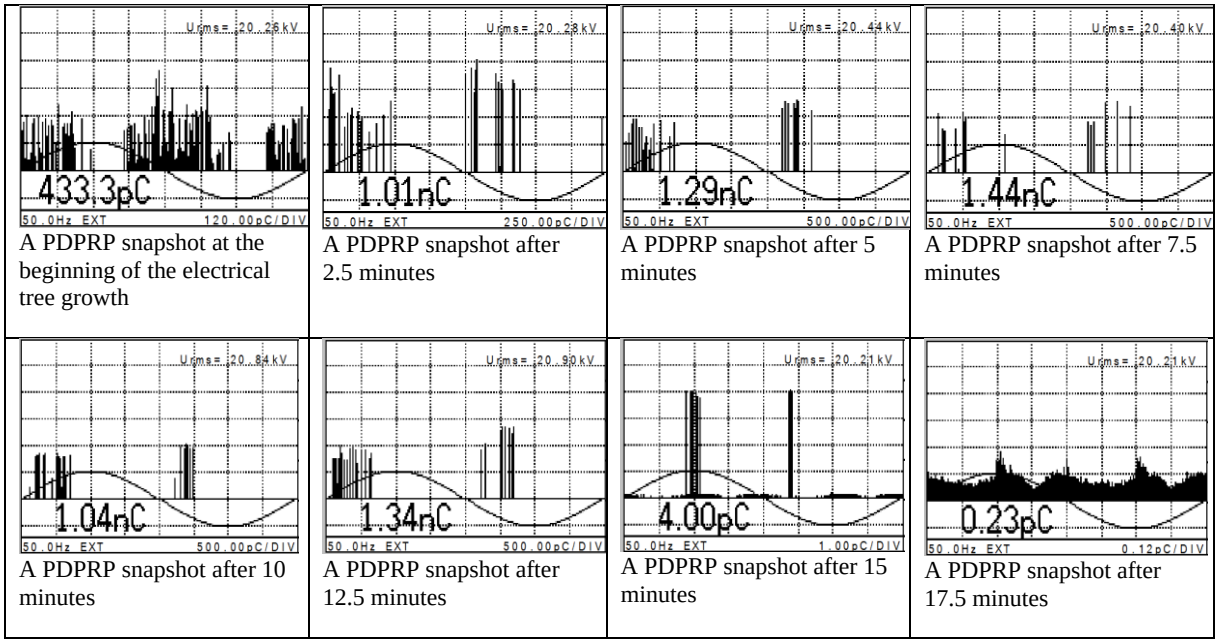


Figure 5.21: The typical PDPRP snapshots of unfilled epoxy every 8 minutes for the first 1 hour of 30 minutes

In the case of SCNs/Epoxy samples, PDPRP were observed at the beginning of the electrical growth for 20 minutes and then disappeared below the noise level as shown in Figure 5.22. After 20 minutes, the charge magnitudes dropped to close to zero as shown in Figure 5.22 and the PDPRP appear randomly with the magnitude less than 5 pC in 3-6 second bursts. The charge

magnitude increased significantly for 27 minutes before the SCNs/Epoxy sample fails. Towards complete failure the PD signal appeared continuously. The typical PDPRP are shown in Figure 5.23. A combination of uniform sized PD pulses, and large varying PD pulse magnitudes are observed on SCNs/Epoxy test sample. The largely small and uniform sized PD pulses correspond to bush trees [11].



A PDPRP snapshot at the beginning of the electrical tree growth

A PDPRP snapshot after 2.5 minutes

A PDPRP snapshot after 5 minutes

A PDPRP snapshot after 7.5 minutes

A PDPRP snapshot after 10 minutes

A PDPRP snapshot after 12.5 minutes

A PDPRP snapshot after 15 minutes

A PDPRP snapshot after 17.5 minutes

Figure 5.22: The PDPRP snapshots of sample 2 of SCNs/Epoxy nanocomposite at 0.31wt% nanofiller loading for every 2.5 minutes for the first hour.

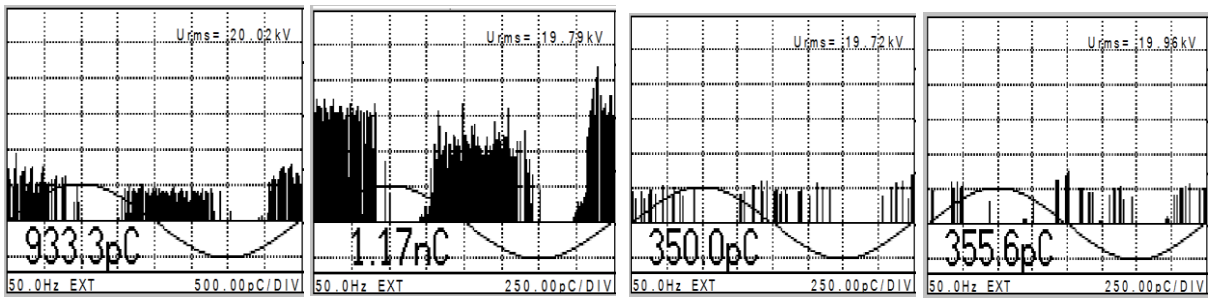


Figure 5.23: The different types of PDPRP snapshots observed 27 minutes before the SCNs/Epoxy sample breaks down.

In HCNs/Epoxy samples the PDPRP appear and disappear sporadically and different types of PDPRP observed are shown in Figure 5.25. The corresponding partial discharge magnitude time-evolution is shown in Figure 5.24c. A combination of small and uniform sized PD pulses and large varying sizes PDPRP were observed on HCNs/Epoxy sample. With the obtained PDPRP it can be deduces that branch-bush electrical trees were grown on HCNs/Epoxy and HCNs/Epoxy samples.

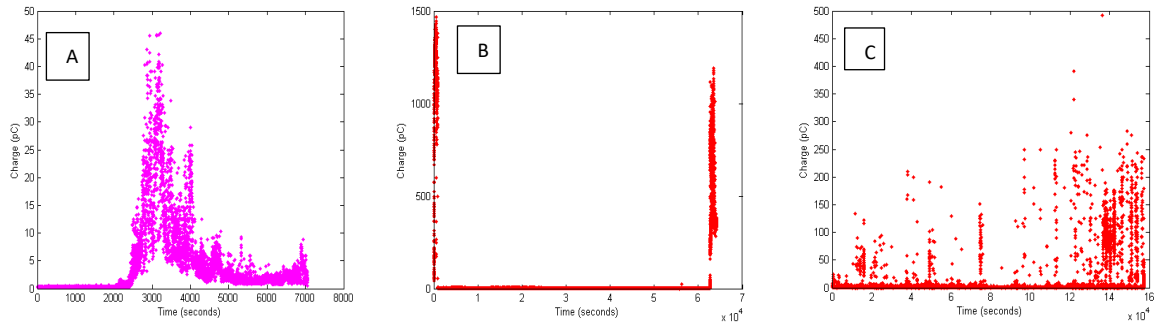


Figure 5.24: The partial discharge magnitude time evolution for a) unfilled epoxy b) SCNs/Epoxy nanodielectric c) HCNs/Epoxy nanodielectric

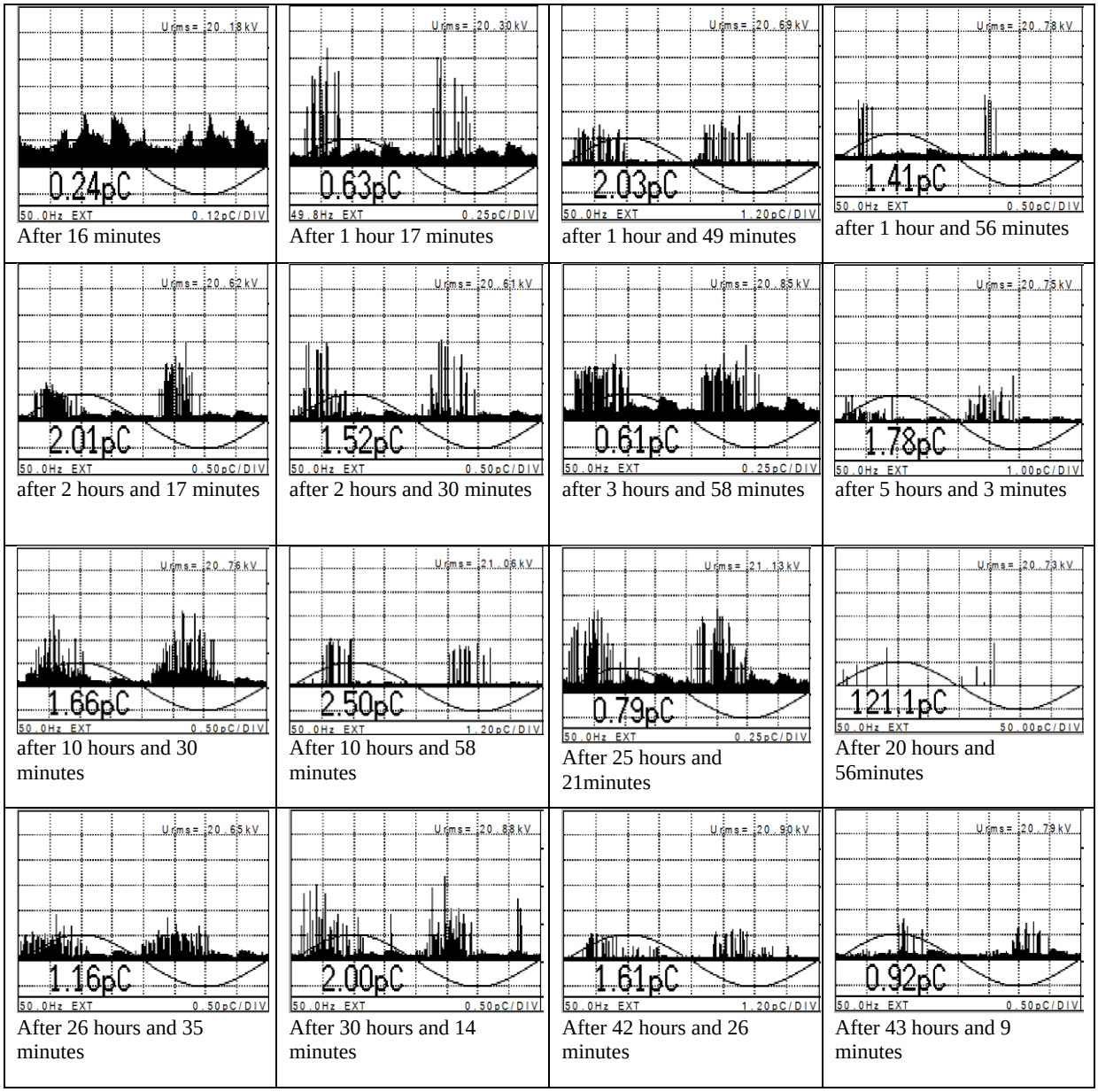


Figure 5.25: Different types of PDPRP snapshots observed on HCNs/Epoxy nanodielectric sample

The next section presents SEM analyses of the test samples which were aged using electrical treeing test and the overall discussion of the obtained results.

5.4.5 Electrical tree microscopic imaging

A scanning electron microscope was used to characterise the electrical trees grown in HCNs/Epoxy and SCN/Epoxy nanocomposite. The analyses did not focus on the particle distribution because both the nanoparticles and the host epoxy are carbon-based. Therefore, it is difficult to distinguish the nanoparticles from the epoxy host insulation. The surface morphology of HCNs/Epoxy nanodielectric is different from that of epoxy and SCNs/Epoxy nanodielectric as shown in Figure 5.26.

A typical electrical tree channel shown in Figure 5.27 has a length and width approximately of 221 µm and 10 µm respectively. The electrical tree partial discharge cavity of HCNs/Epoxy nanodielectric around the needle tip is circular in shape with the diameter approximately 343.5µm shown in Figure 5.28a. Figure 5.28b indicate the partial discharge cavity of SCNs/Epoxy nanodielectric around the tip needle which is ellipsoid in shape with a big and small diameter of approximately is 751 µm and 577 µm respectively. The PD cavity of SCNs/Epoxy nanodielectric is bigger than the one for HCNs/Epoxy nanodielectric.

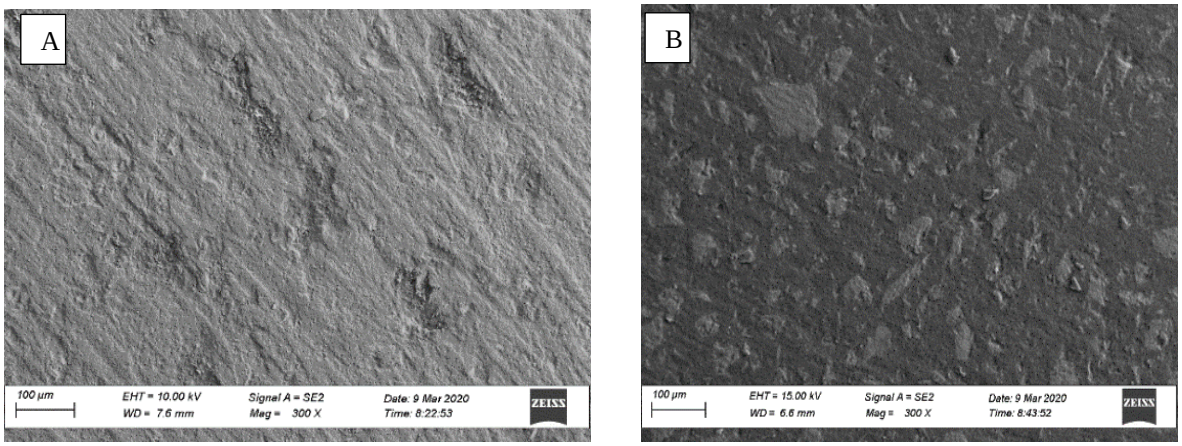


Figure 5.26: The SEM images of (a) unfilled epoxy, (b) HCNs/Epoxy nanodielectric at 0.04 wt%.

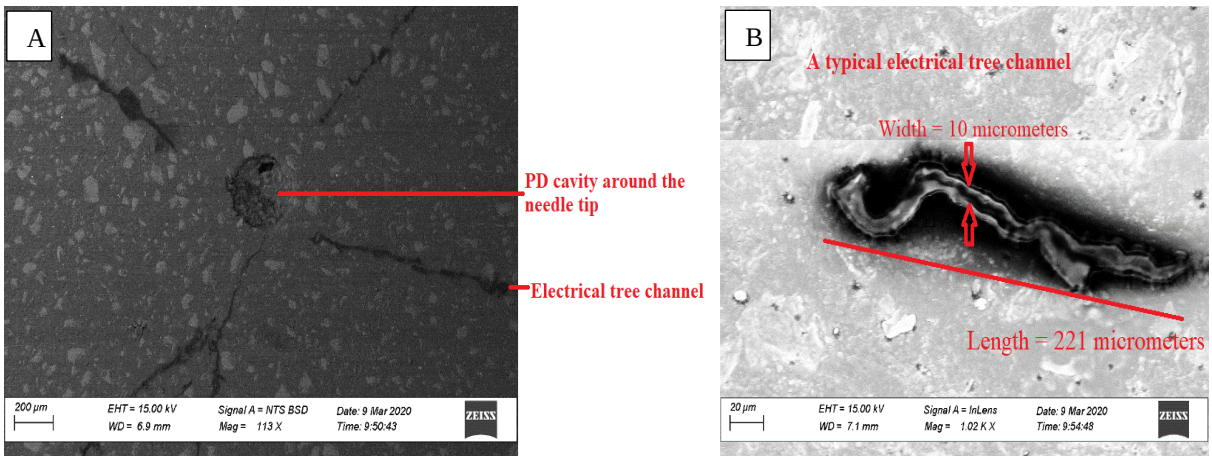


Figure 5.27: The SEM image of a) A top view of the electrical tree in HCNs/Epoxy nanodielectric b) A top view of the electrical tree channel in HCNs/Epoxy nanodielectric.

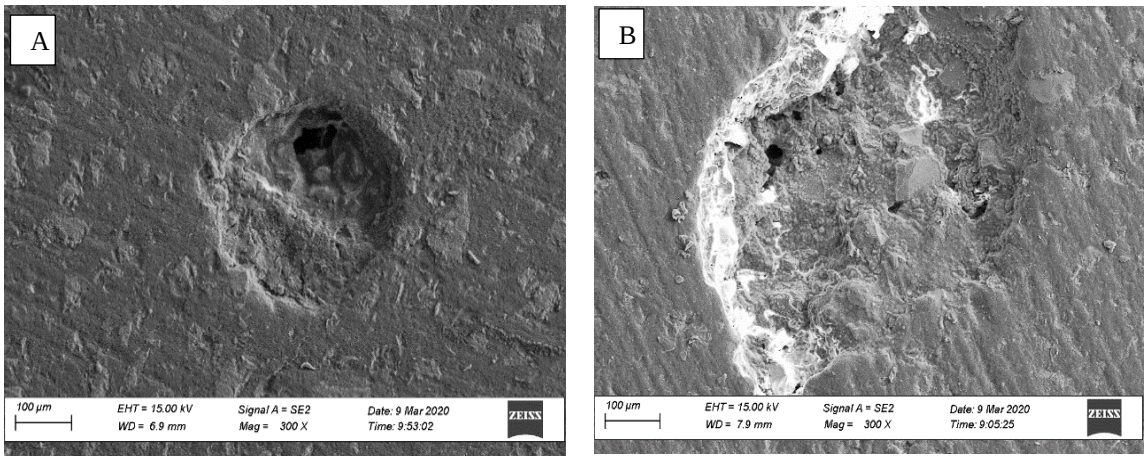


Figure 5.28: The partial discharge cavity around the ogura needle tip for (a) HCNs/Epoxy nanodielectric (b) SCNs/Epoxy nanodielectric.

The region inside the PD cavities around the needle tip were further analysed and SEM images of HCNs/Epoxy and SCNs/Epoxy nanodielectrics are shown in Figure 5.29 and Figure 5.30 respectively. Figure 5.30 presents the SEM image of the generated PD cavity around the needle tip in SCNs/Epoxy nanocomposite and there is an evident of a layer of spherical particles that might be an agglomeration of free nanoparticles that were left behind during partial discharge erosion of interfacial region and epoxy as also reported by Hildinger et al [86] and Fréchette et al [7]. This protective layer absorbs the partial discharge energy therefore prolonging the electrical treeing process in nanocomposite. According to Alapati et al [85] the electrical tree grows through the epoxy resin and interphase region, it however does not grow through the nanofiller. These findings are in agreement with the multicore model proposed by Tanaka et al [17]. The bound and bonded layers are more resistance to partial discharges compared to loose layer and the host insulation which means the tree will grow between the loose layer and epoxy. The SEM image in Figure 5.30a is consistent with what was observed by Hoffmann et al [87]. The morphology of the region inside the PD cavity of HCNs/Epoxy nanodielectric is different from that of SCNs/Epoxy nanodielectric. It is postulated that SCNs/Epoxy and HCNs/Epoxy nanodielectrics might have different electrical treeing mechanisms. There is no evident of the protective layer of nanoparticles formed on HCNs/Epoxy nanodielectric during PD erosions. The hollow carbon nanospheres are mesoporous with a pore size of 2.5 nm and this means that there is a possibility for the electrical tree to grow through the HCNs. Furthermore, the HCNs are filled with air which has low electron affinity compared to epoxy resin. This may explain why HCNs/Epoxy nanodielectric were found to have less electric tree resistance compared to SCNs/Epoxy nanodielectric.

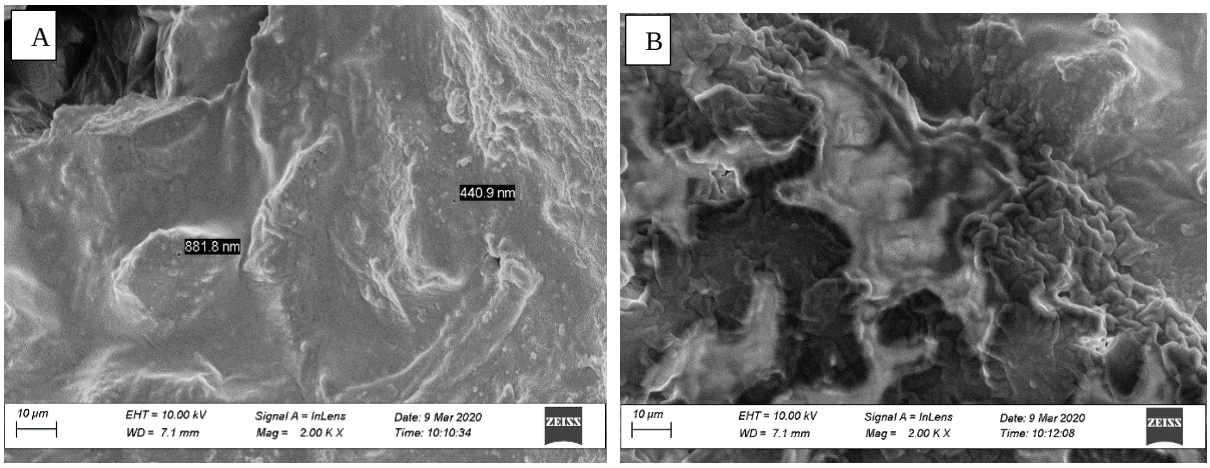


Figure 5. 29: The regions inside the cavity for HCNs/Epoxy nanodielectric.

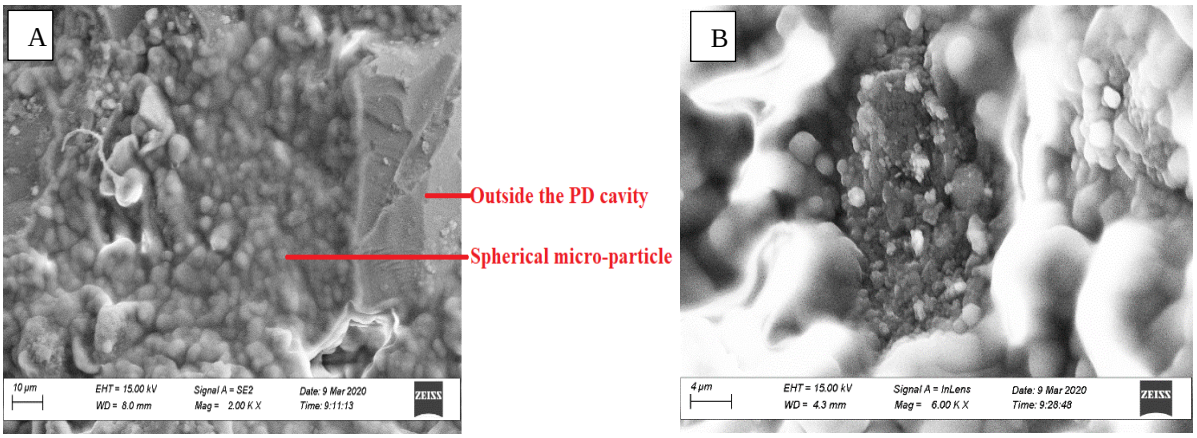


Figure 5.30: The region inside the cavity for SCNs/Epoxy nanodielectric at different magnifications.

5.5 Overall evaluation of the research results in the context of answers to the research questions

The relationship between the average electrical tree time-to-failure and nanofiller concentration of HCNs and SCNs nanofillers is not linear like cases reported for inorganic nanofillers [10]. Outside the optimal filler loading, the properties of nanocomposites are poorer than those of unfilled epoxy. The optimal nanofiller loading level for electrical tree time-to-failure of SCNs and HCNs were found to be 0.31wt% and 0.04 wt% respectively. That of HCNs is lower than of SCNs because the HCNs are lighter in weight. Even with different optimal loading levels, both the SCNs and HCNs nanoparticles increase the electrical tree time-to-failure of epoxy at optimal nanofiller concentration by 195% and 99% respectively. SCNs/Epoxy nanodielectric has longer electrical tree time-to-failure compared to HCNs/Epoxy because solid carbon nanospheres have higher electron affinity compared to hollow carbon nanospheres. Each solid carbon nanoparticle has more carbon layers compared to HCNs nanoparticles. The obtained results are therefore a further proof that the superior electrical tree resistance of SCNs/Epoxy

at optimal nanofiller loading level is attributed to electron scavenging property of carbon and therefore a function of the amount of carbon.

The HCNs and SCNs nanofillers improve the electrical tree time-to-failure of epoxy but they compromise the electrical tree inception voltage. This confirms that there are different mechanisms for electrical tree inception and propagation process. Furthermore, for carbon nanofillers type and host insulation at optimal loading level for electrical tree endurance is not necessarily the same for electrical tree inception voltage. The optimal nanofiller loading level of SCNs in epoxy which is 0.31wt% is different from the one which was obtained by Hank [10] which was 0.11wt%. The average electrical tree time-to-failure of SCNs/Epoxy at optimal nanofiller loading level is 12.76 hours which is less than that obtained by Hank [10] which was 44 hours. The differences in the extent to which the same nanoparticle improve the properties of a dielectric are attributable to the differences in the type of the host epoxy. Furthermore, compatibility between the nanoparticle and the host epoxy resin is important.

In the present work it was assumed that the high shear mixer reduces the agglomeration of nanoparticles as the study was focused on comparing different nanofillers not the agglomeration of nanoparticles. The behaviour of test samples with same nanofiller loading level was inconsistent, some test samples were performing better than the other samples especially the nanocomposites with HCNs. It is speculated that this behaviour is attributed to agglomeration of nanoparticles which can profoundly affect the electrical behaviour of nanocomposite which implies that the nanoparticles were not dispersed and distributed properly, and this resulted into some test samples performing poorly. From the rheology results it was observed that SCNs slightly increased the viscosity magnitude of epoxy and HCNs did not change the viscosity magnitude of epoxy at optimal nanofiller loading. According to Blaszczak et al [69] and Mohammed [67] increase in viscosity might indicate agglomeration of nanoparticles. Khumalo et al [68] claims that the similarity of viscosity magnitude is attributed to weak interactions between the nanofiller and the host polymer. These weak interactions result into agglomeration of nanoparticles. This corresponds to what was reported by Hank [10] that at optimal nanofiller loading level for optimal dispersion and distribution the nanoparticles should decrease the viscosity magnitude of epoxy. Hence this assumption was incorrect in the future work coupling agents should be used to reduce the agglomeration and increase compatibility between the nanofillers and epoxy resin.

The partial discharge magnitude evolution time behaviour observed at 0.31wt% nanofiller concentration of SCNs/Epoxy nanodielectric corresponds to the one observed by Hank [10].

The partial discharge magnitude is relatively very high in the range of 1000-1500 pC at the beginning of electrical tree growth and drops to approximately zero charge after some time. This is an indication of charge suppression by SCNs nanoparticles during electrical tree growth, therefore prolonging the electrical tree growth in epoxy nanodielectric. It is unknown why the partial discharge magnitude is very high at the beginning of the electrical tree growth. The partial discharge magnitude in HCNs/Epoxy nanodielectric fluctuates over time. The PDPRP with varying PD pulse magnitudes observed in epoxy resin suggest the existence of branch electrical trees [11]. Whereas the combination of uniform sized and varying sizes PDPRP as observed in SCNs/Epoxy and HCNs/Epoxy nanodielectric suggest branch-bush and bush electrical trees. It can therefore be concluded that in optimally filled nanocomposites, the electrical tree types are predominantly of branch-bush or bush electrical as also reported by Alapati et al [85] and Pandey et al [88].

The findings in the present study confirm the superiority of solid carbon nanospheres to delay the electrical tree process in epoxy. A nanocomposite with carbon-based nanofillers is a promising next generation of insulation material which is cost effective, reliable and miniaturized. The study has proven the capacity to custom engineer a process to synthesise nanofillers and improved confidence in the ability to tailor nanocomposites with desired specifications. The study has established the opportunity to further enhance the electron scavenging properties of carbon by encapsulating an electronegative material like sulfur hexafluoride gas in the carbon shell. This work contributed knowledge to application of rheology in the nanodielectric development. The incorporation rheology analysis in the manufacturing technique appears to be a promising technique to monitor nanocomposite dispersion and distribution in real time.

5.6 Chapter Conclusion

This chapter has presented the electrical tree time-to-failure, inception voltage, electrical tree partial discharge magnitude time-evolution and PDPRD associated with the electrical tree growth. This chapter comparatively studies characterisation of SCNs and HCNs nanodielectrics through electrical tree PD behaviour and the following key finding were obtained:

- For the same type and size of carbon nanofillers the optimal nanofiller loading level (with regard to electrical tree endurance) is dependent on the type of host epoxy. For epoxy resin of the type Araldite® FR476D and Araldite® the optimal nanofiller concentration of SCNs and HCNs nanoparticles was found to be 0.31wt% and 0.04wt% respectively.

- SCNs/Epoxy nanocomposite have superior resistance to electrical treeing growth compared to HCNs/Epoxy nanocomposite. The good properties are attributed to the electron scavenging property of carbon and therefore the more carbon in the nanoparticle the better is the performance.
- The electrical tree partial discharge magnitude time-evolution behavior of SCNs/Epoxy nanocomposite is consistent with the those studied by Hank [10] even though the type of epoxy used in the present work is different from the one he used. It is still unknown why in the optimally loaded nanodielectrics that gave relatively good endurance to electrical tree degradation, the partial discharge magnitudes are initially very high during the inception phases of the electrical tree growth.
- The SCNs and HCNs nanoparticles enhance the electrical tree time-to-breakdown but compromise the electrical inception voltage in epoxy. It means the improvement in the performance of nanodielectrics with regard to electrical treeing is in the propagation phase of the electrical trees and not the inception stage.
- The electrical trees grown in the SCNs/Epoxy and HCNs/Epoxy nanocomposites are either of bush or branch or bush-branch as manifested in the corresponding PD pulse patterns. Whether the trees are bush or branch or both depend on the time evolution stage in the life of the electrical tree.

The next chapter presents the conclusions of all chapters.

Chapter 6: Conclusion and possible future research

6.1 The conclusions drawn from the present work

In the present work the hollow carbon nanospheres were successfully synthesized using template method with polystyrene as a prototype. The synthesized HCNs have a relatively high surface area and amorphous carbon structure. The synthesized HCNs were then used to fabricate epoxy nanocomposite with HCNs using a direct dispersion method incorporated with rheology. The rheology analysis was used to monitor the nanofiller concentration, dispersion and distribution of nanoparticles within the epoxy matrix during the manufacturing process. From the obtained results it can be concluded that the incorporation of rheology analysis in the nanocomposite manufacturing technique appears to be a promising technique to monitor nanocomposite dispersion in real time and determine the optimal nanofiller loading level for electrical tree resistance efficiently.

It was hypothesised that the excellent electrical tree resistance property of nanocomposites with solid carbon nanospheres is attributed to the electron scavenging properties of carbon. Hence the objective of the present research work was to investigate whether this hypothesis holds when the carbon nanoparticles are of the hollow type. It was confirmed that SCNs give nanocomposite with superior resistance to electrical trees compared HCN. This improvement is attributed to the electron scavenging property of carbon and therefore the more carbon in the nanoparticle the better is the performance. To conclude the dissertation Table 6.1 summarises the answers to the research questions.

Table 6.1: The research questions with corresponding answers as drawn from the research findings.

Research questions	**Answers as obtained from the research findings**
Main question: How do the properties of HCNs/Epoxy nanodielectric compare and contrast with those of solid SCNs/Epoxy nanodielectric?	SCNs/Epoxy nanodielectric has superior resistance to electrical tree compared to HCNs/Epoxy nanodielectric at optimal loaded levels. It was proven that good properties of carbon-based nano-fillers are attributed to electron scavenging property of carbon and therefore a function of the amount of carbon.
Sub-question: Which nanofiller loading level of hollow carbon nanospheres gives best electrical tree resistance in epoxy of type araldite® FR476D and hardener®?	For epoxy resin of the type Araldite® FR476D and Araldite® the optimal nanofiller concentration of HCNs nanoparticles was found to be 0.04 wt%.

Research questions	Answers as obtained from the research findings
Sub-question: Which nanofiller loading level of solid carbon nanospheres gives best electrical tree resistance in epoxy; araldite® FR476D and hardener®?	For epoxy resin of the type Araldite® FR476D and Araldite® the optimal nanofiller concentration of SCNs nanoparticles was found to be 0.31wt% which is approximately three times higher than that found by Hank [10] but using a different epoxy.
Sub-question: What are the rheological properties of unfilled araldite compared to HCNs/Araldite and SCNs/Araldite nanodielectrics in liquid state?	It was found that the HCNs and SCNs changes the viscosity and shear stress profiles at the investigated nanofiller loading levels except for that the nanofiller loading levels that gave the best performance for electrical tree resistance. At optimal nanofiller loading level of HCNs and SCNs nanoparticles for electrical tree resistance the viscosity and shear stress profiles are like those of the unfilled host matrix. Therefore, incorporating rheology analysis in the nanodielectric fabrication method can improve the efficiency of determining the optimal nanoparticle filler loading level for electrical tree endurance.
Sub-question: What are the electrical treeing characteristics of nanodielectric with hollow carbon nanospheres compared to those of unfilled epoxy and nanodielectric with solid carbon nanospheres?	The SCNs and HCNs nanofillers improve electrical tree endurance property of epoxy but compromise the electrical trees inception voltage of epoxy resin. It means the improvement in the performance of nanodielectrics with regard to electrical treeing is in the propagation phase of the electrical trees and not the inception stage.
Sub-question: Which nanofiller between SCNs and HCNs gives a nanodielectric with better resistance to electrical trees?	SCNs nanoparticles gives nanodielectric with better electrical tree resistance compared to HCNs nanospheres.

6.2 Recommendations for future work

Synthesis of hollow carbon nanospheres

- Currently HCNs are manufactured in a smaller scale, new techniques of synthesising hollow carbons nanospheres at larger scale needs to be explored.
- The electron scavenging properties of HCNs can be enhanced further by encapsulating an electronegative material like sulfur hexafluoride gas in the carbon shell.
- A coupling agent can be used to reduce the agglomeration of hollow carbon nanospheres and solid carbon nanospheres.

Rheological properties of nanocomposite material

It is still vague on how the rheological properties of the nanodielectrics are related to the dispersion and distribution of the nanofillers within the polymer matrix and the performance of the nanodielectric. More research is still required to fully understand how the rheological properties of nanodielectrics material are related to the dispersion and distribution of nanoparticles within the polymer. So that the rheology analyses can be used to monitor the particle dispersion in real time during the manufacturing of nanodielectric material.

Dielectric properties of HCNs/Epoxy nanocomposite

- In the present work only the electrical tree endurance and inception voltage properties of HCNs/Epoxy nanodielectric were investigated. It is important to see how the HCNs affect the other dielectric properties of epoxy such as breakdown strength, permittivity, tan delta, partial discharge surface erosion, space charge performance, thermal and mechanical at different nanofiller loadings.
- From the obtained results it can be deduced that SCNs and HCNs nanoparticles improve the electrical tree time-to-failure, but it is still unknown whether the nanoparticles improve or compromise the electrical tree inception time as well.
- It is still unknown why in the optimally loaded SCNs/Epoxy nanodielectrics that gave relatively good endurance to electrical tree degradation the partial discharge magnitudes are initially very high during the early stages of the electrical tree growth. Therefore, research work is required to understand why the charge is very high at the beginning of the electrical tree growth.

References

[1] C. F. Pitt, B. P. Barth and B. E. Godard, "Electrical Properties of Epoxy Resins," *IRE Transactions on Component Parts,* vol. 4, no. 4, pp. 10 - 113, 1957.

[2] I. Plesa, P.V. Notingher, S. Schlögl, C. Sumereder and M. Muhr, "Properties of Polymer Composites Used in High-Voltage Applications," *Multidisciplinary Digital Publishing Institute (MDPI),* vol. 8, no. 5, 2016.

[3] S. Li, S. Yu, Y. Feng, "Progress in and prospects for electrical insulating materials," *IET journals,* vol. 1, pp. 122-129, 2016.

[4] J.C Fothergill, L.A Dissado, J.K Nelson, "Nanocomposite Materials for Dielectric Structures," in *Engineering and Physical Sciences Research Council (EPSRC),* Swindon, 2001.

[5] J. KNelson and J. C. Fothergill, "Internal charge behaviour of nanocomposites," *Nanotechnology,* vol. 15, no. 5, p. 586–595, 2004.

[6] M.F Fréchette, "What are nanodielectrics?," *IEEE Electrical Insulation Magazine,* vol. 29, pp. 8-10, 2013.

[7] M. Fréchette, Convenor, A. Vaughan, Secretary, A. Allais, U. Häring, T. Andritsch, I. Bergmann, J. Castellon, A. Cristiano, E. David, M. Darques, V. Englund, D. Fabiani, A. Germano, S.J. Han, F. Perrot, N. Quirke, C. Reed, T. Shimizu, S. Sutton, T. Tanaka, "Functional nanomaterials for electric power," *CIGRE,* pp. 1-95, 2016.

[8] A. Gustafsson, P. Carstensen, C. Tomkvist, A. Ericsson and U. Nilsson, "Influence of Carbon Black in Polyethylene on Space Charge Accumulation," in *IEEE Annual Report - Conference on Electrical Insulation and Dielectric Phenomena,* Minneapolis, 1997.

[9] M. Jarvid , A. Johansson , R. Kroon , J. M. Bjuggren , H. Wutzel, V. Englun, S. Gubanski , Mats R. Andersson and C. Müller, "A New Application Area for Fullerenes: Voltage Stabilizers for Power Cable Insulation," *Advaned material ,* p. 897–902, 2015.

[10] A. M Hank, "Developing electrical tree resistant epoxy nanodielectrics with improved thermal properties," MSc dissertation at University of Witwatersrand, 2017.

[11] C. Jiang, Y. Hou, J. Yu, Z. Wei, X. Chen and H. Zhou, "Electrical treeing of polyethylene blends with/without voltage stabilizer," in *12th IEEE International Conference on the Properties and Applications of Dielectric Materials* , Xi'an, 2018.

[12] P.O Henk, T.W Kortsen and T. Kvarts, "Increasing the electrical discharge endurance of acid anhydride cured DGEBA epoxy resin by dispersion of nanoparticle silica," *High Performance Polymers,* vol. 11, p. 281–296, 1999.

[13] M.F. Frechette, M. Trudeau, H.D. Alamdari and S. Boily', "Introductory remarks on NanoDielectrics," in *2001 Annual Report Conference on Electrical Insulation and Dielectric Phenomena* , Kitchener, 2001.

[14] S. Li , Q. Lei, "Some Ideas about Engineering Dielectrics Researches," in *2nd International Conference on Electrical Materials and Power Equipment*, Guangzhou - China, 2019.

[15] T. J Lewis , "Interfaces are the dominant feature of dielectrics at the nanometric level," *IEEE Transactions on Dielectrics and Electrical Insulation,* vol. 11, no. 5, pp. 739-753, 2004.

[16] S. Li, G. Yin, S. Bai and J. Li, "A New Potential Barrier Model in Epoxy Resin Nanodielectrics," *IEEE Transactions on Dielectrics and Electrical Insulation,* vol. 18, no. 5, pp. 1535-1543, 2011.

[17] T. Tanaka, M. Kozako, N. Fuse and Y. Ohki, "Proposal of a Multi-core Model for Polymer Nanocomposite Dielectrics," *IEEE Transactions on Dielectrics and Electrical Insulation,* vol. 12, no. 4, pp. 669-681, 2005.

[18] S. Raetzke and J. Kindersberger, "Role of interphase on the resistance to high-voltage arcing, on tracking and erosion of silicone/SiO2 nanocomposites," *IEEE Transactions on Dielectrics and Electrical Insulation,* vol. 17, no. 2, p. 607–614, 2010.

[19] T. Andritsch,R. Kochetov, P.H.F. Morshuis and J.J. Smit, "Proposal of the polymer chain alignment model," in *2011 Annual Report Conference on Electrical Insulation and Dielectric Phenomena (CEIDP),* Mexico, 2011.

[20] E.I. Akpan, X. Shen, B. Wetzel, K. Friedrich, "Design and Sythesis of polymer nanocomposites," in *Polymer Composite with functionalized nanoparticles,* Amsterdam, Elsevier Inc, 2019, pp. 47-83.

[21] W. Wang, D. Min, S. Li, " Understanding the Conduction, Breakdown Properties of Polyethylene Nanodielectrics: Effect of deep traps," *IEEE Transactions on Dielectrics and Electrical Insulation,* vol. 23, pp. 564-572, 2016.

[22] W. Wang, S. Li, F. Tang, J. Li., "Characteristics on Breakdown Performance of Polyethylene/Silica Dioxide Nanocomposites," in *2012 Annual Report Conference on Electrical Insulation and Dielectric Phenomena*, Montreal, 2012.

[23] X. Li, D. Zhang and Y. Chen, "Silicone rubber/hollow silica spheres composites with enhanced mechanical and electrical insulating performances," *Materials Letters,* vol. 205, pp. 240-244, 2017.

[24] Y. Shao, Y. Chen, C. Du, T. Tanaka, "Properties of PS Grafted Alumina/Epoxy Nanocomposites," in *2016 IEEE International Conference on Dielectrics (ICD)*, Montpellier, 2016.

[25] J.Taima, K.Inaoka, T.Maezawa, Y. Tanaka, T. Takada and Y. Murata., "Observation of Space Charge Formation in LDPE/MgO Nano-composite under DC Stress at High Temperature," in *IEEE Conference on Electrical Insulation and Dielectric Phenomena*, Kansas, 2006.

[26] Y. Zhou, J. Hu, B. Dang and J. He, "Titanium oxide nanoparticle increases shallow traps to suppress space charge accumulation in polypropylene dielectrics," *Royal Society of Chemistry (RSC) advances,* 2016.

[27] F. Tian, J. Yao, P. Li, Y. Wang, M. Wu and Q. Lei, "Stepwise Electric Field Induced Charging Current and It's Correlation with Space Charge Formation in LDPE/ZnO Nanocomposite," *IEEE Transactions on Dielectrics and Electrical Insulation,* vol. 22, pp. 1232-123, 2015.

[28] G. Li, G. Chen and S. Li., "Charge Transport Characteristics in Nanodielectrics," in *IEEE Conference on Electrical Insulation and Dielectric Phenomena (CEIDP)*, Toronto, 2016.

[29] R. Kochetov, T. Andritsch, P.H.F. Morshius and J.J. Smit, "Anomalous Behaviour of the Dielectric Spectroscopy Response of Nanocomposites," *IEEE Transactions on Dielectric and Electrical Insulation,* vol. 19, p. 07 – 117, 2012.

[30] X. Zhang, H. Wen, X. Chen and Y. Wu, "Improving Electrical Properties of SrTiO3/Epoxy Nanocomposites with High Thermal Conductivity," in *2016 IEEE International Conference on High Voltage Engineering and Application (ICHVE)*, Chengdu, 2016.

[31] M. Takala, T. Sallinen, P. Nevalainen, J. Pelto and K. Kannus, "Surface Degradation of Nanostructured Polypropylene Compounds Caused by Partial Discharges," in *IEEE Conference International Symposium on Electrical Insulation*, Vancouver, 2008.

[32] M. Kozako, R. Kido, T. Imai, T. Ozaki, T. Shimizu and T. Tanaka, "Surface roughness change of epoxy/TiO2 nanocomposites due to partial discharges , „" in *Proceedings of 2005 International Symposium on Electrical Insulating Materials*, Kitakyushu, 2005.

[33] M. Kozako, N. Fuse, K. Shibata, N. Hirai, Y. Ohki, T. Okamoto and T. Tanaka, "Surface change of polyamide nanocomposite caused by partial discharges," in *IEEE Annual Report Conference on Electrical Insulation and Dielectric Phenomena*, Albuquerque,, 2003.

[34] T. Tanaka, A. Nose, Y. Ohki and Y. Murata, "PD resistance evaluation of LDPE/MgO nanocomposite by a rod-to-plane electrode system," *Proceding of International Conference on the Properties and Applications of Dielectric Materials,* vol. 1, pp. 319-322, 2006.

[35] T. Tanaka, Y. Matsuo and K. Uchida, "Partial discharge endurance of epoxy/SiC nanocomposite," in *Annual Report Conference on Electrical Insulation and Dielectric Phenomena*, Quebec, 2008.

[36] A.D Amit, S. D. Mhlanga and N. J Coville, "Carbon spheres," *Materials Science and Engineering,* vol. 70, no. 1–2, pp. 1-28, 2010.

[37] Y. Zhang, H. Li, P. Liu and Z. Peng, "Study on Electrical Properties and Thermal Conductivity of Carbon Nanotube/Epoxy Resin Nanocomposites with Different Filler Aspect Ratios," in *IEEE International Conference on High Voltage Engineering and Application (ICHVE)*, Chengdu, 2016.

[38] Y. Yao, N. Ning, L. Zhang, T. Nishic and M. Tian., " Largely improved electromechanical properties of thermoplastic polyurethane dielectric elastomer by carbon nanospheres," *RSC advances,* 2015.

[39] X. Gao, D. Gui and J. Liu, "Effect of Chemical Functionalization of Multi-Walled Carbon Nanotubes with 4'-Allyloxy-biphenyl-4-ol on Thermal and Mechanical Properties of Organosilicon Nanocomposites," in *IEEE Conference on Electronic Packaging Technology*, 2013.

[40] C.M. Long, M. A. Nascarella, P. A. Valberg, “Carbon black vs. black carbon and other airborne materials containing elemental carbon: Physical and chemical distinctions,” *Elsevier: Environmental Pollution,* vol. 181, pp. 271-286, 2013.

[41] X. Xie, Y. Mai, X. Zhoub, “Dispersion and alignment of carbon nanotubes in polymer,” *Materials Science and Engineering,* vol. 49, no. 4, pp. 89-112, 2005.

[42] S.L Zhong, Z.M Dang, W. Zhou and H.W Cai, “Past and future on nanodielectrics,” *Institution of Engineering and Technology (IET) Nanodielectrics,* vol. 1, no. 1, pp. 41 - 47, 2018.

[43] S.Li, A. Pasc, V. Fierroa and A. Celzard, “Hollow carbon spheres, synthesis and applications– a review,” *Journal of Materials Chemistry, Royal Society of Chemistry,* no. 33, p. 12686–12713 , 2016.

[44] W. Stöber, A. Fink, E. Bohn, “Controlled growth of monodisperse silica spheres in the micron size range,” *Journal of colloid and interface science,* 1968.

[45] B .Matuma, “Synthesis and Characterization of Solid, Hollow, Core-Shell and Worm-Like Carbon Nanostructures for Applications in Organic Photovoltaic Devices and Chemical Sensors,” University of Witwatersrand, Johannesburg, 2016.

[46] H. Marsh and F. Rodríguez-Reinoso, “Chapter 9 - Production and Reference Material,” in *Activated carbons* , Elsevier, 2006, pp. 454-508.

[47] A. Magubane, “Synthesis of copper nanoparticles contained in mesoporous hollow carbon spheres as potential catalysts for growing helical carbon nanofibers,” MSc thesis at University of Witwatersrand, Johannesburg, 2017.

[48] T.N Phaahlamohlaka, D.O Kumi, M.W Dlamini, L.L Jewell and N.J Coville. , “Ruthernium nanoparticles encapsulated inside porous hollow carbon spheres: A novel catalyst for Fischer_Tropsch synthesis,” *ELSEVIER on Catalysis today,* pp. 76-83, 2015.

[49] “User manual for a FEI Nova NanoLab FIB/SEM,” Wits Microscopy and Microanalysis Unit (MMU), Johannesburg, 2011.

[50] A. C. Ferrari and J. Robertson, “Interpretation of Raman spectra of disordered and amorphous carbon,” *The American Physical Society,* vol. 61, pp. 14 095-14 107, 2000.

[51] S. Choe, “Rheological Properties of Polymers,” Inha University, Korea.

[52] T. Saarinen, “Basics of rheology and rheometry,” Lecture slides from Aalto University, Espoo, 2019.

[53] B. Hochstein, “Institute of Mechanical Process Engineering and Mechanics,” Karlsruhe Institute of Technology , 12 January 2016. [Online]. Available: https://www.mvm.kit.edu/english/697_786.php. [Accessed 17 February 2020].

[54] “An introduction to rheology and its practical uses,” ATA Scientific Pty Ltd, 18 March 2018. [Online]. Available: https://www.atascientific.com.au/an-introduction-to-viscosity-and-rheology/. [Accessed 28 January 2020].

[55] Malvern Instruments Limited, “A Basic Introduction to Rheology,” Malvern Instruments Limited, 2016.

[56] G. Paroline, “Basics of Applied Rheology,” Anton Paar USA, Corvallis, 2016.

[57] C. Green , A. Vaughan, “Nanodilectrics - How much do we really understand?,” *IEEE Electrcal Insulation Magazine,* vol. 24, no. 4, pp. 6-16, 2008.

[58] B. X. Du, Z. L. Ma, Y. Gao, T. Han , Y. S. Xia, “Effects of nano filler on treeing phenomena of silicone rubber nanocomposites,” *IEEE,* pp. 788-791, 2011.

[59] M. Reading and A. S. Vaughan, “Rheological, Thermal and Electrical Properties of Poly(Ethylene Oxide)/Silicon Dioxide Microcomposites,” in *16th International Symposium on High Voltage Engineering (ISH),* Cape Town , 2009.

[60] N.B Singh, S. Rai, S. Agarwal., “Polymer nanocomposites and Cr (VI) removal from water,” *Nanoscience & Technology.,* p. 1–10., 2014.

[61] W. S. Khan, N. N. Hamadneh, W. A. Khan, “Polymer nanocomposites - synthesis techniques , classification snd properties,” in *Science and applications of Tailored Nanostructures,* Italy , One Central Press(OCP), 2016, pp. 50 -66.

[62] T. Andritsch, R. Kochetov, P. H. F. Morshuis, and J. J. Smit, “Influence of manufacturing on dielectric performance of nanocomposites,” in *IEEE International Conference on Solid Dielectrics*, Bologna, 2013.

[63] P.G Bruce, J.T.S Irvine , "Insertion compound," *Encyclopedia of Materials: Science and Technology ,* pp. 4115-4121, 2001.

[64] I. Pleşa, P.V Noţingher, C. Stancu, F. Wiesbrock , S. Schlögl , "Polyethylene Nanocomposites for Power Cable Insulations," *Polymers (Basel),* 2019.

[65] R. Gopal, "Synthesis of nanometerials," 1 December 2014. [Online]. Available: https://www.slideshare.net/RamalingamGopal/sol-gel-synthesis-of-nanoparticles. [Accessed 08 January 20120].

[66] W. E. Mahmoud, "Morphology and physical properties of poly (ethylene oxide) loaded graphene nanocomposites prepared by two different techniques.l," *European Polymer Journa,* vol. 47, pp. 1534-1540, 2011.

[67] N. A. Mohammed, "Rheology, Processing and Properties of Polymer Nanocomposites Based on POSS and Boehmite," Berlin Institute of Technology, Berlin, 2014.

[68] V.M Khumalo, J. Karger-Kocsis and R. Thomann,, "Polyethylene/synthetic boehmite alumina nanocomposites: Structure, thermal and rheological properties," *eXPRESS Polymer Letters 4,* pp. 264-274, 2010.

[69] P. Blaszczak,W. Brostow , T. Datashvili and E. H. Lobland , "Rheology of Low-Density Polyethylene+Boehmite Composites," *Polymer Composites,* pp. 1909-1913, 2010.

[70] L.A Dissado and J.C Fothergill , Electrical degradation and breakdown in polymers, London: Peregrinus, 1992.

[71] T. Tanaka and A. Greenwood, "Effects of charge injection and extraction on tree initiation in polyethylene.," *IEEE Transactions on Power Apparatus and Systems,* Vols. PAS-97, no. 5, pp. 1749-1759, 1978.

[72] M.H Ahmad, N. Bashir, H. Ahmad, A.A. Abd Jamil . and A.A Suleiman, "An overview of electrical tree growth in solid insulating material with emphasis of influencing factors mathematical models and tree suppression," *TELKOMNIKA Indonesian Journal of Electrical Engineering,* pp. 5827-5846, 2014.

[73] J.V Champion,S.J Dodd and G.C Stevens, "Quantitative measurement of light emission during the early stages of electrical breakdown in epoxy and unsaturated polyester resins," *Journal of Physics D: Applied Physics,* vol. 26, no. 5, pp. 819-828, 1993.

[74] M. Bao, S. Tang , J. He ,X. Yin, Q. Wang ,G. Wu and Y. Yang, "The Initiation Phenomena of Electrical Treeing in XLPE Cable Insulation," in *International Conference on High Voltage Engineering and Application,* Shanghai, 2012.

[75] J.V Champion and S.J Dodd, "Systematic and reproducible partial discharge patterns during electrical tree growth in an epoxy resin," *J. Phys. D: Appl. Phys,* vol. 29, p. 862–868, 1996.

[76] L. A. Dissado, S. J. Dodd, J. V. Champion, I. Williams and J. M. Alison, "Propagation of electrical tree structures in solid polymeric insulation," *IEEE Transactions on Dielectrics and Electrical Insulation,* vol. 4, no. 3, pp. 259 - 279, 1997.

[77] J. V. Champion, S. J. Dodd and G. C. Stevens,, "Champion J V, Dodd S J and Stevens G C 1994 J. Phys.D: Appl. Phys. 27 1020–30," *Journal of Physics D: Applied Physics,* vol. 27, pp. 1020-1030, 1994.

[78] N. Qiong, Z. Yuanxiang, C. Zhengzheng and C. Haihang, "Effect of frequency on electrical tree characteristics in silicone rubber," in *9th International Conference on,* Harbin, 2009.

[79] B. X. Du, Z. L. Ma, Y. Gao, T. Han, M. Xiao and X. X. Cheng, "Effects of Frequency on Treeing Phenomena in Silicone Rubber 1," in *2011 International Symposium on Electrical Insulating Materials,* Kyoto, 2011.

[80] B. X. Du, M. M. Zhang, T. Han and L. W. Zhu, "Effect of Pulse Frequency on Tree Characteristics in Epoxy Resin under Low Temperature," *IEEE Transactions on Dielectrics and Electrical Insulation ,* vol. 23, no. 1, pp. 104 - 112, 2015.

[81] I.Iddrissu and S.M. Rowland, "The impact of harmonic frequencies on electrical tree growth in epoxy resin," in *2017 IEEE Conference on Electrical Insulation and Dielectric Phenomenon (CEIDP),* Fort Worth, 2017.

[82] N.S. Mansor, D. Ishak , M. Mariatti, H. S. A. Halim, A. B. A. Basri and M. Kamarol, "Investigation on Electrical Treeing Characteristics of XLPE Containing ZnO Nano-Filler," in *International Symposium on Electrical Insulating Materials (ISEIM),* Toyohashi, 2017.

[83] S. Alapati, J.T.Meledath and A. Karmarkar, "Effect of morphology on electrical treeing in low density polyethylene nanocomposites," *IET Science, Measurement & Technology ,* vol. 8, no. 2, p. 60–68, 2014.

[84] S.J. Dodd, J.V. Champion, Y. Zhao, A.S. Vaughan, S.J. Sutton and S.G. Swingler , “Influence of morphology on electrical treeing in polyethylene blends,” *IEE Proceedings - Science, Measurement and Technology* , vol. 150, no. 2, pp. 58 - 64, 2003.

[85] S. Alapati and M.J Thomas, “Electrical treeeing in polymer nanocomposite,” in *Fifteenth National Power System Conference (NPSC)*, Mumbai, 2008.

[86] T. Hildinger, M. Brockschmidt, P. Gröppel, M. Weil and J. R. Weidner., “Improved Generator Performance with a Nanocomposite High Voltage Insulation System for Stator Windings – A Status Report.,” in *CIGRE*, 2016..

[87] C. Hoffmann, J. Weidner, T. Muth and F. Jenau, “Treeing growth and lifetime of epoxy filled with 26% of silica nanoparticles at 50 Hz AC-voltage,” in *XVII International Symposium on High Voltage Engineering*, Hannover, 2011.

[88] J.C. Pandey and N. Gupta, “Study of treeing in epoxy-alumina nanocomposites using electroluminescence,” *IEEE Transactions on Dielectrics and Electrical Insulation,* vol. 26, no. 2, pp. 648-654, 2019.

Appendix A: Detailed electrical treeing result of unfilled epoxy resin, SCNs/Epoxy and HCNs/Epoxy nanodielectric

Table A.1: The experimental data of electrical tree time-to-failure and inception voltage of unfilled epoxy, HCNs/Epoxy and SCNs/Epoxy nanodielectric data.

Type of the insulation	Sample number	Partial discharge inception voltage (kVrms)	Time to failure (second)	Time to failure (Minutes)	Time to failure a (Hours)
Unfilled epoxy (FR476D) sheared for 10 minutes	1	9,3	3235	53,92	0,90
	2	3,4	3347	55,78	0,93
	3	4,6	3199	53,32	0,89
Average		**5,77**	**3260,333**	**54,34**	0,91
Unfilled epoxy (FR476D) sheared for 15 minutes	5	12,53	13816	230,27	3,84
	6	14,55	28766	479,43	7,99
	7	20	7039	117,32	1,96
	8	18,73	12584	209,73	3,50
Average		**16,453**	**15551,25**	**259,19**	**4,32**
HCNs/Epoxy nanocomposite @ 0.02wt%	1	1,4	3660	61,00	1,02
	2	15,99	15060	251,00	4,18
	3	19,58	18420	307,00	5,12
Average		**12,323**	**12380**	**206,33**	**3,44**
HCNs/Epoxy nanocomposite @ 0.044wt%	1	7,5	15480	258,00	4,30
	2	7,6	157249	2620,82	43,68
	3	7,9	9840	164,00	2,73
	4	10,7	10433	173,88	2,90
	5	11	5807	96,78	1,61
	6	6,8	6423	107,05	1,78
	7	10,12	11580	193,00	3,22
Average		**8,802**	**30973,14**	**516,22**	**8,60**
HCNs/Epoxy nanocomposite @ 0.088wt%	1	8,1	5561	92,68	1,54
	2	6,3	5451	90,85	1,51
	3	8,2	3464	57,73	0,96
Average		**7,533**	**4825,333**	**80,42**	**1,34**
HCNs/Epoxy nanocomposite @ 0.19wt%	1	1,4	2124	35,40	0,59
	2	3,7	6370	106,17	1,77
	3	7,4	1798	29,97	0,50
Average		**4,167**	**3430,667**	**57,18**	**0,95**
HCNs/Epoxy nanocomposite @ 0.31wt%	1	7,5	1189	19,82	0,33
	2	5,2	1451	24,18	0,40
	3	6,5	1910	31,83	0,53
Average		**6,4**	**1516,667**	25,28	0,42
SCNs/Epoxy nanocomposite @ 0.044wt%	1	10,11	2709	45,15	0,75
	2	20	5353	89,22	1,49
Average		**15,055**	**4031**	**67,1833333**	**1,12**
SCNs/Epoxy nanocomposite @ 0.088wt%	1	20	6207	103,45	1,72
	2	6,26	3303	55,05	0,92
	3	5,518	8867	147,78	2,46
Average		**10,593**	**6125,67**	**102,09**	**1,70**
SCNs/Epoxy nanocomposite @ 0.19wt%	1	8,14	16221	270,35	4,51
	2	3,9	9672	161,20	2,69
	3	13,27	27240	454,00	7,57
Average		**8,44**	**17711,00**	**295,18**	**4,92**
SCNs/Epoxy nanocomposite @ 0.31wt%	1	1,45	3104	51,73	0,86
	2	1,45	64109	1068,48	17,81
	3	12,67	70576	1176,27	19,60
Average		**2,60**	**45929,67**	**765,49**	**12,76**
SCNs/Epoxy nanocomposite @ 0.44wt%	1	1,3	8420	140,33	2,34
	2	4,8	5407	90,12	1,50
	3	5,1	2734	45,57	0,76
Average		**3,73**	**5520,33**	**92,01**	**1,53**

Appendix B: Extra rheological results of SCNs/Araldite mixture

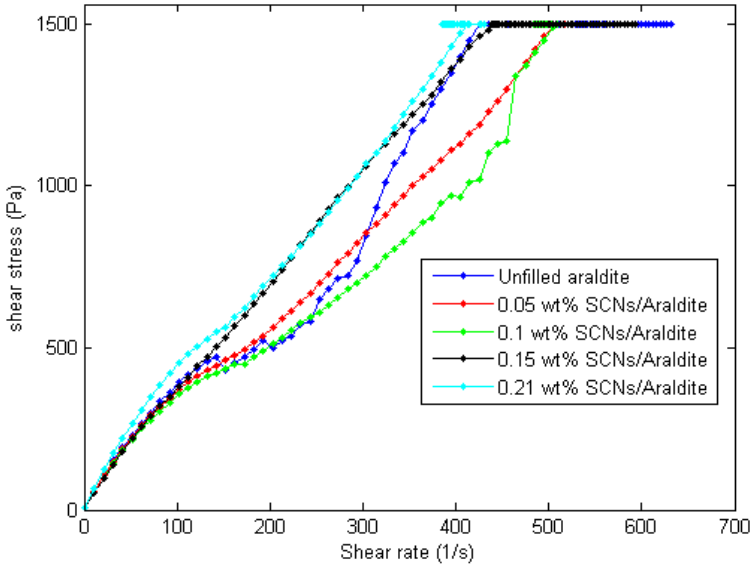


Figure B.1: The comparison of shear stress profiles of SCNs/Epoxy nanodielectric at different nanofiller loading levels and unfilled epoxy measured at 24.6℃.

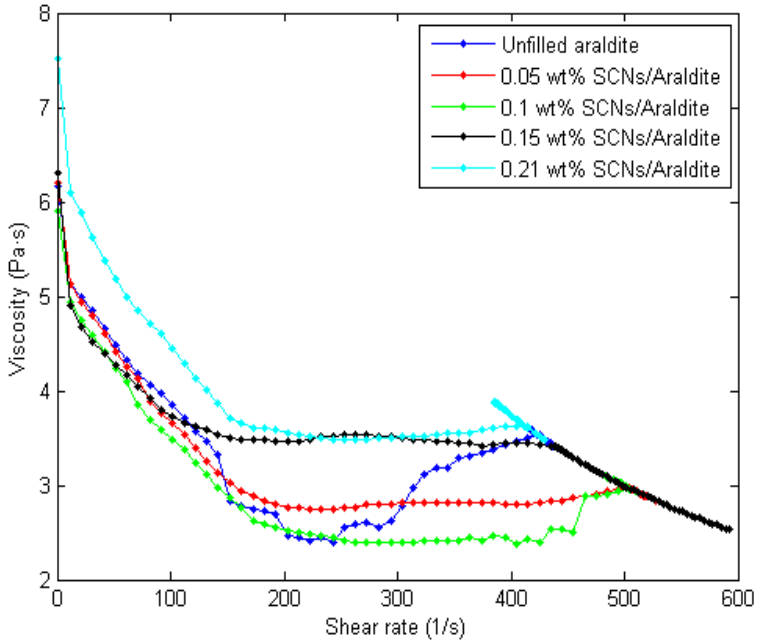


Figure B.2: The comparison of viscosity profiles of SCNs/Epoxy nanodielectric at different nanofiller loading levels and unfilled epoxy measured at 24.6℃.

Appendix C: A paper presented at the 2018 Southern African Universities Power Engineering Conference (SAUPEC) held at University of Witwatersrand, Johannesburg.

EVALUATION OF AC AND DC BREAKDOWN STRENGTH OF CARBON NANOSPHERE/EPOXY NANODIELECTRICS

S. Sitole*, C. Nyamupangedengu and A.M Hank*****

** and ** School of electrical and information engineering, University of Witwatersrand, Johannesburg*
**** System Operator, Eskom, Johannesburg, South Africa*
Email: *sophy.sitole@students.wits.ac.za **cuthbert.nyamupangedengu@wits.ac.za ***hanam@eskom.co.za

Abstract: This paper presents the AC and DC breakdown strengths of epoxy dielectric with solid carbon nanospheres (CNS/Epoxy nanodielectric) at 0.33 vol% loading. A two parameter Weibull distribution and Whisker box plot were used to analyse the data. Dielectric strength tests were done in accordance with the IEC 60243-1 standard which however is for AC voltage. There is no similar IEC standard for DC breakdown strength. It was observed that the median AC breakdown strength of CNS/Epoxy nanodielectric and clean epoxy are approximately the same in the order of 32 kV/mm. The median DC breakdown strength (94.6 kV/mm) was 5.4% less than that of clean epoxy. From the obtained results it was concluded that at 0.33 vol% the AC breakdown strength of CNS/Epoxy nanodielectric was not compromised but the DC breakdown strength was compromised. The DC breakdown strength is three times higher than the AC breakdown strength for both clean epoxy and CNS/Epoxy nanodielectric.

Key words: Breakdown strength, carbon nanosphere/Epoxy nanodielectrics, IEC standard, nanodielectric

1. INTRODUCTION

The conventional polymer insulation technology has reached the performance limit for modern applications such as renewable energy sources, ultra-high voltage transmission, and miniaturized equipment. In the literature it has been shown that adding an appropriate dosage of nanoparticles into a conventional insulation material to form a nanocomposite can enhance the breakdown strength of the insulation [1, 2].

Nanocomposites are a promising new generation of insulating material since they have better performance compared to conventional insulation [1, 2]. Hank [3] found that epoxy dielectric filled with solid carbon nanospheres (CNS/Epoxy nanodielectric) has excellent resistance to electrical treeing compared to clean epoxy and boron nitride/Epoxy nanodielectric at an optimal nanofiller loading level of 0.33 vol%.

This paper is the continuation of the work done in [3], and it presents the AC and DC electrical breakdown strength of CNS/Epoxy nanodielectric at an optimal nanofiller loading level. The purpose of this paper is to determine whether the electrical breakdown strength is improved or compromised at the optimal nanofiller loading level.

2. DIELECTRIC STRENGTH OF NANOCOMPOSITES – A LITERATURE REVIEW

This section discusses the literature review of the electrical breakdown strength of nanocomposites, factors affecting the breakdown strength of nanocomposites and intrinsic breakdown mechanisms in solid insulation.

2.1 Literature review of the electrical breakdown strength of nanocomposites

The selection of nanoparticles for a nanocomposite depends on the desired electrical, thermal and mechanical properties [1, 2]. Thus silica, alumina, magnesia and titania nanoparticles are commonly used as fillers to improve the breakdown strength because they possess high breakdown strength [4, 5]. Li et al [6] reported 95% improvement of DC breakdown strength on hollow silica nanospheres incorporated in silicone rubber compared to unfilled silicone rubber at 5 wt% nanofiller loading. Kochetov et al [7] found that solid silica/Epoxy, aluminium nitrite/Epoxy and magnesia/Epoxy nanodielectrics have an improved AC breakdown strength compared to unfilled epoxy at 0.5 wt% nanofiller loading level. The highest AC breakdown strength enhancement of 4.74% was observed for silica/Epoxy nanodielectric as compared with unfilled epoxy [7].

Wang et al [8] observed an improvement of 12% and 11% for AC and DC breakdown strengths of silica/Low-Density Polyethylene (LDPE) nanocomposite compared to unfilled LDPE at 0.5 wt% loading respectively. In [9] Wang et al reported that DC breakdown strength of aluminium oxide/LDPE nanocomposite increased by 30% compared to unfilled LDPE at 0.5 wt% loading.

From the above review it can be concluded that the breakdown strength is improved at a relatively low level of 0.5 wt% loading for solid inorganic nanoparticles [7-9]. There is however not much literature on the electrical breakdown performance of nanocomposites with conductive/organic nanoparticles which is the motivation for the present work.

However, there are researchers who have looked at electrical breakdown strength of nanocomposites with carbon nanospheres. For example, Yao et al [10] investigated the AC electrical breakdown strength of CNS/Thermoplastic polyurethane (TPU) nanocomposite but their focus was on the mechanical properties above power frequency. They found that the breakdown strength of CNS/TPU decreased from 25 kV/mm of unfilled TPU to 6.3 kV/mm at 5 wt% loading [10]. This was observed for every 1 wt% increment of nanofiller loading i.e. from 1 wt% to 5 wt%. The deterioration of breakdown strength for CNS/TPU nanodielectric might be that the researchers did not investigate the breakdown strength at a nanofiller loading less than 1 wt%. For conductive nanofillers the improvement of electrical properties normally requires that the filler loading level be below the percolation threshold. The percolation threshold is defined as a threshold where the resultant nanocomposite becomes electrically conductive.

Carbon nanospheres have high resistance to electrical treeing, best space charge performance, stable mechanical and thermal properties [3, 11]. The optimal nanofiller loading level of CNS/Epoxy nanodielectric is still unknown for electrical breakdown strength. The challenge with nanocomposites is that for the particle type and host insulation at optimal loading level for electrical tree endurance is not necessarily the same for breakdown strength (DC and AC).

2.2 Factors affecting the electrical breakdown strength of nanocomposites

The electrical breakdown strength of nanocomposites is affected by the method used to fabricate nanocomposites material, electric field distribution, nanofiller loading level and interphase [2, 12]. The method used to fabricate the nanocomposite material affects the dispersion and distribution of the nanoparticles within the host insulation because the nanoparticles tend to agglomerate to form undesired micro-clusters [1]. One of the solutions to agglomeration of nanoparticles is the use of coupling agents to coat the nanoparticles thereby forming functionalized nanoparticles. Coupling agents break up the adhesion forces between the nanoparticles and therefore enabling nanoparticles to be well dispersed within the host insulation [2]. Functionalised nanoparticles have a large improvement of breakdown strength compared to unfunctionalized nanoparticles [2, 12]. It should be noted that some researchers are not in favour of use of functionalized nanoparticles because they further complicate the physics and chemistry of nanocomposites.

The five commonly used techniques to fabricate nanocomposites material are; in-situ polymerization, sol-gel, melt blend, solution compounding and direct dispersion. The electrical field strength is non-uniform in nanocomposites and it is inversely proportional to the distance between the adjacent nanoparticles [13]. The breakdown strength improves at lower nanofiller loading and becomes poor at higher nanofiller loading [2, 7, 14]. The intrinsic breakdown mechanism in nanodielectrics is not yet fully understood. In unfilled dielectrics however, there is considerable understanding of intrinsic breakdown mechanisms as presented in the next section.

2.3 Electrical breakdown mechanisms in solid insulation

The breakdown mechanisms in solid insulations are classified into six types as follows: Intrinsic/ionic, thermal, electrochemical, electromechanical, partial discharges (erosion), electrical treeing and tracking [15, 16]. In the present work the interest is in intrinsic breakdown mechanisms which occur when the electrical field is applied for a short period of time on a uniform insulation. It is assumed that the intrinsic breakdown mechanism is electronic in nature and it occurs when the electrons gain sufficient energy from the applied electric field to move from the valence band to the conduction band [16]. However, insulations are not manufactured perfectly, they have impurities which act as trap sites for free electrons just below the conduction band [16]. At room temperature trapped electrons become excited and move into the conduction band. When the electric field is applied the conduction electrons gain sufficient energy to release electrons from atomic lattice by electron collision process [15,16]. There are models proposed to predict the critical value of the applied field where intrinsic breakdown occurs, but the models have inadequate information [16]. It still cannot be proven experimentally whether the intrinsic breakdown has occurred or not for materials which are not plastic in nature [16].

3. MATERIAL PREPARATION

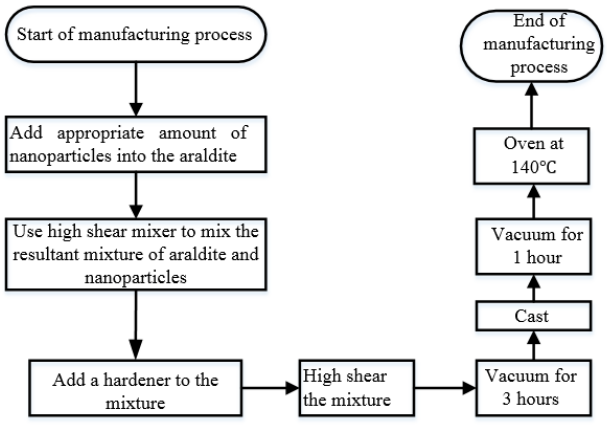


Figure 1: The flow chart of direct dispersion to fabricate the nanocomposite materials

A direct dispersion method shown in Figure 1 from [3] was used to fabricate the nanocomposite material because it is easy to implement. The Araldite and CNS nanoparticles were mixed using a Dispermat AE at a shear rate of 5000 rpm for ten minutes. The resultant mixture was placed in an oven to cure for 16 hours at 140℃. A low viscosity epoxy which comprises of Araldite CY201-3 and Aradur HY 925 from Huntsman™ was used to manufacture the nanocomposites material. The carbon nanoparticles were manufactured at the University of Witwatersrand Johannesburg, School of Chemistry and the process is detailed in [11].

The carbon nanospheres have a diameter of 80-120 nm. A sample cutter was used to partition the cylinder-shaped CNS/Epoxy nanodielectrics and clean epoxy samples into discs with thickness of 1 mm and diameter of 37 mm shown in Figure 2. The test samples were dried in an oven for 14 hours at a temperature of 100℃ to remove air moisture trapped within the test samples. After the conditioning the test samples were placed in a closed container until the day of testing.

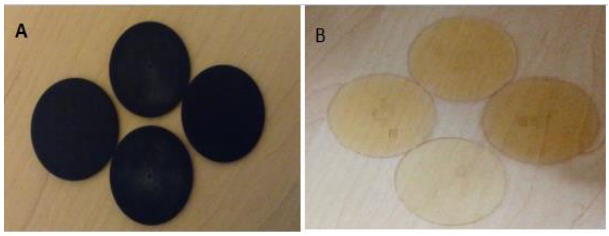


Figure 2: The test samples (a) CNS/Epoxy nanodielectric (b) Clean epoxy

4. DIELECTRIC STRENGTH TEST METHODOLOGY

The circuit diagram in Figure 3 was used to determine AC breakdown strength of unfilled epoxy and CNS/Epoxy nanodielectric according to IEC 60243-1 standard. The same circuit shown in Figure 4 was used to determine the DC breakdown strength of clean epoxy and CNS/Epoxy nanodielectric even though there is no IEC standard yet for DC breakdown strength test. The DC generator has a ripple factor less than 1 %. Spherical electrodes with a diameter of 25 mm were used. The whole test setup was submerged in clean and dry transformer oil to prevent surface flashovers under DC and AC voltages. The AC and DC voltages were increased from zero at a uniform rate of 2kV/s until breakdown occurred. The electrical breakdown strength is defined mathematically by equation 1.

$$E = \frac{V}{d} \tag{1}$$

Where:
V is the breakdown voltage in kV
d is the thickness of the test sample in mm

The measured data is analysed using a two parameter Weibull distribution and Whisker box plot. The Weibull distribution is defined by equation 2.

$$P(E) = 1 - \exp\left(-\left(\frac{E}{\propto}\right)^{\beta}\right) \tag{2}$$

Where:
P(E) is the cumulative probability
α is the scale parameter
β is the shape parameter

The Bernard median rank estimator defined by equation 3 is used to approximate the parameters α and β.

$$MR = \frac{i-0.3}{n+0.4} \tag{3}$$

Where:
n is the number of test samples
i is the order of the n samples. The lowest rank is $i = 1$ and highest is $i = n$

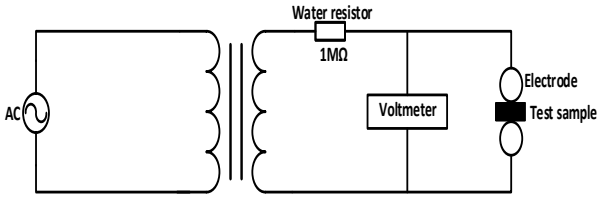


Figure 3: The circuit diagram used to evaluate the AC breakdown strength of clean epoxy and CNS/Epoxy nanodielectric

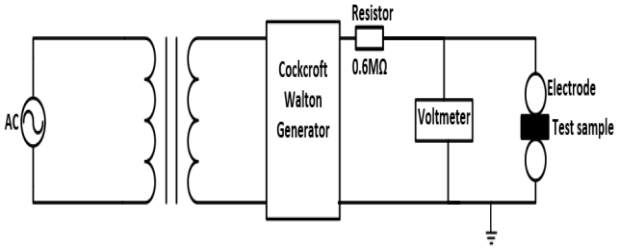


Figure 4: The circuit diagram used to evaluate the DC breakdown strength of clean epoxy and CNS/Epoxy nanodielectric

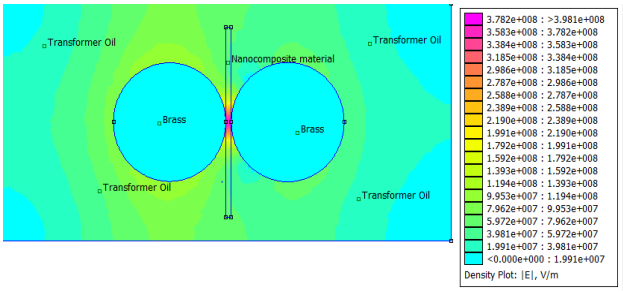


Figure 5: The electric field distribution of CNS/Epoxy nanodielectric under DC voltage

Figure 5 shows the electric field distribution of the test sample. The electric field intensity is more concentrated at the centre of the test sample where the test sample and electrodes are in contact. The electric field intensity is low at the edges of the test sample.

5. RESULTS

Only five samples of clean epoxy were tested under each voltage type AC and DC. Twelve and seven samples of CNS/Epoxy nanodielectric were tested under AC and DC voltages respectively. This imbalance of test samples was due to resource limitations for sample synthesis. Since Weibull analyses require equal number of test specimen and only five samples of clean epoxy were available therefore five samples of CNS/Epoxy nanodielectric were randomly chosen out of twelve to do the analyses.

5.1 AC breakdown strength results

The Weibull distribution plot is shown in Figure 6 and the parameters are in Table 1, but it is inconclusive since the line of best fit does not touch at least three data points for CNS/Epoxy nanodielectrics and the data points are few to draw a reliable conclusion. Hence a Whisker box plot was used to make deductions about the obtained results as shown in Figure 7. The minimum and median AC breakdown strength are approximately the same for CNS/Epoxy nanodielectric and clean epoxy as shown on the Whisker box plot. Therefore, it can be concluded that there is no significant change in the AC breakdown strength of CNS/Epoxy nanodielectric at 0.33 vol%.

At a nanofiller loading level of 0.33 vol% the relative permittivity of CNS/Epoxy nanodielectric and clean epoxy were found to be the same with the value of 3.91 and 3.95 respectively at 50 Hz frequency [3, 17]. Hence it can be speculated that the AC breakdown strength of CNS/Epoxy nanodielectric and clean epoxy are approximately the same because they have similar relative permittivity and conductivity profiles at 0.33 vol%.

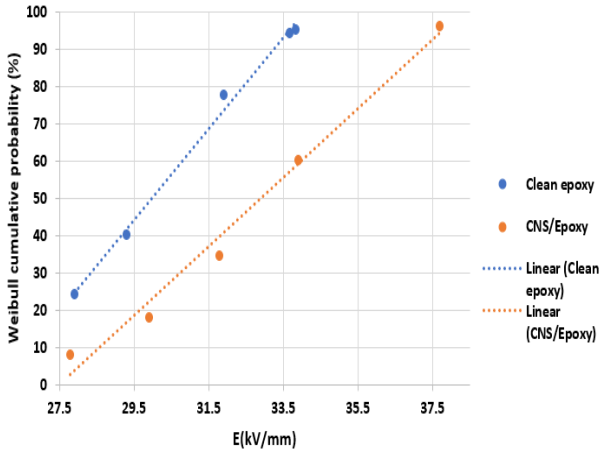


Figure 6: The Weibull distribution plot of AC breakdown strength of the clean epoxy and CNS/Epoxy

Table 1: The Weibull parameters of clean epoxy and CNS/Epoxy nanodielectric under AC voltage

Characteristics	Clean epoxy	CNS/Epoxy
α (kV/mm)	30.88	34.12
Shape parameter (β)	12.5	12

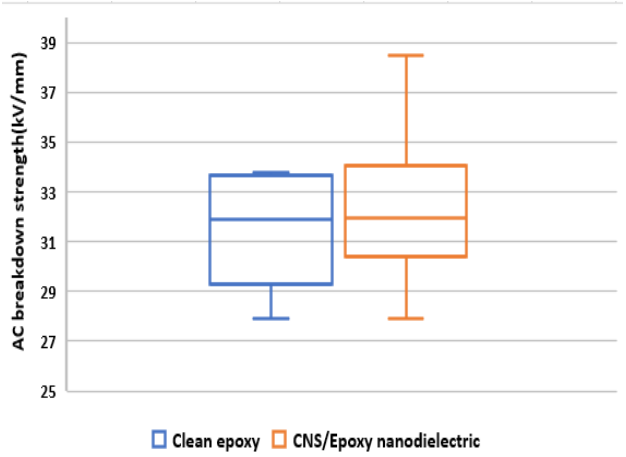


Figure 7: The Whisker box plot of AC breakdown strength of clean epoxy and CNS/Epoxy nanodielectric

5.2 DC breakdown strength results

The Weibull distribution plot shown in Figure 8 and the parameters are in Table 2, is inconclusive since the data points used are few to come up with a reliable conclusion. Thus, Whisker box plot is used to conclude on the obtained results under DC voltage. The median DC breakdown voltage of CNS/Epoxy nanodielectric is less than that of clean epoxy by 5.4%. Therefore, it can be concluded that the carbon nanospheres compromise the DC breakdown strength of CNS/Epoxy nanodielectric at 0.33 vol%.

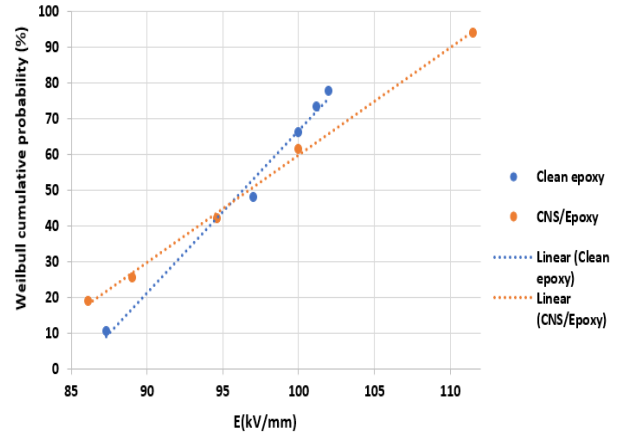


Figure 8: The Weibull distribution plot of DC breakdown strength of the clean epoxy and CNS/Epoxy nanodielectric

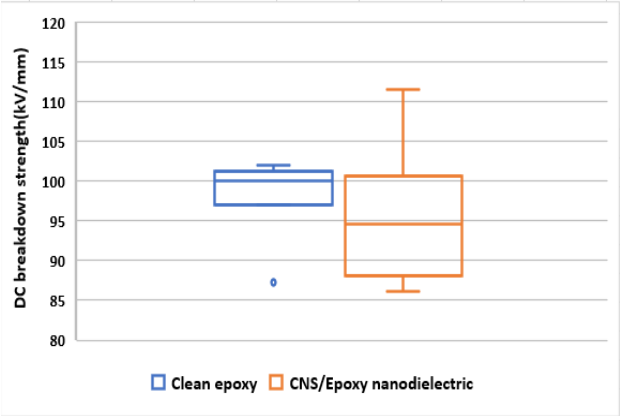


Figure 9: The Whisker box plot of DC breakdown strength of clean epoxy and CNS/Epoxy nanodielectric

Table 2: The Weibull parameters of clean epoxy and CNS/Epoxy under DC voltage

Characteristics	Clean epoxy	CNS/Epoxy
α (kV/mm)	99.5	100.48
Shape parameter (β)	16.7	10

6. DISCUSSION OF RESULTS

The DC breakdown strength magnitude is in the order of three times higher than that of the AC breakdown strength for both CNS/Epoxy nanodielectric and clean epoxy. This is due to the different breakdown mechanisms that occur under AC and DC voltages [8]. It is noted that the measured AC breakdown strength for both clean epoxy and CNS/Epoxy nanodielectric is higher than the specified AC breakdown strength on the datasheet which is 21 kV/mm. The difference could be a manifestation of superiority of the manufacturing process used in the present work.

The similar trends of DC results were observed in [13, 18]. The DC breakdown strength is more sensitive to nanofiller loading, type of nanoparticle and dispersion of nanoparticles within the host insulation more than AC breakdown strength [13, 18]. This behaviour could be attributed to the unidirectional characteristic of the DC electric field.

It can be concluded from the obtained results that carbon nanospheres do not compromise the AC breakdown strength of epoxy at nanofiller loading level of 0.33 vol%. This loading level is the one obtained in [3] as an optimal nanofiller loading for electrical treeing endurance test. This is a positive outcome because many insulation failures are caused by electrical treeing especially in alternating currents. It is acceptable to improve one property of the insulation without compromising the other property. More research still needs to be done to determine how carbon nanospheres influence the space charge performance and accelerated ageing and among other insulation properties of epoxy nanocomposite at 0.33 vol%. However, the carbon nanospheres compromise the DC breakdown strength of epoxy.

7. CONCLUSION

This paper presented the AC and DC breakdown strength of CNS/Epoxy nanodielectric in comparison to clean epoxy at a nanofiller loading level of 0.33 vol%. From the Whisker box plot it was concluded that AC breakdown strength of CNS/Epoxy nanodielectric and clean epoxy are approximately the same. The DC breakdown strength of CNS/Epoxy nanodielectric is lower by 5.4% compared to clean epoxy. The overall conclusion is that AC breakdown strength of CNS/Epoxy nanodielectric is not compromised and DC breakdown strength is compromised. Further investigation can be done to improve the accuracy of the obtained results by using more data quantity.

8. ACKNOWLEDGEMENTS

The authors would like to thank merSETA for funding one of the authors to pursue master's studies, and Eskom and National Research Foundation (NRF) for their support of the High Voltage Engineering Research Group at the university of Witwatersrand Johannesburg. Special thanks to these two schools within the university of Witwatersrand Johannesburg which are as follows; school of chemistry for manufacturing the solid carbon nanoparticles and school of chemical and metallurgy engineering for equipment and insight to manufacture the nanocomposite materials.

9. REFERENCES

[1] I. Plesa, P.V. Notingher, S. Schlögl, C. Sumereder and M. Muhr: "Properties of Polymer Composites Used in High-Voltage Applications", Multidisciplinary Digital Publishing Institute (MDPI), Vol. 8, Issue 5, April 2016.

[1] M. Fréchette, Convenor, A. Vaughan, Secretary, A. Allais, U. Häring, T. Andritsch, I. Bergmann, J. Castellon, A. Cristiano, E. David, M. Darques, V. Englund, D. Fabiani, A. Germano, S.J. Han, F. Perrot, N. Quirke, C. Reed, T. Shimizu, S. Sutton, T. Tanaka and J. Weidner: "Functional nanomaterials for electric power", Cigré, 2016.

[2] A. M Hank: "Developing electrical tree resistant epoxy nanodielectrics with improved thermal properties", MSc dissertation at University of Witwatersrand, March 2017.

[4] R. Nandanwar, P Singh, F.Z Haque: "Synthesis and properties of silica nanoparticles by Sol-gel method for the application in green chemistry", Material Science Research India, Vol. 10, May 2013.

[5] W.A Izzati, Y.Z. Arief, Z. Adzis and M. Shafanizam "Partial Discharge Characteristics of Polymer Nanocomposite Materials in Electrical Insulation: A Review of Sample Preparation Techniques, Analysis Methods, Potential Applications, and Future Trends", The Scientific World Journal, 2014.

[6] X. Li, D. Zhang, Y. Chen: “Silicone rubber/hollow silica spheres composites with enhanced mechanical and electrical insulating performances”, Elsevier, Vol. 205, pp 240-244, October 2017.

[7] R. Kochetov, T. Andritsch, P.H.F. Morshuis, J.J. Smit: “Evaluation of the Influence of various Nanofillers on the AC Breakdown Strength of Epoxy-based a nanocomposite”, IEEE Electrical Insulating Materials, pp. 383- 386, 2011.

[8] W. Wang, S. Li, F. Tang, J. Li: “Characteristics on Breakdown Performance of Polyethylene/Silica Dioxide Nanocomposites”, IEEE Electrical Insulation and Dielectric Phenomena, 2012.

[9] W. Wang, D. Min and S. Li: “Understanding the Conduction, Breakdown Properties of Polyethylene Nanodielectrics: Effect of deep traps”, IEEE Transactions on Dielectrics and Electrical Insulation. Vol. 23, pp. 564-572, February 2016.

[10] Y. Yao, N. Ning, L. Zhang, T. Nishic and M. Tian: “Largely improved electromechanical properties of thermoplastic polyurethane dielectric elastomer by carbon nanospheres”, Royal Society of Chemistry (RSC) advances, February 2015.

[11] A. A. Deshmukh, S. D. Mhlanga, and N. J. Coville: “Carbon spheres”, Materials Science and Engineering: R: Reports, Vol. 70, pp. 1–28, September 2010.

[12] Y. Shao, Y. Chen, C. Du and T. Tanaka: “Properties of PS Grafted Alumina/Epoxy Nanocomposites” IEEE International conference, 2016.

[13] K.Y. Lau a, M.A.M. Piah and K.Y. Ching: “Correlating the breakdown strength with electric field analysis for polyethylene/silica nanocomposites”, Elsevier Journal of Electrostatics, 2017.

[14] M. Gao, P. Zhang, F. Wang: “Effect of Percolation and Interfacial Characteristics on Breakdown Behavior of Nano-Silica/Epoxy Composites”, IEEE International forum, 2013.

[15] D. Tommasini: “Dielectric insulation and high-voltage issues”, CERN Geneva Switzerland, https://cas.web.cern.ch/sites/cas.web.cern.ch/files/lectures/bruges-2009/tommasini.pdf, last accessed 19 November 2017.

[16] E. Kuffel, W.S. Zaengl and J. Kuffel; "High Voltage Engineering Fundamentals" Oxford: Butterworth-Heinemann, 2nd edition, pp. 368-373, 2000.

[17] N.M. Maphundu, T.I. Rakoma, A.M. Hank and C. Nyamupangedengu, “Investigating the percolation threshold of carbon/epoxy nanodielectrics using dielectric spectroscopy”, SAUPEC, 2016.

[18] K.Y. Lau, A.S. Vaughan, G. Chen and I.L. Hosier: “Polyethylene nanodielectrics: the effect of nanosilica and its surface treatment on electrical breakdown strength”, IEEE conference, pp. 21-24, 2012.

Appendix D: The paper presented at the 2019 International Symposium on High Voltage Engineering (ISH) conference held at Budapest, Hungry.

Comparing electrical tree inception in epoxy and polyethylene using Fowler-Nordheim based model

S. Sitole[1*[0000-0001-7219-5028]] and C. Nyamupangedengu[1[0000-0001-8738-9191]]

[1] University of Witwatersrand, Johannesburg, South Africa
*sophy.sitole@students.wits.ac.za

Abstract. Endurance to electrical treeing-induced degradation is an important design parameter of electrical insulation. This paper presents a study of the electrical tree inception time in epoxy resin in comparison to that in polyethylene and Cross-Linked Polyethylene (XLPE). The electrical tree inception time is inversely proportional to the electric field strength and the relationship can be represented using the Fowler-Nordheim model. The model parameters are; the threshold electrical field strength (E_0) and material constants (C' and B). In the paper, the model parameters for electrical treeing in epoxy resin are derived through curve fitting on experimentally obtained data. The time to electrical tree inception for a range of applied electric field strengths were measured using partial discharge detection technique. For comparison, the experimental data obtained from the literature was used to determine the material constants of Fowler-Nordheim based model for polyethylene and XLPE. The derived Fowler-Nordheim based model constants C', B and E_0 of epoxy resin were found to be 3, 100 and 150 kV/mm respectively compared to 11, 100 and 441 kV/mm for XLPE and 0.3, 400 and 400 kV/mm for polyethylene. Electrical treeing inception characterisation using the Fowler-Nordheim model enables quantitate comparative evaluation of endurance to treeing degradation of various polymer solid insulation material and can be a useful tool in insulation material design.

Keywords: Electrical tree initiation, Epoxy, Fowler-Nordheim model, Partial discharges.

1 Introduction

Electrical trees are pre-breakdown mechanisms in solid polymeric insulation under enhanced localized electric stress. The electrical trees are gas-filled micro-tunnels that progressively grow through localized partial discharge (PD) activity [1]. The electrical treeing process is divided into three stages; initiation (inception), propagation and breakdown [2]. In the literature, studies of electrical treeing phenomena have mainly focused on the propagation mechanisms. It can be argued however, that an understanding of electrical treeing initiation mechanisms is necessary for informing improved insulation designs. This paper therefore focuses on the electrical tree initiation mechanisms.
Electrical tree inception time has been regarded as the time taken to produce a hollow channel large enough (about 10μm) to accommodate gaseous discharges [1, 3]. The time-to-inception for electrical trees is a function of the applied electric field strength. The relationship between the electric field strength and the time-to-inception of the electrical trees can be represented using the Fowler-Nordheim model [3]. The model parameters are unique for each polymer. It can be postulated that for a given polymer type under a known maximum electric field strength, it should be possible to estimate the time it takes for electrical trees to initiate. The converse could also be true that if the electrical treeing inception has to be delayed by a certain time, the maximum applied electric field strength has to be below a known value. This paper presents a study of the electrical tree inception time in epoxy resin in comparison to that in polyethylene and Cross-Linked Polyethylene (XLPE).

The rest of the paper is structured as follows; section 2 gives an overview of the theory on electrical tree inception mechanisms and the Fowler-Nordheim based model for electrical tree inception time. The experimental work is presented in section 3 followed by results and discussion in section 4. The paper conclusion is drawn out in section 5.

2 Background

This section gives an overview of the electrical treeing initiation mechanisms and electrical tree inception time in the context of the Fowler-Nordheim based model.

2.1 Electrical tree initiation mechanisms

Electrical trees are initiated in the region of enhanced localised electric field caused by irregularities in the insulation such as metallic inclusions, small cavities or cracks [1, 3, 4]. The electrical treeing process is driven by cyclic charge injection and extraction at the interface between the electrode and insulation under alternating electric field [2, 3]. The electrons are repetitively emitted/injected into the insulation in the negative half cycle and drawn back during the positive half cycle. In every cycle, injected/emitted electrons may extract sufficient energy from the electric field to initiate the physio-chemical reaction which causes disintegration of the polymer molecular chains. The electrical treeing process will then start when the polymer

disintegration produces hollow channels that are sufficient enough to sustain gaseous discharges. Alternatively, due to the Maxwell compressive forces prevailing in the regions of enhanced electric field, micro-cracks may form. The micro-cracks then facilitate initiation of progressively growing electrical trees through partial discharge (PD) activity in the cracks.

Charge injection is a characteristic initial process in electrical tree initiation [5]. The evidence of charge injection in electrical treeing in polyethylene was reported by Tanaka et al. [3] and in epoxy by Champion et al. [6]. The charges are injected by either Fowler-Nordheim tunnelling or Richardson-Schottky emission. Although there is some knowledge in the literature on electrical tree initiation mechanisms, the phenomenon is not yet fully understood due to the complexity and numerous factors influencing the process [7]. Despite the challenges however, there has been convergence on the knowledge on how to relate the incubation time of electrical treeing with the attendant maximum electric field; and this is commonly presented as the Fowler-Nordheim model for electrical tree inception as explained in the next section.

2.2 Fowler-Nordheim based model of electrical tree inception time

The time it takes for an electrical tree to initiate in a given polymer at a given electric field is defined by equation 1 which can be regarded as the Fowler-Nordheim based model [3, 8]. The model was derived using field emission and equi-energy theory. The model assumes that electrical tree inception is caused by charge injection and extraction from the tip of the electrode to the polymer. An assumption is made that the injected/emitted electrons can only contribute to electrical tree initiation if they have acquired sufficient energy which is above a specific critical value. The symbols E_0, C' and B are unique for each polymer. The present work derives these parameters for epoxy resin through curve fitting on experimentally obtained test data.

$$t = C'(\exp\left[-\frac{B\emptyset^{3/2}}{E}\right] - \exp\left[-\frac{B\emptyset^{3/2}}{E_0}\right])^{-1} \quad (1)$$

$$E = \frac{2V}{rln(1+\frac{4d}{r})} \quad (2)$$

The symbols in the equations are defined as follows: $C'$and B are material constants, $\emptyset$ is the effective work function of the insulation and electrode. It is the difference between work function of the electrode and electron affinity of the dielectric. Electron affinity is very small compared to the work function and therefore considered insignificant. E_0 (kV/mm) represents the resilience of the molecular structure to the push-pull effect of the energetic electrons and therefore is the threshold electric field strength beyond which the molecular bonds breakdown. E (kV/mm) is the applied electric field strength around the needle tip defined by the Mason equation 2 [3]. It is assumed that electrical tree initiates when applied electric field is greater than E_0. The value of C' corresponds to the tensile strength of the polymer [1] and is a measure of the resilience of the mechanical boring effect of the treeing micro-tunnels. V (kV) is the applied peak voltage, r (mm) is the radius of needle tip and d (mm) is the electrode spacing.

In order to study the relationship between the electric field strength and treeing initiation time in epoxy, electrical trees were deliberately initiated by applying AC voltage to a needle-plane electrode geometry cast in the epoxy under study. Using a PD measurement setup, the time-to-inception of the electrical trees were measured. The obtained data was then analysed. Details of the experimental work are presented in the next section.

3 Experimental

The experimental work entailed the preparation of the epoxy test specimens and conducting the electrical treeing measurements.

3.1 Sample preparations

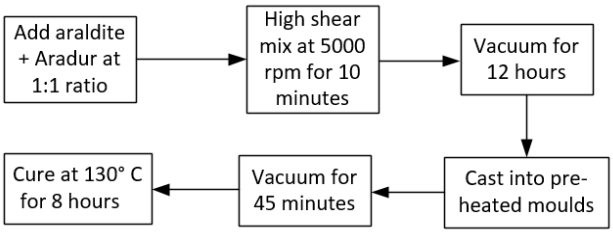


Fig. 1. Method to fabricate the epoxy resin treeing test samples

The procedure followed in fabricating the electrical tree test samples is presented schematically in Figure 1. The epoxy resin was of the type Araldite® CW 229-3 and Aradur® HW 229-1 obtained from Huntsman™. An image of some of the fabricated test samples is shown in Figure 2. Ogura™ needles with a tip radius of 5μm were used in the needle-plane electrode setup cast in the epoxy.

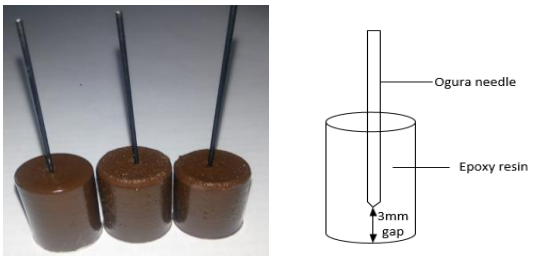


Fig. 2. An image of epoxy resin and drawing of electrical tree test samples

3.2 Electrical treeing inception detection using PD measurements

Imaging techniques have been commonly used in the studies of electrical tree inception in insulation. In non-transparent insulation however, the microscopic imaging techniques cannot be used to visualize and measure the electrical tree initiation time. Assuming that at inception the electrical trees immediately give detectable PD, the initial appearance of PD can be regarded as manifesting electrical tree initiation. The partial discharge measurement circuit shown in Figure 3 was used to determine the electrical tree inception time in the epoxy resin. The test sample was submerged in insulation oil to prevent surface discharges. The high voltage coupler to the needle part of the test specimen was custom designed to be corona-free. The applied voltage was increased at a rate of 1 kV/s up to the desired test voltage and held at that value until PD signals appeared. The voltage would then be lowered back to zero. The inception time of the electrical trees in epoxy resin was measured at voltage levels of 4, 5, 6, 8 and 10 kV_{rms}. Four samples were tested at each voltage value. For each test event, PD measurement and data was continuously recorded using the ICM compact™ PD measurement instrument.

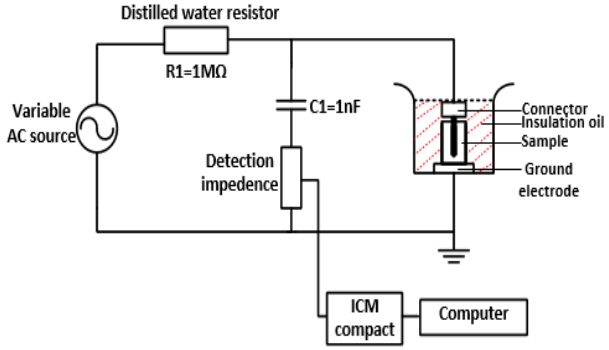


Fig. 3. The circuit diagram to measure the first partial discharges pulse according to IEC 60270.

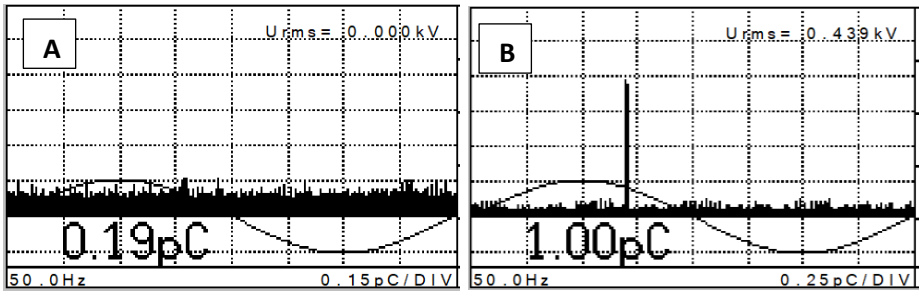


Fig. 4. a) A snapshot of PDPRP associated with the noise level at the lab, b) A snapshot of PDPRP of 1 pC signal used to calibrate the circuit.

The experiment was conducted in a shielded high voltage laboratory where the average noise level was 0.2 pC as shown in Figure 4a. The partial discharge test circuit was calibrated using 1 pC pulse as shown in Figure 4b. The 1 pC pulse is clearly distinguishable such that the PD magnitudes between 1 pC and the noise level can be deem traceable.

4 Results and discussion

The measured electrical tree inception times of epoxy resin at different electric field strengths are presented and discussed in this section. Furthermore, the derived parameters of the Fowler-Nordheim based model for epoxy resin, polyethylene and XLPE are presented.

4.1 The experimental results of electrical tree initiation time in epoxy resin

The PD Phase-Resolved-Patterns (PDPRP) associated with the initial PD pulses and charge magnitude measured for the electrical tree inception time in epoxy resin were recorded and studied to determine the time-to-electrical tree inception. Figure

5 presents typical results of a sample showing the time lapse before appearance of PD signal (indicating the initiation of electrical trees) with magnitude above the noise level. For this sample the first PD pulses were observed after 180 seconds. A snapshot of the PDPRP of the detected PDs at 180 s is shown in Figure 6. With reference to Figure 5 and 6, the following electrical tree PD characteristics are notable: Although the PD pulses are clearly distinguishable from the background noise level of about 0.2 pC, the PD magnitudes are relatively very small with indicated maximum magnitude of 0.6 pC. The relatively small measured electrical tree PD magnitude corresponds to very narrow (micrometer) gas-filled electrical tree tunnels at initiation and this is consistent with electrical treeing mechanisms presented in the literature [1, 3]. The PDPRP in Figure 6 are distinctly typical PD. The PD pulses are located on specific regions of the positive and negative half cycles of the test voltage. The PD pulses are small and of generally uniform sizes. Such characteristics typically depict PD signatures of bush type electrical trees as observed by Iddrissu et al. [9].

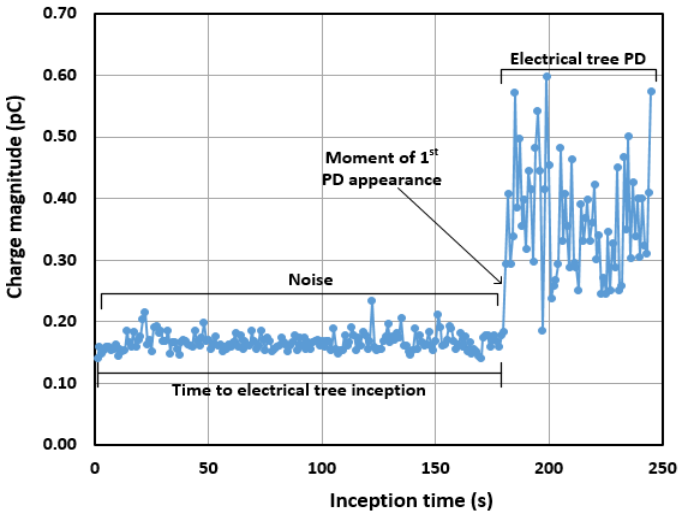


Fig. 5. Inception time as a function of charge magnitude at 4 kV corresponding to E_{max} of 206 kV/mm at the needle tip.

The plot of the measured time-to-electrical tree inception as a function of the applied electric field strength in epoxy is shown in Figure 7. At each data point the statistical spread of the four measurements is indicated. As expected, it is evident that at lower electric field strengths, the electrical tree takes relatively long to initiate compared to higher stress. At higher stress the differences in the time-to-inception becomes insignificantly small; in fact becomes statistically difficult to differentiate. Another notable characteristic is the significantly wide statistical spread of the time-to-electrical tree inception values at lower stress compared to higher stress values. At relatively low stress the time it takes for the initial micro-tunnels to grow big enough to support PD is relatively long. The repetitive process of charge injection/extraction causes physio-chemical degradation which initiate the electrical treeing process. At low electric field there is low probability of each event of charge injection/extraction causing insulation erosion. The corresponding time-to-electric tree inception is longer and with wider variations of the corresponding electric field values. At higher electric field however, the charge injection/extraction events are more effective resulting in shorter inception times and narrower spread of the corresponding electric field values. At low stress the process is slow and there are other factors such as inhomogeneity of the material which may become more dominant in influencing the electrical tree inception process [10]. Consequently, there would be a wider range of inception times at low electric field as evident in Figure 7.

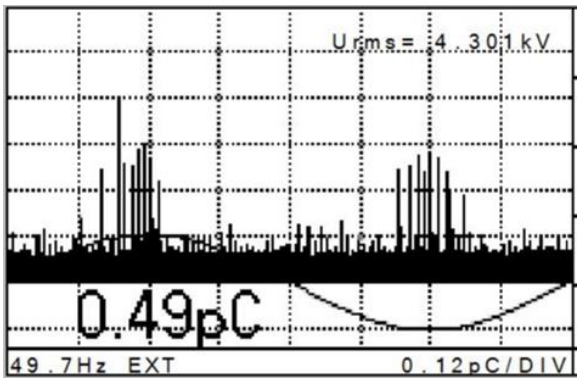


Fig. 6. An example of the PDPRP associated with the first PD pulses at 180s electrical tree inception time on Figure 5.

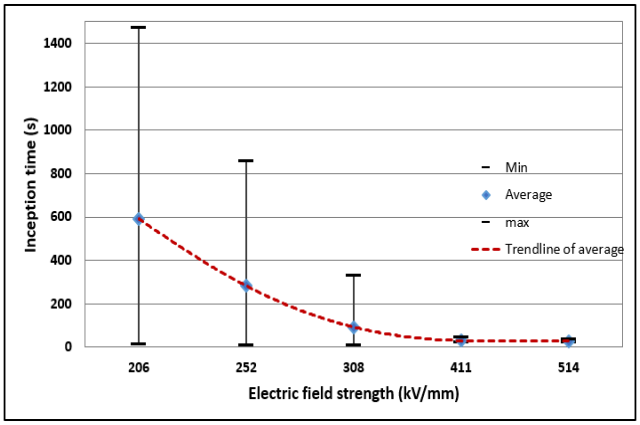


Fig. 7. Average-Max-Min chart for inception time as a function of maximum electric field strength.

The measured PD pulses are barely above the background noise level as shown in Figure 5 and 6. Sensitive and traceable measuring system is therefore imperative in the detection and measurement of electrical tree partial discharges. Some of the PD pulses associated with electrical initiation might have a magnitude equal to or less than the background noise therefore making it difficult to distinguish between the background noise and PD pulses related to the electrical tree. Due to the limitations brought by the capability of the measuring system it is possible that not all the PD pulses associated with the electrical tree inception were captured.

Notwithstanding the randomness in the electrical treeing inception process and measurement sensitivity limitations, the trends in the relationship between the electric field strength and time-to-electrical tree inception is distinct as shown in Figure 7. In the next section, through curve fitting, the corresponding constants in the Fowler-Nordheim model for the epoxy are derived.

4.2 Approximation of Fowler-Nordheim based model parameters for epoxy resin, polyethylene and XLPE

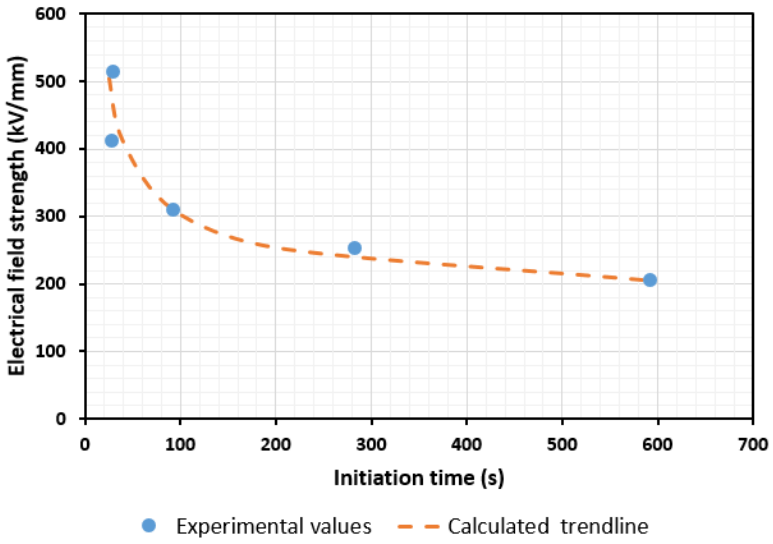


Fig. 8. The electrical tree inception time as function of applied electric field strength profile for epoxy resin.

A trend line can be fitted on the measured data points of electrical field versus time to electrical tree inception plot. By iteratively choosing and adjusting the E_0, C' and B values of the Fowler-Nordheim model (equation 1), the trend line can be reproduced that closely fits that of the measured data points as shown in Figure 8. Using a similar technique but on experimental test data obtained from the literature, the Fowler-Nordheim constants C' and B for polyethylene and corresponding trend lines were produced as shown in Figure 9 and for XLPE the plots are presented in Figure 10.

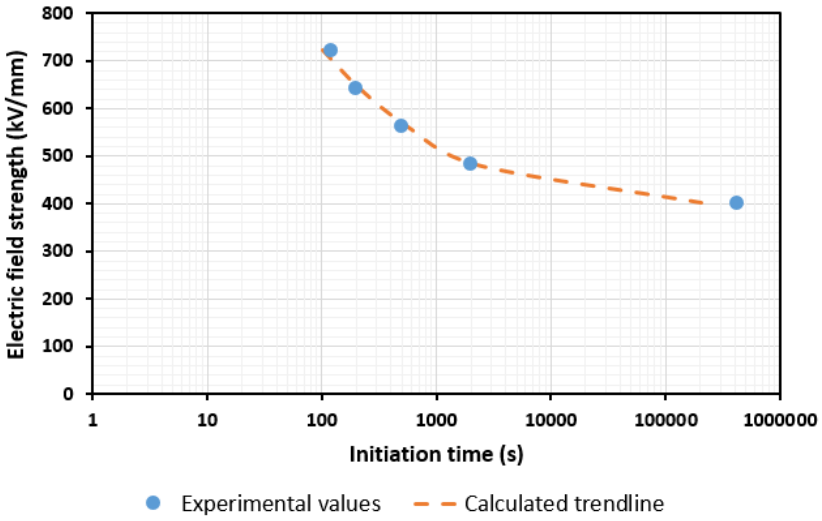


Fig. 9. The electrical tree inception time as function of applied electric field strength profile for polyethylene.

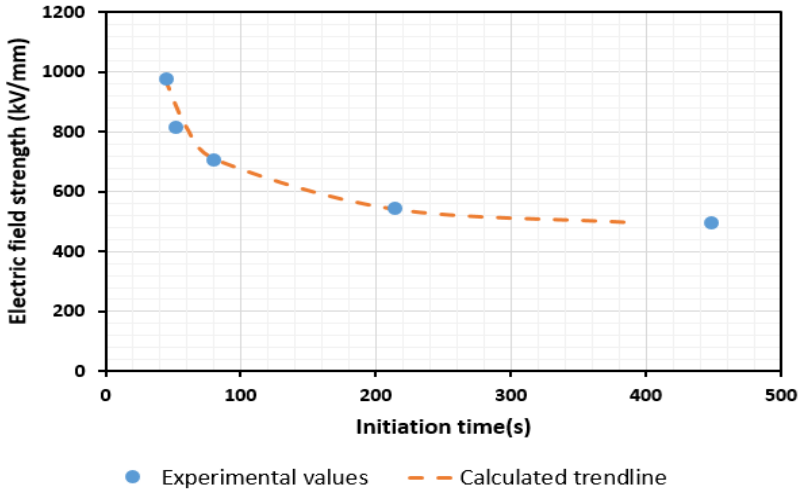


Fig. 10. The electrical tree inception time as function of applied electric field strength profile for XLPE.

Table 1 summarises the derived Fowler-Nordheim model constants of epoxy resin, polyethylene and XLPE. The E_0 values of XLPE and polyethylene were taken from the work by Hu et al. [10] and Dissado et al. [11] respectively. It can be deduced from the experimental data that the applied maximum electric field has to be greater than E_0 to initiate electrical trees. XLPE has a E_0 value greater than that of polyethylene and epoxy resin as shown in Table 1.

Table 3. A summary of derived Fowler-Nordheim model parameter for epoxy resin, polyethylene and XLPE

Insulation type	**Threshold electric field (E_0) (kV/mm)**	**Material constant C'**	**Material constant B**
Epoxy resin	150	3	100
Polyethylene	400	0.3	400
XLPE	441	11	100

The value of C' corresponds to the tensile strength in solid insulation material [11]. With reference to Table 1, XLPE has C' value greater than both polyethylene and epoxy resin. According to equation 1, B is inversely proportional to the electrical tree initiation time hence B should be lower to prolong the electrical tree initiation. The value of B is the same for both XLPE and epoxy resin. XLPE has a B value less than that of polyethylene and this confirms the superiority of XLPE over polyethylene. The Fowler-Nordheim based model can be used to compare the electrical tree inception time in epoxy resin and nanocomposites material.

5 Conclusion

This paper has presented the electrical tree inception time in epoxy resin which was measured using PD detection circuit. The measured PD pulse magnitudes are relatively small corresponding to the micrometer hollow channels formed at electrical tree initiation. The electrical tree inception time decreases with an increase in applied electric field strength. At lower electric field

the differences in the time-to-electrical tree inception is large and insignificantly small at higher electric field strength. The measured electric tree inception time of epoxy resin was compared to that of XLPE and polyethylene using Fowler-Nordheim based model parameters. It was found that B constant is the same for both XLPE and epoxy resin, and XLPE has a C' value greater than of epoxy resin and polyethylene.

Acknowledgments

Sincere gratitude is extended to MerSETA for financial support to the first author enabling here to conduct her post-graduate research work at the University of Witwatersrand. Gratitude is also extended to Eskom and the National Research Foundation (NRF) for their support of the High Voltage engineering research programme at the University of Witwatersrand.

References

1. Dissado L. A., Fothergill J. C.: Electrical degradation and breakdown in polymers. Peregrinus, London (1992).
2. Barclay A.L, Stevens G.C.: Statistical and fractal characteristics of simulated electrical tree growth. In: 6th International Conference on Dielectric Materials, Measurements and Applications, pp.17–20. IET, Manchester (1992).
3. Tanaka T., Greenwood A.: Effects of charge injection and extraction on tree initiation in polyethylene. IEEE Transactions on Power Apparatus and Systems PAS-97(5), 1749-1759 (1978).
4. Ahmad M.H., Bashir N., Ahmad H., Abd Jamil A.A. and Suleiman A.A.: An overview of electrical tree growth in solid insulating material with emphasis of influencing factors mathematical models and tree suppression. TELKOMNIKA Indonesian Journal of Electrical Engineering 12(8), 5827-5846 (2014).
5. Dissado L.A.: Understanding electrical trees in solids: from experiment to theory. IEEE Transaction on Dielectrics and Electrical Insulation 9(4), 483-497 (2002).
6. Champion J.V, Dodd S.J, Stevens G.C.: Quantitative measurement of light emission during the early stages of electrical breakdown in epoxy and unsaturated polyester resins. Journal of Physics D: Applied Physics 26 (5), 819-828 (1993).
7. Bao M., Tang S., He J., Yin X., Wang Q., Wu G., Yang Y.: The Initiation Phenomena of Electrical Treeing in XLPE Cable Insulation. In: 2012 International Conference on High Voltage Engineering and Application, pp.431–434. IEEE, Shanghai (2012).
8. Montanari G.C., Mazzanti G., Simoni L.: Progress in electrothermal life modelling of electrical insulation during the last decades. IEEE Transaction on Dielectrics and Electrical Insulation 9(5), 730-744 (2002).
9. Iddrissu I., Rowland S.M, Zheng H., Lv Z., Schurch R.: Electrical Tree Growth and Partial Discharge in Epoxy Resin Under Combined AC and DC Voltage Waveforms. IEEE Transactions on Dielectrics and Electrical Insulation 25(6), 2183-2190 (2018).
10. Hu L., Xu Y., Chen X., Li H., Feng Y., Ren Z.: The electrical trees initiation at different electric field strength in XLPE cable insulation. In: 2012 IEEE International Symposium on Electrical Insulation, pp.14–17. IEEE, San Juan (2012).
11. Dissado L.A., Hill R. M.: The statistics of electrical tree inception. IEEE Transaction on Electrical Insulation 25(4), 660-666 (1990).

Synthesis of hollow carbon spheres for fabrication of C\Epoxy nanocomposite insulation

Sophy Sitole
School of Electrical and Information Engineering
University of the Witwatersrand, Johannesburg
South Africa
sophycharism@gmail.com

Cuthbert Nyamupangedengu
School of Electrical and Information Engineering
University of the Witwatersrand, Johannesburg
South Africa
cuthbert.nyamupangedengu@wits.ac.za

Alice Magubane
School of Chemistry
University of the Witwatersrand, Johannesburg
South Africa
alice.magubane@students.wits.ac.za

Neil Coville
School of Chemistry
University of the Witwatersrand, Johannesburg
South Africa
neil.coville@wits.ac.za

***Abstract*— Nanocomposites are new generation electrical insulation made up of nano-fillers in a host insulation matrix. Such insulation technology has a potential for tailor engineering the properties to desired specifications. This paper presents a review of the nanocomposites insulation technology followed by an account of the experimental method and results of a methodology used in synthesising mesoporous hollow carbon nano-sphere (MHCNs) fillers. The obtained nanoparticles are characterised using SEM, TEM, Raman spectra, Banauer Emmett-Teller (BET), and thermogravimetric analysis techniques. The MHCNs have a diameter and BET surface area of 383±14 nm and 341.5 m^2/g respectively. In the ongoing research, the synthesized MHCNS are then used as fillers to fabricate C\Epoxy nanocomposite.**

Keywords— nanocomposites, nano-dielectrics, hollow carbon nano-spheres

I. Introduction

There is a need to explore development of the next generation electrical insulation to meet the evolving needs and increasing performance demands of modern and future electric power industry. Nanocomposites have been found to exhibit improved properties compared to conventional insulation [1]. The present paper focuses on the synthesis and characterisation of mesoporous hollow carbon nano-spheres (MHCNs). These nanoparticles are then used as fillers to fabricate epoxy nanocomposites. Some other applications where MHCNs have been used include water purification, energy storage, catalysis and biomedical application [2]. To the authors' knowledge use of MHCNs as nano-fillers in nanocomposites for high voltage applications has not yet been explored. In the literature however, other types of carbon nano-fillers such as fullerenes have been used and found to give nanocomposites with profoundly improved dielectric properties [3].

The good properties of carbon-based nano-fillers have been attributed to the electron scavenging properties of carbon. The overall aim of the ongoing research work is to fabricate a nano-composite epoxy using hollow carbon nano-spheres as fillers. The hollowness of the nanoparticles opens up other possibilities of further enhancing the electron scavenging properties of carbon such as by encapsulating electron negative material in the carbon nanoparticle shell. This paper however only focuses on the synthesis process of the hollow carbon nano-spheres which as a critical stage in the fabrication of nanocomposites.

Section 2 presents the literature review of nanocomposite electrical insulation technology. The methodology used to synthesise MHCNs is discussed in section 3. Section 4 presents the characterisation results and analysis of the nanoparticles.

II. Nanocomposites-A Literature Review

The science of nanocomposite technology evolves around the interphase region. There are key factors that influence the properties of nanocomposites and these include the interphase region, type and size of nanoparticles, nano-filler loading level and method used to fabricate the nanocomposite especially with regard to particle dispersion and distribution in the host material. In the next sections each of the factors are reviewed in more detail.

A. The Interphase Region

The improved dielectric properties of nanocomposites are attributed to the existence of the interphase region between the individual nanoparticle and the host insulation matrix [4]. The interphase region has different properties from the nanoparticle and host insulation [5]. There are several models proposed in the literature to describe the interphase region, but it is still vague on how the interphase predominates the resultant bulk properties of the nanocomposites insulation.

There are four prominent models in the literature that characterise the interphase region. The models are the multi-core, the new potential barrier, interphase volume and polymer chains model. Tanaka [6] proposed the multi-core model which states that the interfacial region comprises of three different layers which are the bonded layer, bound layer and loose layer as depicted in Figure 1. The bonded layer represents the chemical bonds between the nanoparticle and host matrix. The polymer chains are interfaced with the nanoparticle and bonded layer on the bound layer. The loose layer is the outermost layer and has different structure from

the first two layers. In this model the influence of the nano-filler loading level and type of nanoparticle are parameters not taken into account.

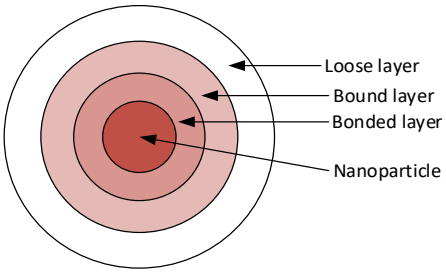


Fig. 1: The multi-core interphase model according to Tanaka [6]

The new potential barrier model is an extension of the multi-core model [5]. The transition region is made up of bound and loose layers of the multi-core model. The charge carries are restricted within the transition region at low nano-filler loading level. The restriction reduces the mobility and density of the charge carriers resulting in reduced electrical conductivity and increased breakdown strength. At high nano-filler loading however, the opposite occurs (especially for conductive nano-fillers) as the interphase regions overlap resulting in reduced breakdown strength.

The other model is the Interphase Volume model that is based on the multi-core model and has mathematical equation representations [7]. The following assumptions were made in the development of this model; the nanoparticles are spherical in shape, the thickness of the interphase is constant, the nanoparticles have the same diameter and, there is good distribution and dispersion of nanoparticles within the host insulation. The volume of the interphase is influenced by the nano-filler loading level, particle size, type of nanoparticle and host matrix. The maximum interphase volume is found at the optimal nano-filler loading and beyond this point the nanoparticles cease to enhance the properties of nanocomposite. This model is relatively more comprehensive and consistent with many findings in the literature as the nano-dielectrics give best performance at the optimal nano-filler loading level.

Another model is the polymer chain alignment model that is built on the multi-core layered, the intensity, the interphase volume and the double layer models [8]. The interaction between the nanoparticle and host insulation is enhanced by surface conditioning of the nanoparticles. The coupling agents align the polymer chains as illustrated in Figure 2. The model states that the interphase region is influenced by the physical properties of the nanoparticle (size and shape), type of nanoparticle as well as the type of coupling agent used to modify the surface of nanoparticle.

The nature of the interphase region depends on the type of the nanoparticle and compatibility with the host matrix. The selection of the nanoparticle type therefore becomes an important factor in the design and synthesis process of nanocomposites.

B. Selection of nanoparticles

The choice of type of nanoparticle for the nanocomposite insulation depends on the desired electrical, thermal and mechanical properties [1, 9]. When selecting a nanoparticle, it is desired that the nanoparticle enhances the dielectric characteristics such as good space charge performance, high breakdown strength, resistance to electrical treeing-induced degradation, good thermal and mechanical properties, among other important properties. Table 1 shows the properties of commonly investigated nanoparticles. MHCNs are a potential candidate because they have high surface area, high mechanical strength, high capacitance, thermally stable, low density and electrical conductive [2, 10]. The present work therefore focuses on MHCNs.

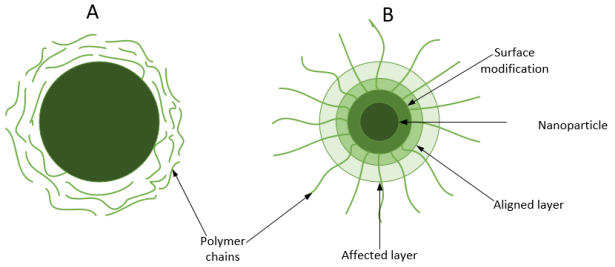


Fig.2: The polymer chain alignment model (a) the particle without surface conditioning (b) a surface conditioned particle adapted from [8]

THE CHARACTERISTICS OF COMMONLY INVESTIGATED NANOPARTICLES IN THE LITERATURE [1, 13-15]

Nanoparticles	Properties
Silicon dioxide (SiO_2)	High breakdown strength, resistance to electrical treeing and poor thermal properties.
Titanium oxide (TiO_2)	High breakdown strength, resistance to partial discharge and good mechanical properties.
Alumina (AlO_3)	It has high breakdown strength and good thermal properties
Magnesium oxide (MgO_2)	Good space charge performance, thermal properties, resistance to electrical treeing and partial discharge
Hollow silica nanospheres	High surface area, high breakdown strength, stable thermal and mechanical properties

C. Nano-filler loading level

There is no enhancement in nanocomposite insulation properties when the nanoparticles are not optimally loaded and in fact this may further compromise the properties the base insulation. The breakdown strength, space charge performance and dielectric properties of nanocomposites are enhanced at lower nano-filler loading while thermal properties are enhanced at higher nano-filler loading. Possible methods of finding the optimal nano-filler loading level include trial and error iterative and rheology techniques. In the trial error methods the nanocomposites with different nano-filler loadings are manufactured and then characterized to deduce which nano-filler loading is optimal. The drawback of trial error method is wastefulness. Rheology is the study of flow and deformation of matter in a liquid state under the influence of exerted force [11]. The rheology technique has been explored and reported to give promising results in the fabrication of epoxy nanodielectrics of solid carbon nanospheres in. It was found that the optimal nano-filler loading level of solid carbon nanospheres for treeing resistance is 0.33 vol% [12].

Related to the optimal loading level is the criticality of the rest of the process of mixing the nanoparticles in the host matrix as reviewed in the next section.

D. Methods used to fabricate nano-composite insulation

Agglomeration of nanoparticles during the fabrication of nanocomposite material negatively affect the properties of nanocomposites. For the enhanced performance to occur, a good distribution and dispersion of nanoparticles within the host insulation is essential. There are five commonly used methods to fabricate nanocomposite material; in-situ polymerization, sol-gel, melt blend, solution compounding and direct dispersion. The in-situ polymerization technique can be used in a variety of host insulation but not suitable for large scale production [16]. The sol-gel technique can disperse the nanoparticles much better compared to in-situ polymerization. The melt blend technique is effective and cost efficient, but it cannot be used on thermosetting host insulation. Direct dispersion technique is the least complicated and therefore used in the present work [16].

In most research articles on nanocomposites, the nanoparticles are presented as received from suppliers and therefore there is little focus on characterizing the nano-particles. This could be regarded as a possible source of inconsistences in the research results because the characteristics of the nanoparticles themselves have been proven to have a significant influence on the overall quality of the resultant nano-dielectric. The rest of this paper therefore details the customized hollow carbon nano-spheres synthesis process and characterization of the resultant nanoparticles through various established scientific test techniques. In the subsequent publications on the ongoing work, characterization of the resultant nanocomposite will be presented.

III. Synthesis methodology of the Mesoporous Hollow Carbon nano-spheres (MHCNs)

This section presents the method used to synthesize MHCNs. The MHCNs were manufactured using specialized facilities in the School of Chemistry at the University of Witwatersrand, Johannesburg. Spherical nanoparticles such as silica and polystyrene are used as the templates in synthesizing the MHCNs [10]. In the present work polystyrene was found to be the most convenient template. In summary the process entails initially coating the solid polystyrene nanoparticle templates with carbon material; resorcinol-formaldehyde polymer. The polystyrene template is then decomposed at 350°C to leave behind the mesoporous hollow carbon nano-spheres. The details of how the polystyrene is made followed by the coating process and release of the polystyrene are presented in the sections below.

A. Synthesis of the Polystyrene Template

16 mL of styrene and 0.2 g of polyvinyl pyrrolidone are added into 200 mL of ethanol and 50 mL of distilled water and the resultant mixture is stirred for 10 minutes [17]. 0.3 g of potassium persulfate is then dissolved in 20 mL of distilled water. The two solutions are mixed together, and resultant mixture is stirred at 80°C for 24 hours, the setup is shown in Figure 3. The mixture is centrifuged at 15000 rpm for 15 minutes and the resultant solids are washed three times with ethanol to give wet polystyrene nanoparticles. The wet polystyrene nanoparticles are then dried in an oven for 6 hours at 60°C to get ready for the coating phase of the process.

B. The Resorcinol-formaldehyde (RF) coating and carbonization process

The first solution comprises of 2 g of polystyrene nanoparticles and 1.5 mL ammonia solution which is dispersed in 100 mL of ethanol using a sonicator [17, 18].

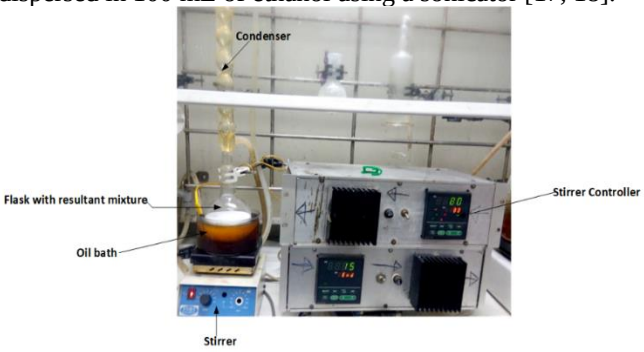


Fig. 3:The setup used to reflux the resultant mixture

In a separate glass beaker, a 1.5 mL formaldehyde solution, 0.75 g of resorcinol, 1 g of hexadecyltrimethylammonium bromide and 50 mL of ethanol are mixed to form the second solution. The two solutions are mixed, and the mixture stirred at room temperature for 24 hours to initiate the reaction. The resultant mixture is then stirred at 100°C for 24 hours. The solution is then filtered to give the solids which are washed with distilled water to remove unreacted precursors. The solids are then dried in an oven at 60°C overnight to give a polystyrene coated with resorcinol-formaldehyde polymer (PSS@RF).

The experimental setup for the carbonization process is schematically shown in Figure 4. A 0.5g of PSS@RF is placed inside the quartz boat which is then placed at the centre of a quartz tube inside the furnace. Nitrogen gas is used as carrier at a flow rate of 50 mL/minute. Figure 5 shows how the furnace temperature is ramped upto temperatures at which the polystyrene decomposes and temperatures where annealing process occurs. Annealing process is where carbon-carbon bonds are formed to make MHCNs and any residual polystyrene is removed. Approximately 80 mg of MHCNs are obtained at each run of the carbonization reaction.

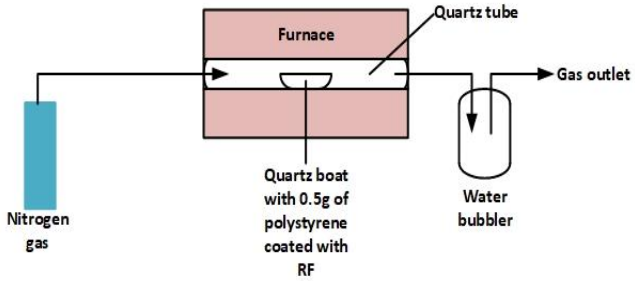


Fig. 4: A schematic of the experimental setup used for carbonation reaction

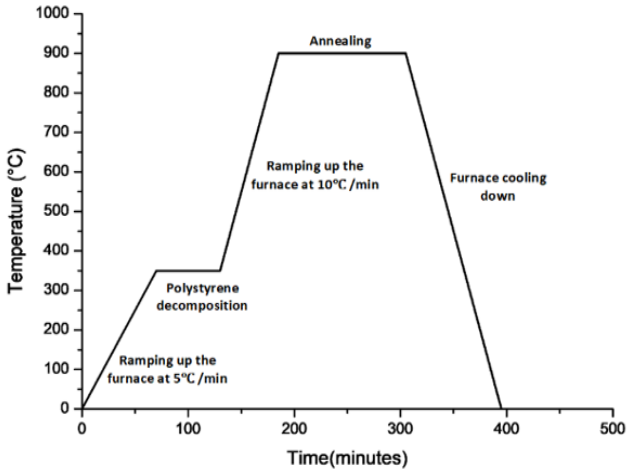


Fig. 5: The temperature profile which is set of the furnace as function of time

After the synthesis process, there is need to characterize the obtained hollow carbon nano-spheres, determining and confirming parameters such as dimensions, and chemical composition. The next sections present the various measurements conducted in that regard.

IV. Results and Analysis

A. Scanning electron microscopy (SEM)

The FEI Nova nanolab 600 scanning electron microscopy was used to determine the surface morphology and the diameter of the nanoparticles. The nanoparticles are uniformly dispersed on a carbon tape which is attached to an aluminium stab. The nanoparticles are coated with a single layer of palladium gold on top to make them more conductive. The aluminium stab is then placed inside the vacuumed chamber of SEM. The sample is subjected to a beam of electrons and based on their interaction, the detector generates an image depicting the surface of the nanoparticles [19]. In Figure 6, the SEM images of the MHCNs are shown. The spherical shape of the particles and tendency to agglomerate is evident.

B. Transmission electron microscopy (TEM)

Transmission electron microscopy technique is used to view the interior of the nanoparticles and confirm whether the manufactured nanoparticles are hollow or solid. TEM also uses a beam of electron to generate images depicting the tested sample. A small quantity of nanoparticles is placed inside a small vase in which 3 ml of methanol is added. The mixture is sonicated at room temperature for 15 minutes to disperse and distribute the nanoparticles within methanol solution. One drop of the mixture is placed on a copper grid and dried. The dry copper grid is placed on the TEM holder which is inserted into the TEM chamber. A beam of electrons is transmitted onto the copper grid which contains the nanoparticles to generate an image as shown in Figure 7 [20].The MHCNs have a diameter of 383±14nm and a shell thickness of 36±10nm. Less than 5% of the nanoparticles were found broken.

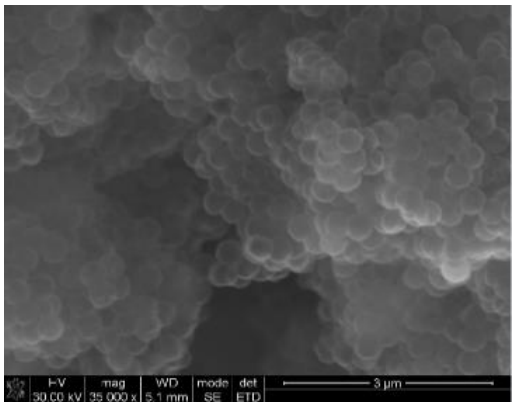


Fig. 6:The SEM pictures of the MHCNs

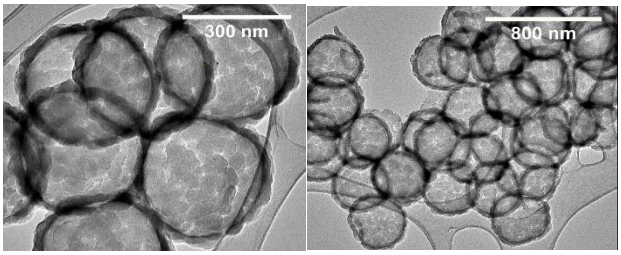


Fig 7: TEM images of the MHCNs

C. Branauer Emmett-Teller (BET) analysis

The BET is used to measure the surface area and the pore size distribution of nanoparticles [21]. 200 mg of MHCNs are placed in BET sample holder and degassed at 250 ºC in nitrogen gas for 4 hours. The BET method uses the nitrogen adsorption data to calculate the surface area and pore size distribution. The nanoparticles have a BET surface area and a pore size of 341.5 m^2/g and 2.5 nm respectively. The BET results show that the MHCNs have a high surface area.

D. Thermogravimetric Analysis (TGA)

The thermogravimetric analysis (TGA) of the nanoparticles is conducted to measure the thermal stability of MHCNs. TGA measures the mass loss of the samples as the temperature is increased from 36°C to 900°C at a rate of 10°C/minute [22]. A 10 mg of the test sample is placed on the sample pan inside the furnace of thermogravimetric analyser. The thermogravimetric analyser gives two curves which are thermogravimetric and derivative thermogravimetric analyses (D-TGA) curves. The TGA curve gives information about the thermal stability of the sample and sample composition. The D-TGA curves provides information about the rate of change of weight percentage loss with respect to temperature.

The thermogravimetric of results of synthesized polystyrene nanoparticles and MHCNs are shown in Figure 8 and 9. Figure 8 shows that there is a 2% weight loss at 100-150°C and this is attributed to the moisture. The polystyrene nanoparticles start to decompose at 300°C and the residual mass is zero at 430°C. The MHCNs start to decompose at 500°C as shown in Figure 9 and this confirms that all the polystyrene is decomposed during the carbonization process. The decomposition temperature of MHCNs is above 450 °C which means that they have a graphitic type of carbon.

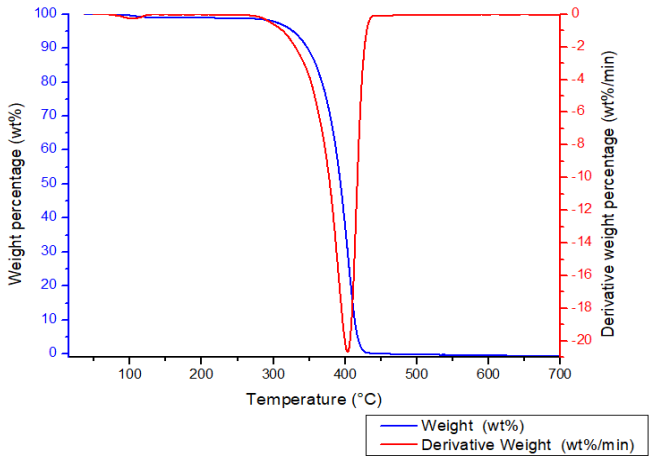


Fig. 8: The TGA and D-TGA curves of polystyrene nanoparticles

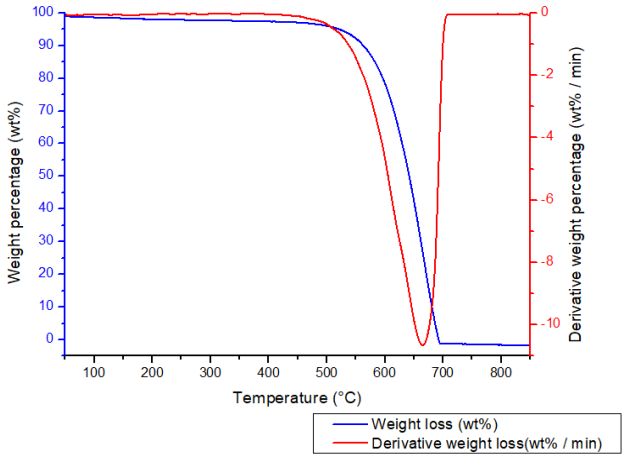


Fig. 9: The TGA and D-TGA curves of MHCNs

E. Raman spectroscopy

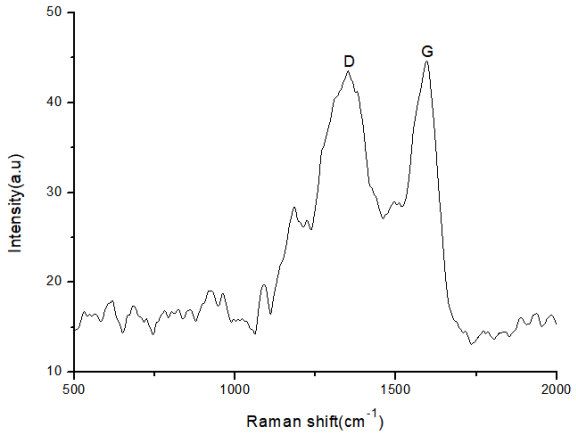


Fig. 10: Raman spectroscopy results of MHCNs

The Raman spectra technique gives information about the molecular vibrations and crystal structure of the nanoparticles [23]. The positions of Raman bands are used to characterize different structure of carbon materials. The two Raman band positions are observed for MHCNs which are the D and G bands. The D and G peaks positions are at 1350 cm^{-1} and 1597 cm^{-1} respectively as shown in Figure 10. The G band is attributed to the vibrations of sp^2 carbon atoms and it characterizes the graphitic carbon material [23]. While the D band is activated by the disorder [23]. The I_D/I_G (intensity of D peak to G peak) ratio is 0.98 as indicated on Raman spectroscopy results in Figure 10 and this means that the MHCNs have a disordered carbon structure. The disordered carbons comprise of sp^2 and sp^3 [23]. The synthesized MHCNs have more sp^3 hybridized carbon than sp^2 carbon.

V. Conclusion

Among the factors that influence the properties of each nanodielectric is the type and characteristics of the nano-filler. This paper has presented a template based synthesis process of hollow carbon nanosphere particles. Results of comprehensive measurements conducted to characterize the nanoparticles are presented and discussed. It is thus concluded that with the proven capacity to custom engineer a process to synthesise nano-fillers, there is improved confidence in the ability to tailor fabricate nanocomposites to required specifications.

Acknowledgment

Special thanks to MerSETA for funding one of the authors towards her Master of Science in engineering at the University of Witwatersrand. Eskom and the National Research Foundation (NRF) for their support of High Voltage engineering research work at the University of Witwatersrand.

References

[1] M. Fréchette, Convenor, A. Vaughan, Secretary, A. Allais, U. Häring, T. Andritsch, I. Bergmann, J. Castellon, A. Cristiano, E. David, M. Darques, V. Englund, D. Fabiani, A. Germano, S.J. Han, F. Perrot, N. Quirke, C. Reed, T. Shimizu, S. Sutton, T. Tanaka, J. Weidner. "Functional nanomaterials for electric power", CIGRE, 2016.

[2] S.Li, A. Pasc, V. Fierroa and A. Celzard, "Hollow carbon spheres, synthesis and applications– a review", Journal of Materials Chemistry, Royal Society of Chemistry, pp.12686-12713, 2016.

[3] M. Jarvid , A. Johansson , R. Kroon , J. M. Bjuggren , H. Wutzel, V. Englun, S. Gubanski , Mats R. Andersson and C. Müller, "A New Application Area for Fullerenes: Voltage Stabilizers for Power Cable Insulation", Advanced Materials, pp. 897-902, 2015.

[4] T. J Lewis, "Interphases are the Dominant Feature of Dielectrics at the Nanometric Level", IEEE Transactions on Dielectrics and Electrical Insulation, Vol. 11, pp. 739- 753, 2004.

[5] S. Li, G. Yin, S. Bai and J. Li., "A New Potential Barrier Model in Epoxy Resin Nanodielectrics", IEEE Transactions on Dielectrics and Electrical Insulation Vol. 18, pp. 1535-1543, 2011.

[6] T. Tanaka, M. Kozako, N. Fuse,Y. Ohki, " Proposal of a Multi-core Model for Polymer Nanocomposite Dielectrics", IEEE Transactions on Dielectrics and Electrical Insulation, Vol. 12, pp. 669- 681, 2005.

[7] Raetzke and J. Kindersberger "Role of interphase on the resistance to high-voltage arcing, on tracking and erosion of silicone/SiO2 nanocomposites", IEEE Transactions on Dielectrics and Electrical Insulation, Vol. 17, No. 2, pp. 607–614, 2010

[8] T. Andritsch,R. Kochetov, P.H.F. Morshuis and J.J. Smit, "Proposal of the polymer chain alignment model", 2011 Annual Report Conference on Electrical Insulation and Dielectric Phenomena (CEIDP), Mexico, , pp. 624-627, 16 – 19, Oct 2011.

[9] I. Plesa, P.V. Notingher, S. Schlögl, C. Sumereder and M. Muhr, "Properties of Polymer Composites Used in High-Voltage Applications", Multidisciplinary Digital Publishing Institute (MDPI), Volume 8, Issue 5, 2016.

[10] A.D Amit, S. D. Mhlanga, N. J Coville. Carbon spheres, Elsevier, July 2010.

[11] "Rheology. Definition of viscosity; Non-newtonian behaviour" http://dragon.unideb.hu/~kolloid/colloid/lectures/chembsc/lecture%2009.pdf , Last accessed 14 September 2017.

[12] A. M Hank, "Developing electrical tree resistant epoxy nanodielectrics with improved thermal properties", MSc dissertation at University of Witwatersrand, March 2017.

[13] X. Li, D. Zhang, Y. Chen, "Silicone rubber/hollow silica spheres composites with enhanced mechanical and electrical insulating performances", Elsevier, Vol 205, , pp 240-244, October 2017.

[14] T. Tanaka, A. Nose, Y. Ohki and Y. Murata, "PD resistance evaluation of LDPE/MgO nanocomposite by a rod-to-plane electrode system", Proc. ICPADM, Vol. 1, No. L-1, pp. 319-322, 2006.

[15] C. Nyamupangedengu, D. R. Cornish, " Time-evolution Phenomena of Electrical Tree Partial Discharges in Magnesia, Silica and Alumina Epoxy Nanocomposites", IEEE Transactions on Dielectrics and Electrical Insulation, Vol 23, 2016.

[16] T. Andritsch, R. Kochetov, P. H. F. Morshuis, and J. J. Smit, "Influence of manufacturing on dielectric performance of nanocomposites", IEEE International Conference on Solid Dielectrics, Italy, 30 June 30- 4 July 2013.

[17] A. Magubane, "Synthesis of copper nanoparticles contained in mesoporous hollow carbon spheres as potential catalysts for growing helical carbon nanofibers", MSc thesis at University of Witwatersrand, 2017.

[18] T.N Phaahlamohlaka, D.O Kumi, M.W Dlamini, L.L Jewell and N.J Coville. Ruthernium nanoparticles encapsulated inside porous hollow carbon spheres: A novel catalyst for Fischer_Tropsch synthesis, ELSEVIER on Catalysis today , pp. 76-83, 2015.

[19] "User manual for a FEI Nova NanoLab FIB/SEM", University of Witwatersrand Microscopy and Microanalysis Unit (MMU), 2011.

[20] " User manual for a FEI spirit 120kV TEM", University of Witwatersrand Microscopy and Microanalysis Unit (MMU), 2011.

[21] "A Beginner's Guide: Thermogravimetric Analysis (TGA)", PerkinElmer Inc, 2010-2015.

[22] R. Matshitse, "Brunauer-Emmett-Teller (BET) surface area analysis", Presentation slides from Rhodes University.

[23] A. C. Ferrari and J. Robertson, "Interpretation of Raman spectra of disordered and amorphous carbon", The American Physical Society,Vol 61, pp. 14 095-14 107, 2000.